QATAR UNIVERSITY

COLLEGE OF ENGINEERING

A FINITE ELEMENT INVESTIGATION OF EXISTING PIPEWORK VIBRATION ACCEPTANCE CRITERIA

BY

MEHDI KHAMMASSI

A Thesis Submitted to

the College of Engineering

in Partial Fulfillment of the Requirements for the Degree of

Masters of Science in Mechanical Engineering

June 2020

COMMITTEE PAGE

The members of the Committee approve the Thesis of
MEHDI KHAMMASSI defended on 03/05/2020.

Dr. Jamil Renno
Thesis/Dissertation Supervisor

Professor. Sadok Sassi
Committee Member

Professor. Ahmet Yigit
Committee Member

Approved:

Khalid Kamal Naji, Dean, College of Engineering

ABSTRACT

KHAMMASSI, MEHDI, Masters : June : 2020,

Masters of Science in Mechanical Engineering

Title: A Finite Element Investigation of Existing Pipework Vibration Acceptance Criteria.

Supervisor of Thesis: Jamil Renno.

In this thesis, a literature review was conducted to cover the assessment techniques for Oil and Gas (O&G) pipework that includes Small Bore Pipes (SBP). The various methods that were studied are the most commonly found in the field today. The advantages and disadvantages were analyzed. Multiple studies performed for the SBP connection which is the most susceptible area for fatigue failure (where it is usually welded on).

A robust Finite Element Analysis was carried out that initially analyzed the variations to the maximum stress, SBP tip velocity, and the first mode by changing the geometry of the system including the length and schedule of pipes.

Finally, a sample system was designed, and hundreds of results were gathered from the FEA models which were fed to multiple machine learning programs that trained them. To evaluate the accuracy of the programs, a sample system‘s geometrical parameters were inputted, the first mode frequency was predicted, and the percentage error was calculated. The output of this research would help inspectors to determine the system’s first natural frequency easily and thus expedite the fatigue risk assessment using existing vibration guidelines such as ASME.

DEDICATION

This thesis is dedicated to my mother.

ACKNOWLEDGMENTS

I would like to thank Dr. Jamil Renno who showed me unconditional support during this thesis by guiding me to achieve milestones in order to be able to finish my thesis. Additionally, I express my gratitude to my parents who encourage me throughout this journey.

TABLE OF CONTENTS

LIST OF TABLES

LIST OF FIGURES

Chapter 1: Introduction

Background

In recent decades the problem of metal fatigue has proven to be a popular topic in the industry. This type of failure is described by the gradual degradation effect due to an applied load that varies with time. These loads are cyclic but not necessarily periodic. Les Pook [1] divided metal fatigue into two categories: metallurgical and mechanical. The former category is concerned about studying the historical state of the metal before, during, and after applying fatigue loads. On the other hand, the mechanical category is about investigating the system's mechanical response due to the load applied (i.e. the number of cycles remaining for failure to occur).

Metals are heavily used in a plethora of industrial applications, one of these industries is the O&G industry. O&G is considered one of the most important/crucial sectors of today's economy. Pipes made from metals are used for pipework and pipeline in order to transfer the energy supply from the plant to various destinations [2].

Piping systems are categorized into two main groups, utility piping, and process piping. The latter is the system of pipes responsible for process fluids transportations (i.e. glycol, hydrocarbons, etc.). While, the utility piping is used to transport fluids that are used to support the hydrocarbon production process (i.e. cooling water, steam, etc.). Pipes, in general, are classified into mainline piping and Small-Bore Piping (SBP) [3]. The need for SBP during the production process is important, where these types of pipes are responsible for carrying pressure safety valves, drains, instrumentation ports, etc. In fact, the mainline and the SBP are connected (welded) thought SBC [4].

Fatigue failure of the SBC in the O&G industry is a universal concern. Vibration assessment of the SBC becomes a daily routine in every O&G plant. International standards provide guidelines and curves for the maximum acceptable levels of vibration

to ensure operational safety. However, these guidelines are described as unduly conservative by field experts. A wrong assessment could be declared, and process pipework might be categorized as unsafe to operate according to the measurement obtained. This often happens for offshore and onshore systems due to the low mechanical damping in the structure and thus leads to over-conservative operational limits as well as excessive cost manufacturing due to the high safety factor used in the design criteria [5].

The first target of an O&G plant is production. Vibration is considered to be a major hurdle along with corrosion. Statistics performed by the UK Health and Safety Executive show that Vibration Induced Fatigue is responsible for over 20% of all incidents of loss of containment in the North Sea (UK) [6]. Vibration can cause a loss of millions of dollars for companies and thus a reliable and rapid accurate methodology is required in the field to reduce the failure possibilities and thus maintain or increase production rates. Safety is considered the first and foremost priority for companies. It has been proven that the plant is more reliable and productive if the environment is safe for work.

Problem Statement

This research study is aiming to determine the geometry factors that are affecting the stress concentration within a vibrating SBP. Pipe inspectors rely on qualitative assessment to identify the risk in pipework plant. This assessment is described to be a visual survey by using guidance such as [7] & [8]. Since this assessment is not based on any taken measurements then it is mostly subjective to the inspector. On the other hand, the existing vibration criteria are reported to be conservative and ineffective since it eliminates the effect of the mechanical natural frequency as well as it ignores the importance of the system configuration.

As a result, the pipeline's condition in the United States is ranked as “Relatively poor condition” due to the immense failure cases (exceeds 10,000 case) and consequently leads to six (6) Billion US dollars loss [9]. Such failures may cause long term impact and irreversible damages to the human and natural environment.

Objectives

The main objectives of this research are the following:

1. To compare between the commonly used vibration criterion assessment.
2. To study the effect of the main pipeline dimensions on natural frequency, stress, and vibration.
3. To study the effect of the SBP dimensions on natural frequency, stress, and vibration.
4. To predict the first mode of the frequency of the system (main pipe + SBP) based on its geometrical dimensions to accurately assess the pipe’s vibration.

Outline of the Thesis

This thesis covers five chapters. The first chapter is the introduction where a background of the thesis been provided. The problem statement was defined, and the objectives were stated. For chapter Two “Research and Literature Review”, a definition of the fatigue was introduced and a detailed guideline for vibrations assessment was presented. Chapter Three covers the “Methodology” and the different phases followed throughout this research. Chapter Four discusses the findings and results. These results were validated and presented in Chapter Five And finally, conclusions and recommendations are provided in Chapter Six.

Chapter 2: Literature Review

The O&G industry is known for its huge usage of pipelines and pipework. Pipelines are considered to be critical components for the O&G field since it transports dangerous and invaluable goods. However, pipelines are known to be the safest petroleum products transportation (compared to highways trucks and rail). Nowadays, pipeline systems are efficient and ecofriendly. Nevertheless, any failure will cause a catastrophic impact on both environment and economy [10].

The pipelines are described to be a series of welded straight pipes that cover a long distance (e.g. 8200km is the Chinese West-East pipeline distance [11]). Such pipelines are operating above or under the ground and even in sub seas (see Figure 1). On the other hand, the pipework system is a complex pipes network within a specific boundary inside a plant. The latter is responsible for transporting liquids between vessels and equipment (see Figure 2).

Figure 1. Gas Pipeline [12]

Figure 2. Gas pipework system [13]

The gas pipework system is known by the use of a large number of SBCs as stabbings, instrument connections, or vent points. Due to it is geometry, the SBC is more apt to fatigue failure as a consequence of the vibration excitation. Fatigue failure may lead to a gas release and thus the safety of the plant can be at risk. A tragic example of vibration-induced fatigue in an O&G plant is the Gudrun incident in the North Sea, Norway, where this fatigue failure accident could have caused a big disaster where huge damage to the facility resulted. Such incidents have a negative environmental impact due to methane leakage, which is a prime element of the natural gas where it contributes heavily to global warming [14].

Kacprzyski et al. [15] mentioned that an inaccurate assessment of a mechanical system can lead to underutilizing of assets or on the flip-side overtax the equipment which is reaching the end of their lifespan. Thus, accurate prediction of fatigue failure is a necessity to ensure safety during production, both for human life and for financial aspects [16], [17].

Fatigue Life Assessment

Fatigue life assessment determines how many stresses cycles a system can safely handle until failure. In industry, fatigue life assessment is a crucial aspect of the operation. One of the challenges faced in such assessments is the huge uncertainty due to the service conditions that the system may encounter due to the internal operations of the plant or external conditions (service loading etc.) [18]. However, researches conducted in this field have developed different techniques to predict fatigue life. Mainly three approaches are the most commonly found in the field [19]:

- The stress life approach.
- The strain life approach.
- The linear elastic fracture mechanics approach.

Olson [20] claims that due to the large number of stress cycles experienced during the steady-state vibration, the allowable stress needs to be obtained from the fatigue curves. Indeed, using strain gauges will accurately help to determine pipe stresses and thus assist in analyzing the effects of vibration. The vibratory maximum stress is used to specify the piping acceptance criterion. Therefore, strain data would be sufficient along with the endurance limit for the piping material to determine whether the vibration amplitude measured was acceptable or not [21].

The challenge is that the dynamic stress measurement is a complicated and time-consuming approach. That is why it's considered as an unpractical technique in the industry. Thus, the tendency in the O&G field is to depend on velocity vibration measurement to assess the pipeline vibration. This is done since the maximum vibration amplitude is proportional to stress in the piping span vibrating at its resonance frequency [22]. In fact, the vibration severity is linked to fatigue due to several factors, in particular, the stress magnitude variation occurred, the anticipated numbers of this

variation throughout the piping system lifetime, and the distinct tolerance of cyclic loading for different steel grades [23].

The vibration assessment guidelines are made according to the operational experience of the plant. Due to this, the O&G industry is largely reluctant in the implementation of such guidelines. As a result, being able to accurately assess the pipework vibration is considered a difficult mission. These guidelines are not only based on empirical methods but are also stated in implicit terms without detailed derivation [23].

Minimizing the fatigue failure in the O&G plants is a priority and thus having a rapid and reliable criterion of assessment is essential in order to identify the risks. One of the earliest screening methodologies was based on the displacement and it was suggested by Wachel and Bates to the petrochemical plants [24]. This proposed criterion assumes that the additional masses attached to the main pipework are negligible and treats the first mode vibration of the main pipework as a simple beam. More extensive studies and surveys have been conducted in a nuclear power plant station in order to review the vibration problems and find a solution for the vibrated pipes [25]. Unfortunately, the suggested method was limited to a maximum of 300 Hz which is often considered below the natural frequencies of connections that possibly will be excited to higher frequencies.

The Southern Gas Association in Texas (USA), established an acceptance criterion for the vibration levels. The vibration readings are compared to the acceptance curves to determine the condition of the pipe [26]. These curves are no longer efficient for the reason that many fittings and connections have been introduced to the piping work design since that criterion was established in the early ’80s. Furthermore, this published technique does not take into consideration the geometry variation of the pipe and therefore the risk of wrong pipe condition assessment is maximum.

In the ’90s Motriuk proposed an approach that is based on the Rayleigh principle to assess the main pipe vibrations [27]. Motriuk builds this approach based on the phenomena of proportionality. The kinetic energy resulted from the vibration is proportional to the square of the velocity whereas the potential energy is proportional to the strain energy. This explains the connection between strain and velocity. Consequently, assumptions were made to introduce a constant (K) between the maximum strain in the structure with the maximum velocity obtained from the measurement. By determining the proportionality constant (K), the use of an accelerometer to assess the pipe will be justified. However, the reliability of this method depends on minimizing the uncertainty to determine this proportional constant (K). On the other hand, this approach allows the user to use a standard instrument to measure the velocity and this is considered as an advantage since this method is applicable for any vibrational mode and does not limit the application of the first mode only.

Small Bore Connection (SBC)

The SBC (see Figure 4) is described as a branched connection attached (welded) to a mainline pipe where it has a nominal size of usually 2 inches or smaller. This branch connection category also includes the branches welded to the mainline with a ratio of less than 10%, at the same time it excludes the connections with a ratio above the 25% (branch ratio) [28] (See Figure 3A for inch dimensions and Figure 3B for metric dimensions “mm”).

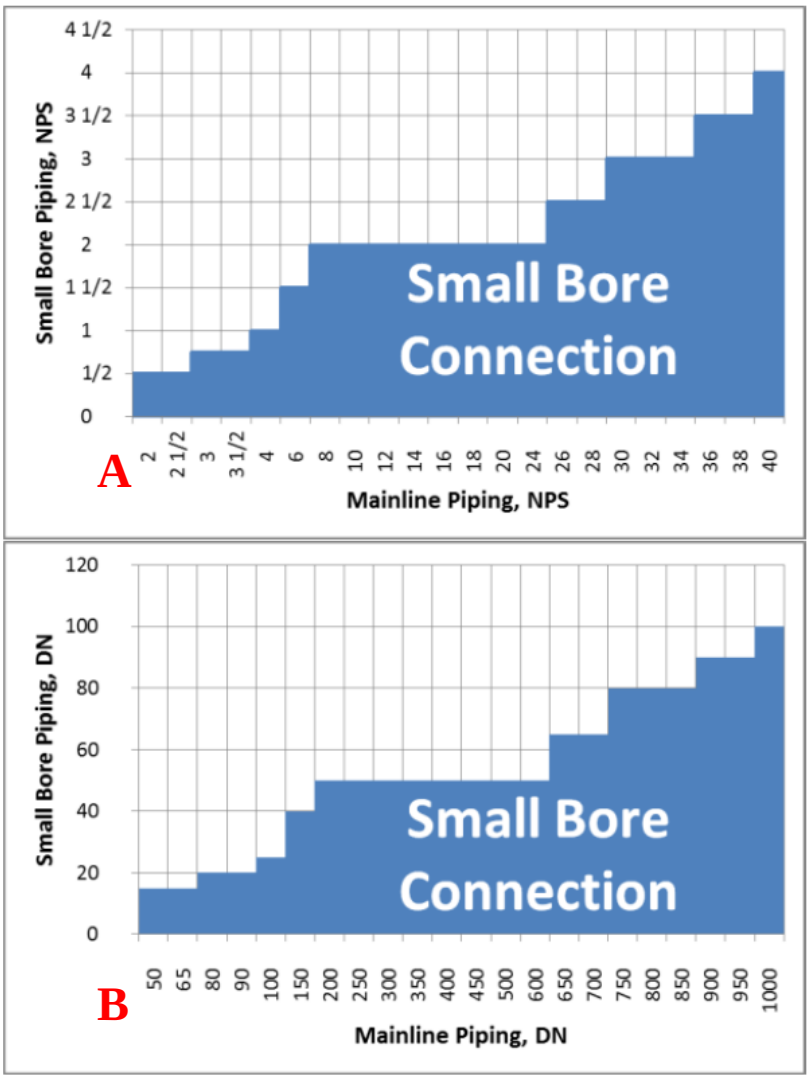

Figure 3. Small bore connection definition ([A] inch dimensions , [B] metric dimensions) [29].

The SBP is described as an attached pipe to the SBC where it contains fluid at its production pressure (see Figure 4).

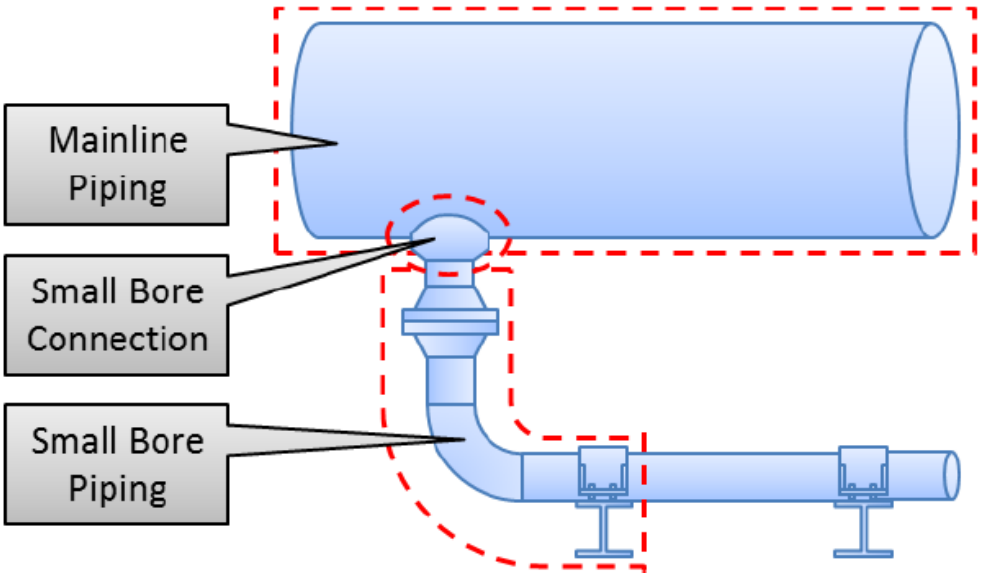

Figure 4. SBC and SBP definition [29]

According to the European Forum for Reciprocating Compressors Guidelines [30], in some cases, the vibration of the mainline (main pipe) could be acceptable but this vibration can be magnified at the SBC. Based on the geometry of the SBP and if the SBC is in resonance the vibration could be 30 times multiplied by the process piping which means that the SBP will experience very high cyclic stresses. Therefore, potential failure could occur anytime.

All the existing vibration guidelines for the SBC aim to classify the vibration levels in order to lower the risk of fatigue failures. However, recommended practices confirm that the location of the measurements, direction, and selection of the right guideline will play a major role to determine the accuracy of the decision.

Most of the installed rotatory systems (compressors/pumps) are used in the field without taking into consideration the geometry factor of the SBC, SBP, and valve mass. However, such a decision may lead to unpleasant consequences during the operational stages. Designers argue that the layout of the SBC and SBP are not provided during the design stage. Also, in the case that the SBC design and dimensions are already given

the mass will remain unknown until the procurement departments take an action and select them, and thus ignoring the accuracy of the SBC's mass may lead to misleading natural frequencies results.

In addition to what is been mentioned above, the human factor is still considered as a gap during the evaluation of the SBC in the field. Technicians cannot easily decide which one of the vibration guidelines needs to be followed. Furthermore, a proper evaluation requires full coordination between internal departments in the same company as well as good coordination with the other organizations (contractors and consultants). This could be explained by the fact that the procurement engineer is involved during the shop test, and the operation engineer is involved during the field evaluation. That is why solving the practical challenges during the design stage will help to solve the risks coming along with the SBC.

Nominal Pipe Size

Figure 5 below represents the dimensional parameters of a pipe. Abbreviations used for these parameters are the following:

- NPS: Nominal Pipe Size
- OD: Outside Diameter
- ID: Inside Diameter

For pipes with Nominal Pipe Size 14 inches or above, Its NPS refers to the Outer Diameter (OD). However, for small pipes with an NPS starting from 1/8 inch until 12 inches this is not the case (see Figure 5).

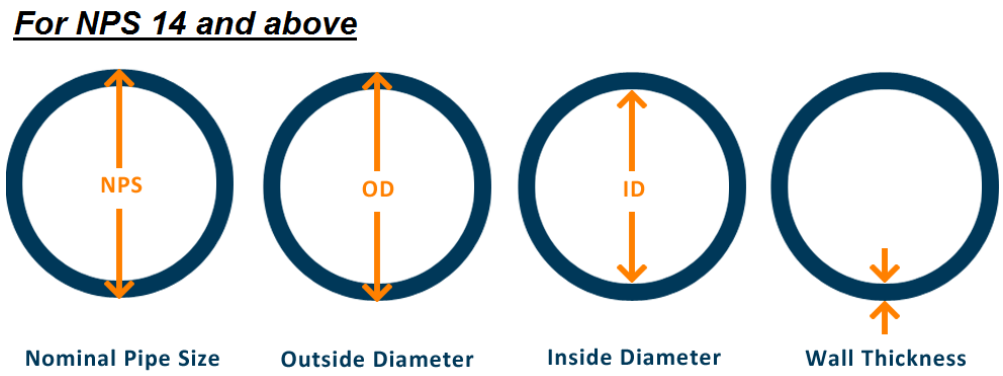

Figure 5. Pipe dimensions definition for NPS 14'' and above [31]

Figure 6 shows that the NPS does not represent the OD of a small pipe. In fact, pipes are described by the OD and a non-dimensional number stands for the wall thickness called by pipe schedule (SCH). Early in history, only three pipe schedules were in use, Standard (STD), Extra Strong (XS) and, Double Extra Strong (XXS).

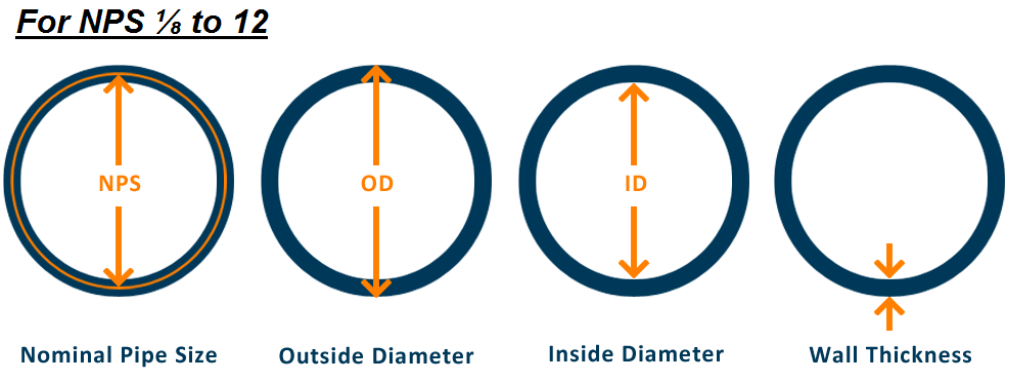

Figure 6. Pipe dimensions definition for NPS 1/8 to 12'' [31]

Nowadays, due to the wide use of pipes in various applications and the harsh/extreme operational conditions (High pressure and temperature, etc.). The industry adapted, and a new range of schedules was introduced (i.e. SCH 5, 10s, 40S, etc.).

Appendix (E) shows the standard pipe sizes and schedule dimensions that are used commonly in the industry. These dimensions are used to create the different models which the analysis was built on in this thesis as described in Chapter 3.

Piping Vibration

The awareness of the dynamic impact in the pipework systems leads the O&G community to evaluate the vibration measurements on-site and thus highlighting the importance of the natural frequency for a better understanding of the fatigue failure phenomena.

As the vibration is definable in three different terms [32] (displacement, velocity, and acceleration). Figure 7 illustrates the relationship between these three terms and the relative frequency.

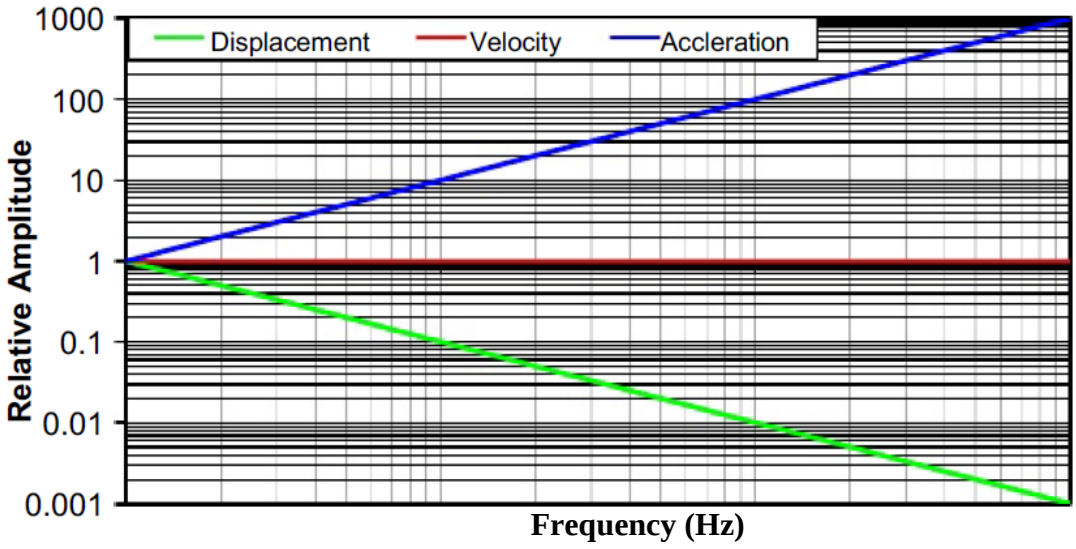

Figure 7. Displacement, acceleration and velocity comparison to frequency [8]

Figure 7 above proves that the displacement is dependent on the frequency. For the same amount of energy, results show that the displacement will be maximum at low frequency and minimal at high frequency. On the contrary, acceleration will be at its

maximum for a high frequency.

The velocity shows a uniform behavior over the needed frequency range (0 to 1000Hz) since its directly related to the dynamic stress [32]. As a result, velocity measurement is the most reliable technique to assess the problem severity.

The Natural Frequency

The natural frequency of the pipe is dependent on the pipe dimensions (e.g. pipe schedule, pipe length, location of the SBC) as well as the distribution of the mass and stiffness (see Figure 4).

Codes and standards such as EI-AVIFF guidelines [32] confirm that the pipe's supports designed only according to the static conditions may behave abnormally under dynamic excitations.

The modes shape associated with the different natural frequencies has unique deflection appearances. However, the system of the study in this thesis is a combination of two different pipes attached (welded) together which essentially makes the visualization and the calculation of the mode shapes more challenging. Also, the response of the system to any applied excitation is quantified as a relationship between the natural frequency of the entire system and the frequency of the excitation (considering the amount of excitation and its location).

Excitation Types

The Energy Institute [32] categorizes the excitation found in pipework into three different categories:

The Resonant Tonal Excitation:

The resonant tonal excitation is a result of frequency matching between the natural frequency and the excitation frequency. In this case, a significant level of vibration is recorded regardless of the amount of excitation. During the design stage, the selection

of material may help to reduce the impact of the tonal excitation resonant due to unique material damping values. In general, operational recommendations determine that the existing excitation frequency is bounded between ±20% of the system's modes [32].

The Forced Tonal Excitation:

Contrary to the resonant tonal excitation the excitation frequency in forced tonal does not match with the natural frequency. Nonetheless, high levels of vibration may result due to the high energy excitation level.

Broadband Excitation:

The broadband excitation is always taken into account since some of the energy may coincide with the natural frequency of the system and thus may lead to critical failure. Even though this type of excitation is less dangerous than the Resonant Tonal Excitation, it is nonetheless considered the most common type recorded in the field due to the flow in pipes.

Reasons for Piping Vibration

For a better understanding of the vibration assessment, grasping the most common cases encountered in the field that cause serious piping vibration problems can only be beneficial [32]:

Flow-Induced Vibration:

Turbulence resulted from the Flow-Induced Vibration (FIV) is well known in the oil & gas industry. However, this turbulence is dangerous whenever the system has a discontinuity geometry shape (i.e. SBC, elbow, expansion joints, etc.). As a result, the dynamic pressure is concentrated around the SBC (or any geometry discontinuity). It is remarked that the excitation is mainly localized at low frequencies (under 100 Hz) and this explains the existing excitation due to the likeliness of matching the system's natural frequency (see Figure 8).

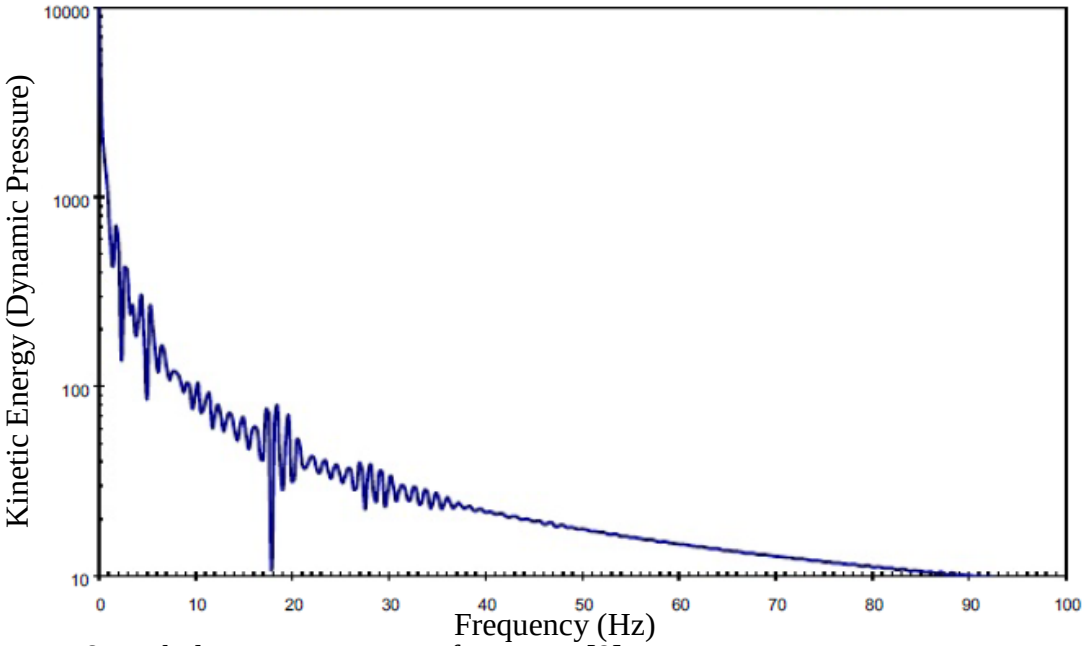

Figure 8. Turbulent Energy against frequency [8]

Mechanical Excitation:

The existence of the mechanical components with the pipework system (i.e. positive displacement compressor) causes the transmission of dynamic forces to the connected pipework and thus produces an excitation within the system. In fact, failure occurs when the multiple running speeds of the components as a whole coincide with the natural frequency of the structure. To mitigate this, avoidance of the ±20% structure's natural frequencies is mandatory during the operational phase.

Pulsation:

Similar to the failures associated with natural frequencies, the running fluid inside the pipework also causes acoustic natural frequency which in turn leads to undue shaking forces. Acoustic natural frequency is dependent on the pipe's length as geometry and other process factors such as molecular weight and fluid density [32].

Section T-13 in the Energy Institute Guidelines [32] suggest geometrical parameters for better operational durability. The following items need to be considered regarding

the main pipeline:

- Pipe supports are to be added at any heavy masses.
- Long unsupported spans need to be avoided (add supports).

Regarding SBC, the following recommendations are given:

- The SBC's length needs to be minimized.
- The mass of the unsupported valves on the top of the SBC needs to be minimized.
- The heavy masses at the free end of the SBC needs to be supported perpendicularly in both directions to the axis of the connection.
- The diameter of the SBC needs to be minimized.

In short, the two main reasons for the main piping excitation are commonly Broadband and Discrete. The Broadband excitation is primarily due to the high-velocity flow turbulence where it is spread over a wide frequency range but with a low amplitude compared to the discrete excitations. Discrete excitations are mainly caused due to pulsation from positive displacement pumps, cavitation, and impeller vane pass frequency. However, the available guidelines are designed to minimize the risk of SBC failure due to such problems. But if any of these excitations coincide with any of the structural system natural frequencies, then the vibration amplitude will be considerably amplified by a factor between 10 and 50 [33].

Natural Frequency

Introducing an SBC in the main pipeline may lead to a change in the natural frequency of the entire structure (mainline & SBC). The SBC is susceptible to a high vibration with huge displacement levels. As a result, high levels of displacement along with bending stresses increase the risk of the Vibration Induced Fatigue (VIF).

In order to avoid the VIF, designers need to consider a high fundamental natural frequency to avoid having a critical response such as a high displacement. McGhee [34] explains the relationship between the tip displacement of an SBC and the frequency associated (See Figure 9 below). It can be seen from Figure 9 that the tip displacement increases as the vibration magnitude (velocity) are increased at the same frequency. On the other hand, the tip displacement significantly reduces by increasing the frequency.

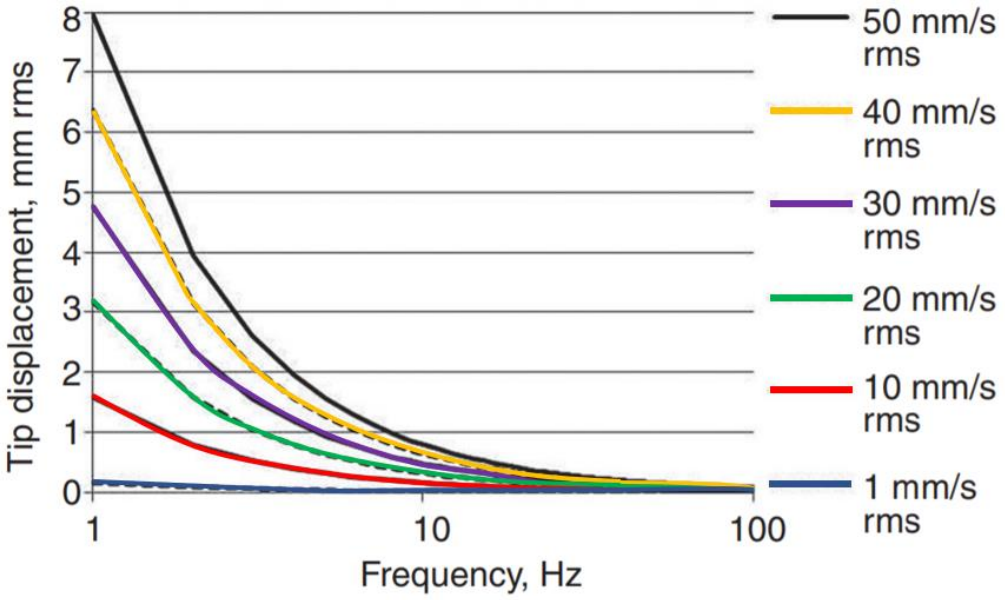

Figure 9. The vibration magnitude and response frequency of the SBC's tip [34]

McGhee [34], claims that the kinetic energy (dynamic pressure) decays with an increase in the frequency. Consequently, he argues that a fundamental natural frequency needs to be defined in a way that the risk of the VIF will be negligible. This frequency is named the cut-off natural frequency. However, this is not always possible at the design stage since many other disciplines (e.g. process and production engineering) will be taken into account to determine the size of the valve at the end of the SBP.

The SBC natural frequency is mainly a function of the spool’s stiffness as well as the

end mass attached to the SBP (see Figure 10). The SBC stiffness is primarily dependent on the second moment of area and the spool length as shown in Equation 1 [35].

$$K = \frac{3EI}{L^3} \qquad \text{Equation 1}$$

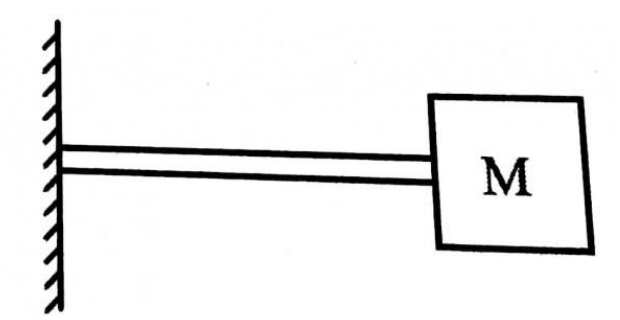

Figure 10. Cantilever beam with attached mass

This thesis will vary the length of the SBC as well as the wall thickness of the SBP (schedule) according to the industrial use and the applications implemented in the O&G pipework plant. In addition, the end mass attached to the SBP will vary amongst the different conducted analyses to understand its effects on the SBC and its contribution to fatigue failure if it exists.

Guidelines for Vibrations Assessments

This section explains established guidelines that are popularly utilized in assessing vibration in SBC. Each of the described guidelines has its own procedures, measurement techniques, and evaluation curves. The advantages and disadvantages of the presented guidelines are discussed in this section.

European Forum for Reciprocating Compressors

The appendices section (Annex E) in the European Forum for Reciprocating Compressors (EFRC) describes the measurement procedures and the classification process for the mechanical vibration within the SBC. Recommendation of the best measurement locations and direction of measurement are also provided.

The EFRC zones are split into 4 distinct categories:

- Zone A, which is considered as a good zone for the SBC to vibrate in.
- Zone B, which is considered as an **acceptable** zone for the SBC to vibrate in.
- Zone C, which is considered as a **marginal** zone for the SBC to vibrate in.
- Zone D, which is considered an **unacceptable** zone for the SBC to vibrate in.

Figure 11 represents the overall vibration velocity plots for the SBC. Where the assessment is performed by comparing the operational frequency with RMS and then verify the peak in which zone.

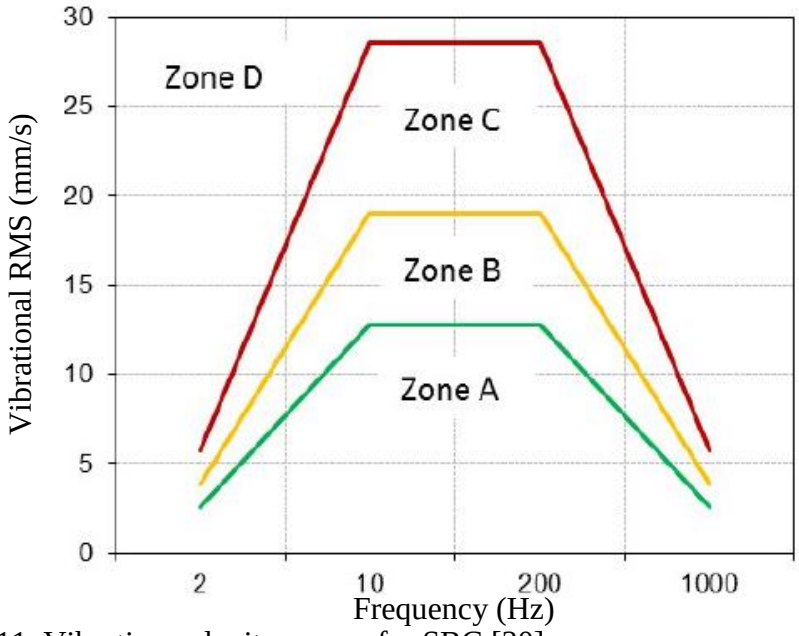

Figure 11. Vibration velocity curves for SBC [30]

The three (3) different curves used to differentiate between the zones are derived using the following piecewise functions:

Equation 2: EFRC Equations

The **unacceptable** curve (Red curve) =

$$\begin{cases} f < 10 \ , \ 2.875 \times f - 0.25 \\ 10 < f < 200 \ , \ 28.5 \\ f > 200 \ , \ -0.0288 \times f + 34.25 \end{cases}$$

The **marginal** curve (Orange curve) =

$$\begin{cases} f < 10 \ , \ 1.9 \times f + 7 \times 10^{-14} \\ 10 < f < 200 \ , \ 19 \\ f > 200 \ , \ -0.019 * f + 22.8 \end{cases}$$

The **acceptable** curve (Green curve) =

$$\begin{cases} f < 10 \ , \ 1.2625 \times f + 0.075 \\ 10 < f < 200 \ , \ 12.7 \\ f > 200 \ , \ -0.0126 \times f + 15.225 \end{cases}$$

Using the EFRC guideline, the technician is required to measure the vibration. This measurement is projected into the graph presented in Figure 11 and based on the amplitude of the vibrational RMS the assessment is made as explained above.

Energy Institute - Avoidance of Vibration Induced Fatigue Failure

Similar to EFRC, EI-AVIFF (Energy Institute - Avoidance of Vibration Induced Fatigue Failure) guideline use Figure 12 to assess the vibration within the SBC. This empirical method does not apply for frequency above 300 Hz. Nevertheless, the ease and speed of the process favor this approach among others when it comes to field measurements.

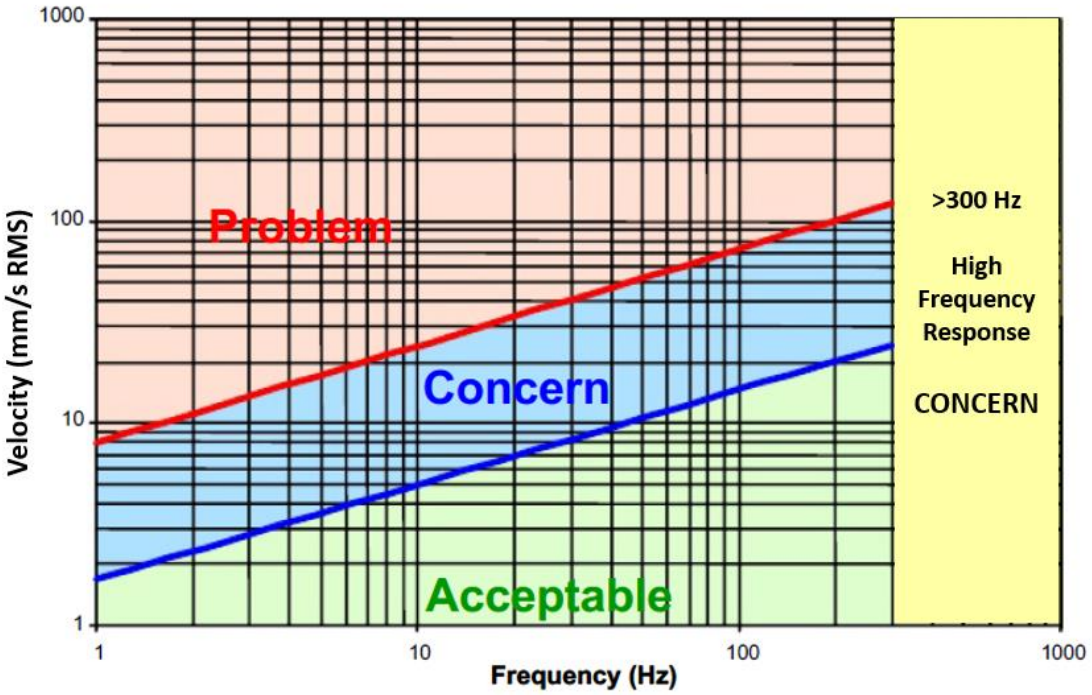

Figure 12. EI vibrational acceptance criteria [32]

Frequencies between 0-300 Hz are categorized into 3 categories ("Problem", "Concern", and "OK" regions). These regions are expressed by the below formula [32]:

$$Concern\ Vibration\ \geq 10^{\frac{(\log(f)+0.48017)}{2.127612}}$$

$$Problem\ Vibration\ \geq 10^{\frac{(\log(f)+1.871083)}{2.084547}}$$

According to the EI-AVIFF guidelines [32], four major factors lead to classify the VIF (Vibration Induced Fatigue) within the pipework as major concerns, which are the safety of the operation, the loss of production time, the cost of corrective maintenance, and the environmental impact of the hazardous leaked fluid.

The EI-AVIFF guidelines [32] claims that the failure in petrochemical plants are mainly a result of poor management decisions during the operation as well as non-operational reasons such as poorly designed pipes. Increasing the production flow rate or using the thin-walled pipework (e.g. duplex stainless-steel alloys) contribute heavily to the fatigue failure of certain hotspots such as SBC due to the occurrence of concentrated stresses.

The EI-AVIFF guideline evaluation is considered a robust methodology, this is due to the reason that the guideline based on the SBC's characteristics (such as pipe diameter, location of the SBC on the main pipeline, etc.). Even though, the EI-AVIFF assessment is taking the (rough/approximate) SBC and SBP geometries into account it ignores the effect of the mechanical natural frequencies. As such, an unexpected issue can result in the case of accepting the Likelihood of Failure (LoF) results as guaranteed. In addition, the EI-AVIFF guidelines utilize an empirical method to determine the LoF, which is based on a scoring system on-site vibration survey. In short, the LoF is not an absolute failure measurement technique neither an absolute failure probability method [32].

Gas Machinery Research Council Design Guideline

The Gas Machinery Research Council (GMRC) evaluation of the SBC is built on the models of Finite Element Analysis (FEA), this model determines the structure's mechanical natural frequency (MNF) as well as performing quasi-static stress analysis resulted by a 1.5G load applied horizontally [36]. This guideline is based on 3 different variables (mass, length, and configuration) to evaluate the SBC's maximum stress.

The main difference between using the GMRC and the EI-AVIFF guidelines is that the GMRC approach ensures that the mechanical natural frequency of the SBP is estimated in order to avoid any chance that the main pipe excitation frequency is close to the MNF of the SBP. Therefore, it assumes that the LoF is very low since the resonance frequency

is avoided. However, the GMRC guidelines ignore important factors such as the schedule of the main pipe and the SBP as well as the used fitting type.

Woodside Energy Guideline

Woodside Energy claims [37] that a direct calculation of the vibration-induced bending stresses using acceleration is more accurate when compared to using velocity or displacement readings for assessments. The authors of [37] said that the possibility to calculate stress for the SBC allows assessment for design alternatives in the future. On the other hand, adopting this technique will introduce some limitations such as:

- Piping vibration is commonly assessed by measuring displacement or velocity (not acceleration).
- This method is only applicable to the first mode of frequencies.
- The measurement needs to be taken at the center mass of the concentrated mass to have a meaningful (accurate) result.

ASME OM-S/G 1991

The authors of [29] recommend using ASME OM-S/G to calculate the allowable vibration amplitude as well as allowable displacement limit based on Equation 3 below:

$$Y_{all} = K_a \frac{L^2}{D} \qquad \text{Equation 3}$$

Where:

Y_{all}: peak to peak displacement amplitude [m].

L: The pipe (SBP) length [m].

D: The pipe outer Diameter [m].

K_a: The allowable vibration factor for the first mode of vibration (see Table 1).

Now converting Equation 3(which represents the allowable deflection (Y_{all})) into a velocity allowable limit (V_{all}) gives the following Equation 4.

$$V_{all} = Y_{all} \frac{f_{meas}}{318.31} \qquad \text{Equation 4}$$

where:

V_{all} : velocity allowable limit [m/s].

Y_{all} : peak to peak displacement amplitude [m].

f_{meas}: The first mode Mechanical Natural Frequency (MNF) [Hz].

The onshore and offshore installed pipeworks are designed to satisfy the static requirement. Modal analysis or any vibrational tests is usually ignored and that explains severe failures that have previously occurred due to fatigue and resonance. For that reason, ASME OM-S/G is a valuable guideline since it includes the natural frequency in the assessment.

Table 1 shows different possible configurations for the SBP along with the allowable vibration factor for the first mode of vibration based on the shown diagrams.

Table 1. Allowable factors of vibration [29]

Configuration	Diagram	K_a
Fixed-Free	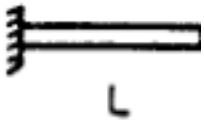	0.0569
Simply Supported	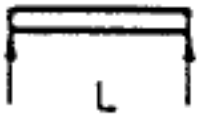	0.0203
Fixed Supported	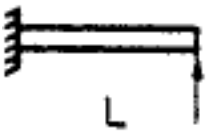	0.00979
Fixed-Fixed	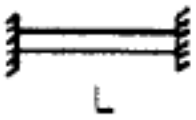	0.00710
L-Bend, Out-of-Plane, Equal Leg Length	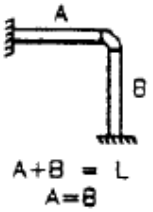	0.0110
L-Bend, In-Plane, Equal Leg Length	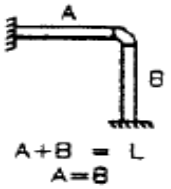	0.00267
U-Bend, Out-of-Plane, Equal Leg Length	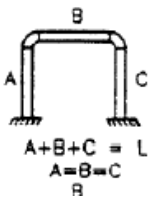	0.00746

Southwest Research Institute

In the 1960s the Southwest Research Institute (SwRI) published allowable vibration curves (see Figure 13). These curves are based on multiple running tests and on the accumulated experiences [20]. However, according to Wachel [38], these curves are only valid for bending vibration and not for pipe wall vibration. The guideline uses recorded peak-to-peak vibrational amplitudes as an indicator for assessment.

The SwRI curves categorize the condition of the system into four (4) zones, where:

Zone A: The design range zone.

Zone B: The marginal range zone.

Zone C: The correction range zone.

Zone D: The dangerous range zone.

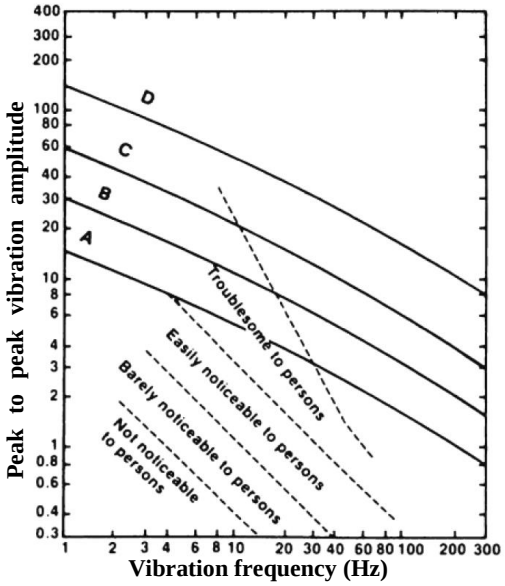

Figure 13. SwRI assessment curves [39]

Verein Deutsher Ingenieure 3842:2004-06

VDI standard 3842 (Verein Deutsher Ingenieure) is based on vibration velocity RMS at the corresponding frequency. Similarly, to EI and EFRC this method is based on measuring the vibration magnitude and then comparing it to plots presented in Table 14. This standard is derived from SwRI curves and the empirical curves were converted to metric units. The peak to peak amplitude is represented as an RMS value. Finally, the velocity is a derivation of the displacement [31].

Equation 5 & Equation 6 consecutively are used to assess the risk of vibration where the velocity is considered to be acceptable if the vibration is below V_{all} value in Equation 5. While it will be unacceptable if it reaches or exceeds $V_{failure}$ (see Equation 6).

$$V_{all} = 4\,\pi\sqrt{\frac{f}{8000}} \qquad \text{Equation 5}$$

$$V_{failure} = 2.5\ \times V_{all} = \pi\sqrt{\frac{f}{80}} \qquad \text{Equation 6}$$

where:

V_{all} : Allowable (acceptable) vibration velocity RMS [mm/s].

$V_{failure}$: Unallowable (failure) vibration velocity RMS [mm/s].

f : Frequency [Hz].

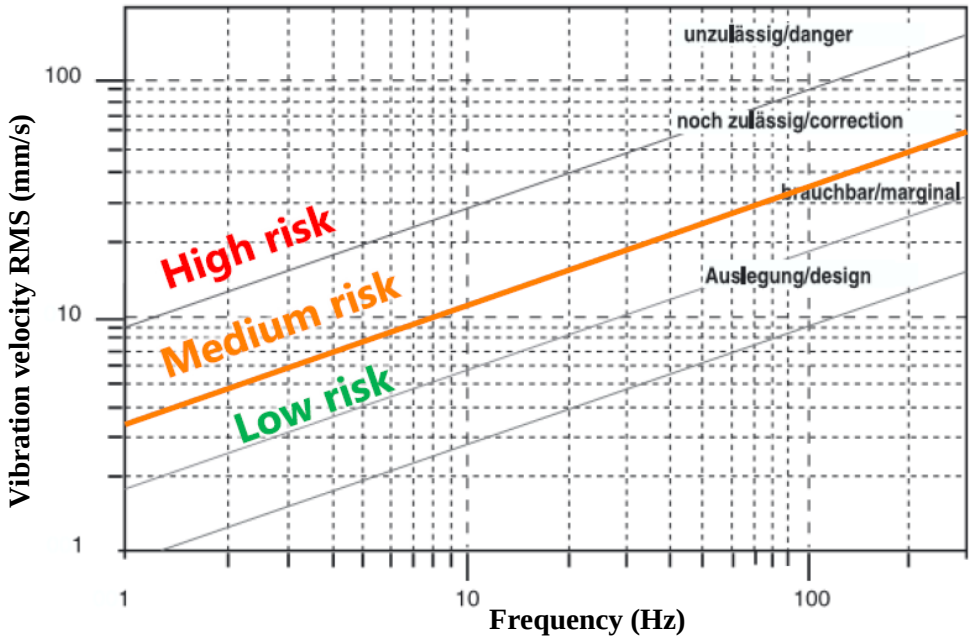

Figure 14. Allowed velocity values for permissible pipe vibrations [40]

Gamble and Tagart Limits

In 1991, Gamble and Tagart suggested new limits for pipe vibration at low frequencies. The new limits presented are again based on experience. These limits recommended a displacement lower than 0.5 mm (0-peak) for all the vibrations under 10 Hz. For the vibrations bounded between 10-40 Hz, the displacement is not supposed to exceed 0.25mm (0-peak) [41].

Figure 15 shows a comparison between the Gamble & Tagart limits, and the VDI 3842 standard. The curves of Gamble & Tagart clearly exists within the correction zone of the VDI 3842 [31].

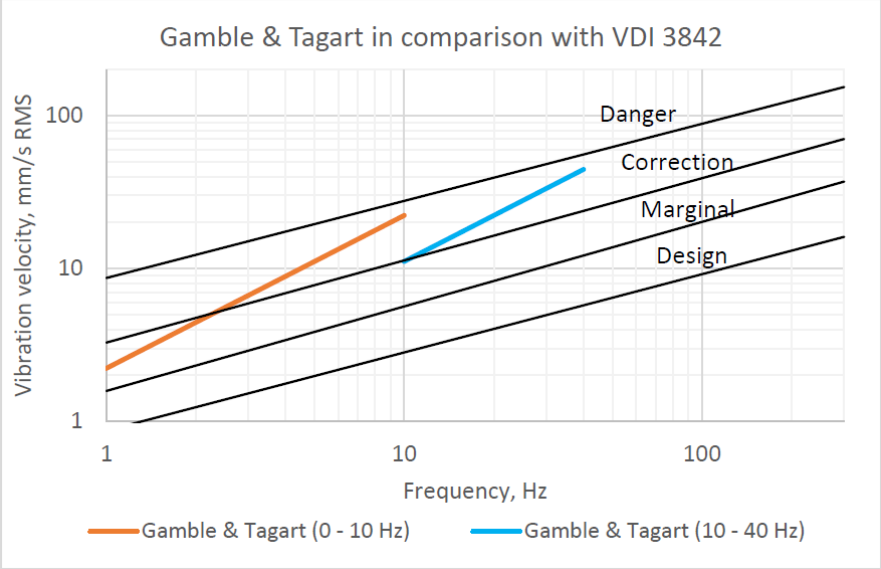

Figure 15. Comparison of Gamble and Tagart vibration velocity limits and VDI 3842 [31]

ASME OM-S/G 2007

The uniqueness of ASME OM-S/G-2007 is that the assessment does not depend on the frequency of vibration. However, the level of screening vibration velocity is 12.7 mm/s.

According to the appendix D in ASME OM-S/G code [42], the presented method for piping system screening is calculated based on the following equation:

$$V_{allow} = \frac{C_1 C_4}{C_3 C_5} \frac{\beta (S_{el})}{\alpha C_2 K_2}$$ Equation 7

where the used parameters are the correction factors which they refer to:

C_1 : The effect of the concertation weight factor.

C_2 K_2 : The stress indices factor.

C_3 : The pipe contents and insulation factor.

C_4 : The configuration factor.

C_5 : The frequency factor (comparing the measured frequency with the first natural frequency).

α : The stress reduction factor.

Making this guideline more practical ASME recommends using a conservative value for the correction factors to ensure a safe level of piping vibration for different piping configurations. Thus, 0.5 in/sec (12.7 mm/s) is the screening criterion, where:

C1 = 0.15

C2 K2 = 4

C3 = 1.5

C4 = 0.7

C5 = 1.0

$\frac{S_{el}}{\alpha}$ = 53 MPa (7,690 Psi)

Finite Element (FE)

Finite Element Analysis (FEA) has major applications in today's industry. Many analyses are easier, faster, and economical if FE is applied (compared to the actual experimental analysis).

Previous studies used FEA and vibration measurement to assess the components' fatigue life under random vibration loading [43], [44]. Xue et al. [45] used FEA (ABAQUS) to evaluate the vibration at a welded pipe socket by finding the mode shape and vibration stress. As a result, Xue et.al [45] succeed to control/decrease the vibration velocity to an acceptable level by introducing fixed rigid support to the valve. The modification was based on the time domain dynamic stress data and vibration modes obtained from the FEA.

FEA is a specific numerical method approach used to find a solution for partial differential equations. This solution approach works by dividing the system into simpler and smaller parts called finite elements [46]. Then, the system of nodes grouped to form a mesh and represent the finite elements. The Mesh is responsible to contain all the structural properties such as the material and boundary conditions [47]. The numerical domain for the solution (mesh) results in an algebraic equation system which is by itself assembled in a bigger system of equations that represent the entire model (all the elements) [48].

Dividing the entire system into subdivisions (simpler parts/elements) helps to model accurately any complex geometry and represent easily the global solution as well as capturing the local effect (i.e. stress at a specific location) [49]. Figure 16 below summarizes the FEA process starting from analyzing the physical problem until results and final decision.

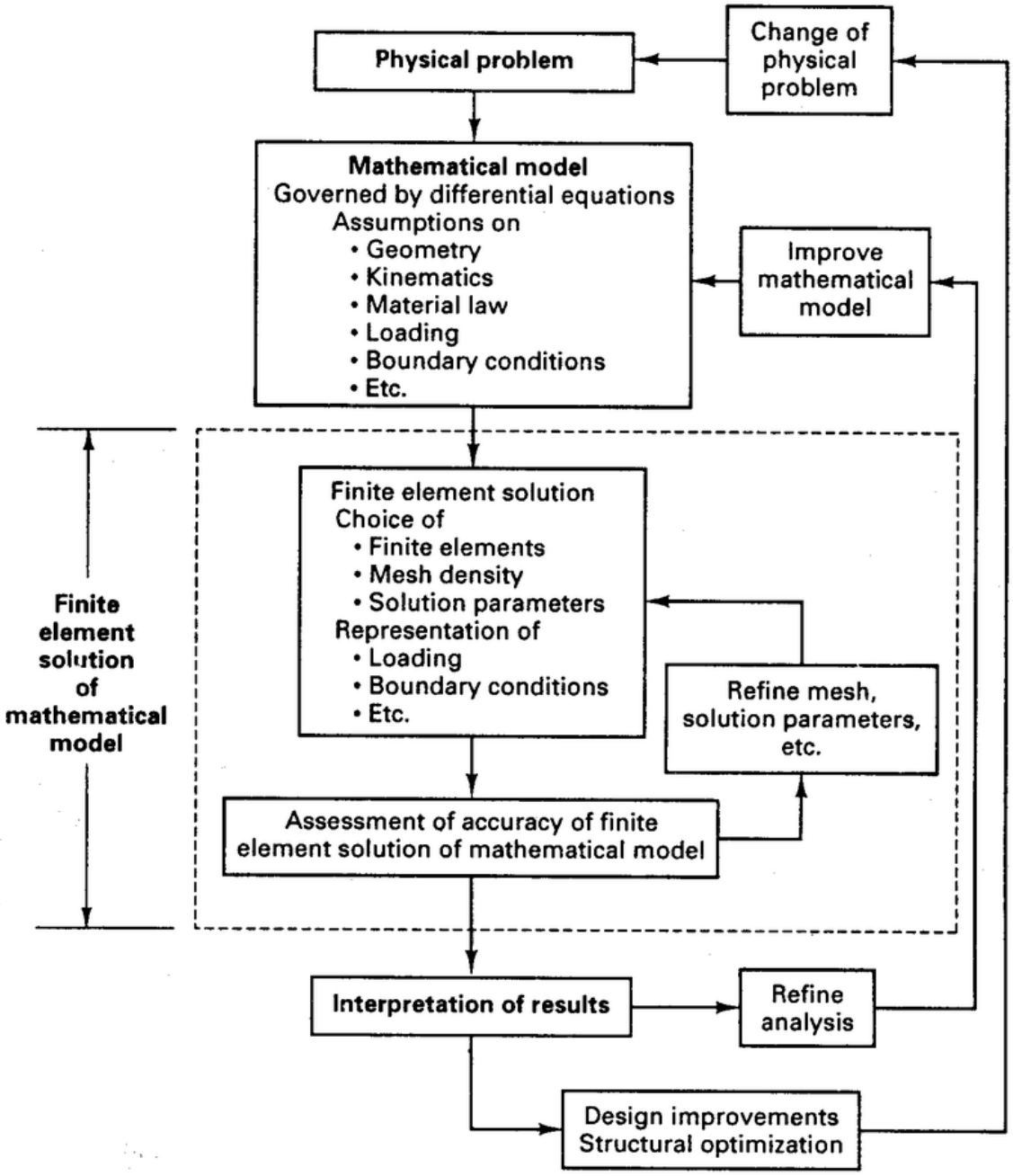

Figure 16. Finite Element Analysis Process [50]

Machine Learning (ML)

Running multiple FEA models guarantee a huge database. This database could be beneficial if it's analysed properly. Saito et.al suggested using machine learning for better handling a huge FE dataset [51].

Machine learning (ML) is known as the science that learns patterns through a set of computational theories in Artificial Intelligence (AI). ML is capable to make predictions after feeding its data sets through an algorithm; these steps will generate data-driven output. However, the precision of the results will highly depend on the inputs used to feed the model (algorithm), as well as the approach, used [52].

The learning algorithms of ML are classified as supervised and unsupervised. The supervised algorithm needs input-output pairs of data sets. These data sets will be used to build a mapping procedure starting from the given inputs to the prediction of the outputs. Unlike supervised learning which requires human interaction, the unsupervised learning method consists of providing input data and the algorithm, in this case, will have to study the data distributions [53].

The Artificial Neural Network (ANN) is one of the major branches applied and used in ML [54]. ANN has a variety of applications in different engineering and science fields like structural health monitoring [55], vibration control systems [56], and O&G Pipelines failure [57].

According to [58], ANN is an effective solution for nonlinear and complex problems. This technique is based on mimicking the learning process of the human brain and recalling the neuron patterns.

The main elements of ANN are eight [59] :

1. Activity aggregation
2. Neurons

3. Signal function
4. Environment
5. Connectivity pattern
6. Activation rule
7. Activation state vector
8. Learning Rules

The Neurons of the ANN are connected by transfer functions in three (3) layers (see Figure 17): input, hidden and output [60]. After the biasing and weighting process, the data is saved in the neural network (NN). Finally, tuning needs to take place (modification of weights) to meet the needed tolerance [61].

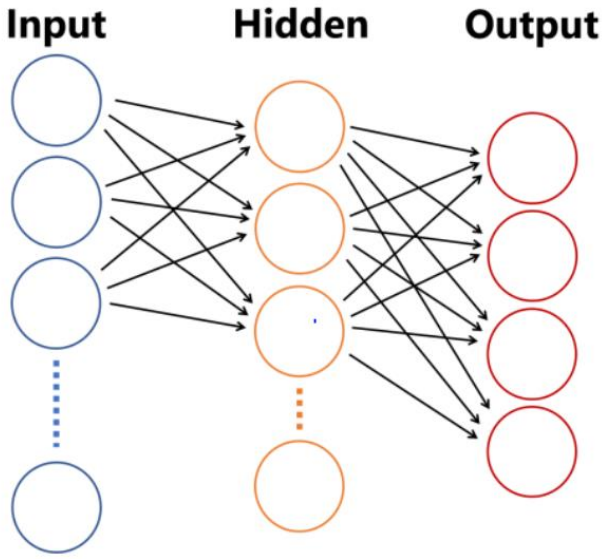

Figure 17. Schematic graph of ANN.

Chapter 3: Methodology

This chapter covers the methods applied in each phase of this thesis. Figure 18 shows the sequence of the research and the different analysis tests performed.

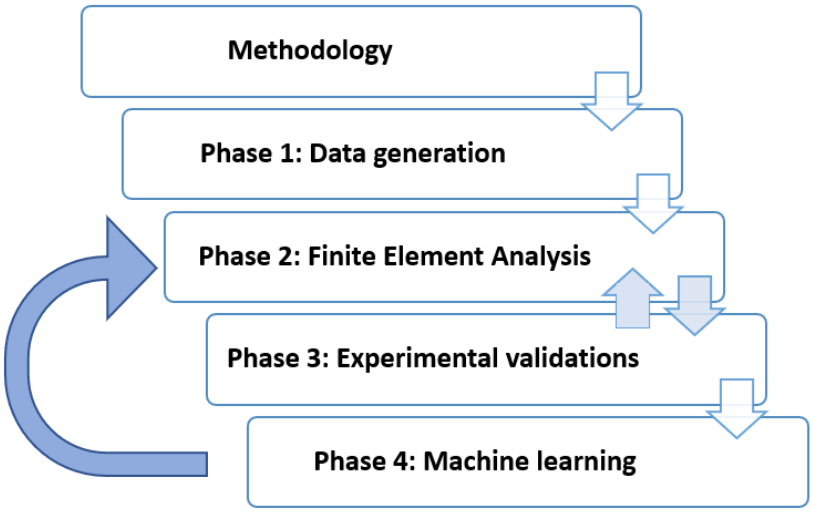

Figure 18. The phases of the research

The first phase is concerned with generating datasets of pipe standards used commonly in the O&G industry. The standard specifications were then modeled and analyzed with finite model analysis software (ANSYS-APDL). In the succeeding stage, experimental analysis was conducted to verify the results found through ANSYS. In case of discrepancies between the two independently retrieved results, iterations were carried out and the models were revised until the results were within acceptable tolerances. Finally, the generated output datasets were fed into a custom machine learning algorithm, and the program was tuned to make predictions of a selected sample pipework system.

Phase 1: Database Generation

The first phase of this research was to find the parameters for the pipe model. These parameters are the outer diameter, inner diameter, and pipe's schedule. Appendix [E] has a wide variety of used pipelines and pipe works dimensions manufactured and used in O&G plants.

The entire system consists of an SBP connected to a mainline as shown in Figure 19. The SBP's outer diameter is kept constant (NPS 2") however the mainline's outer diameter, both pipes' length, and schedule are varied.

The following describes the bounds of the changed dimensions:

- The SBP schedule is varied from 0.065" [1.651 mm] to 0.436" [11,074 mm] (ASME standards 5S to XX).
- The SBP's length is varied from 1.97" [5.004 cm] to 12" [30.48 cm] in order to accommodate a wide range of possible applications.
- The mainline's length is varied from 19.7" [50.05 cm] to 79" [200.66 cm].
- The mainline outer diameter is varied from 6.63" [16.83 cm] to 36" [91.44 cm].

Phase 2: Finite Element Analysis

Finite Element Analysis (FEA) software ANSYS-APDL was used to generate the models that were documented in phase 1. Figure 19 represents the different components that make up the system that was used for modal and stress analysis. This thesis mainly focused on one type of pipework configuration which consisted of:

- A mainline that is fixed at both ends.
- A straight SBP connected perpendicularly to the mainline.
- The two pipes were connected (welded) with one single SBC type.
- A single mass was added to the tip of the SBP to represent a valve.

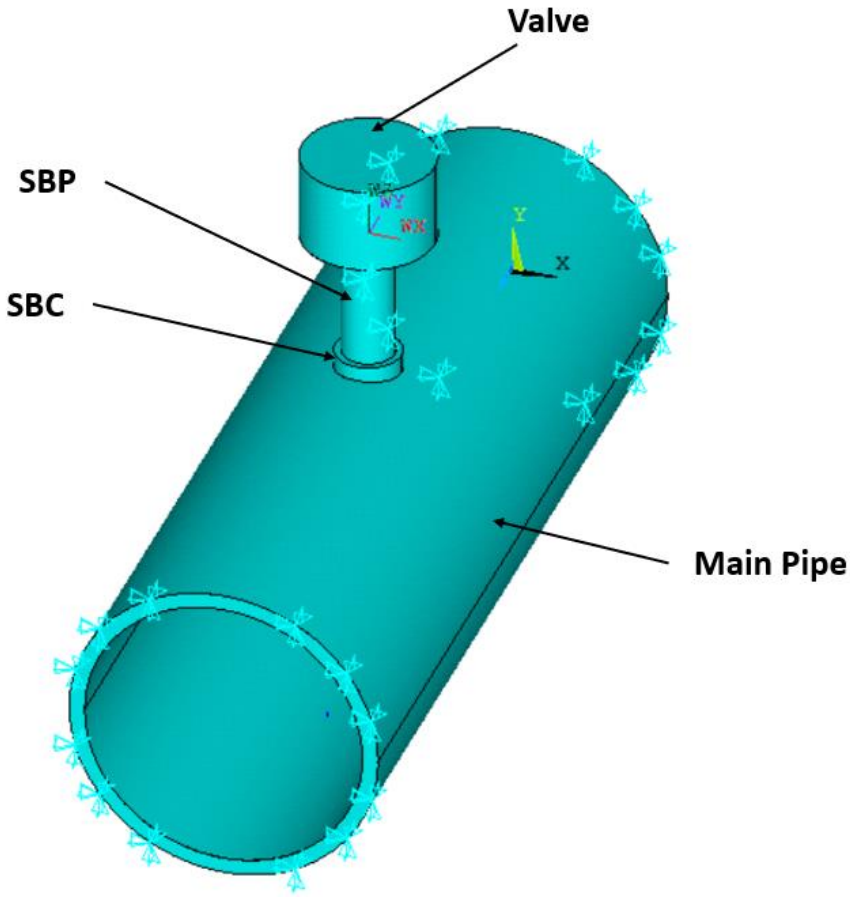

Figure 19. Model components

Figure 20 demonstrates the main pipe cross-section specification. Where:

MaID : Main Pipe Inner Diameter.

MaOD: Main Pipe Outer Diameter.

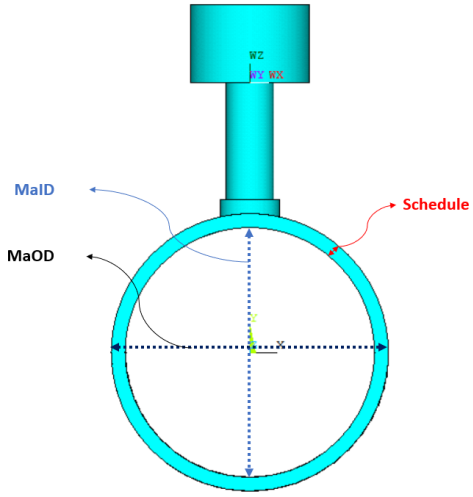

Figure 20. Main pipe details

Figure 21 below shows the SBP parameters, including:

BIN: Branch inner diameter.

BOD: Branch outer diameter.

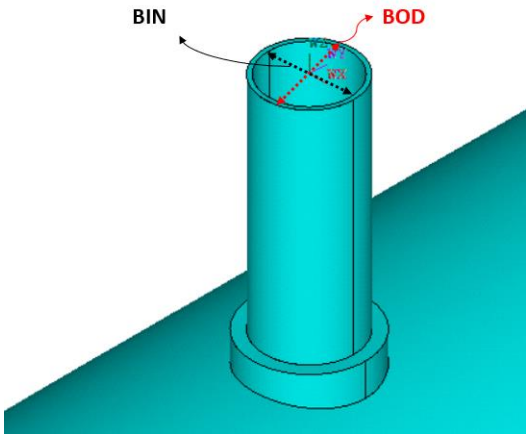

Figure 21. SBP details

Figure 22 similarly shows the main pipe length (MALength) and the SBP length (BLength). A wide range of configurations was covered by varying the SBP's length from 1.97" to 12". For the same reason, the mainline's length is varied from 19.7" to 79" (please refer to Appendix F for alternative views of the model).

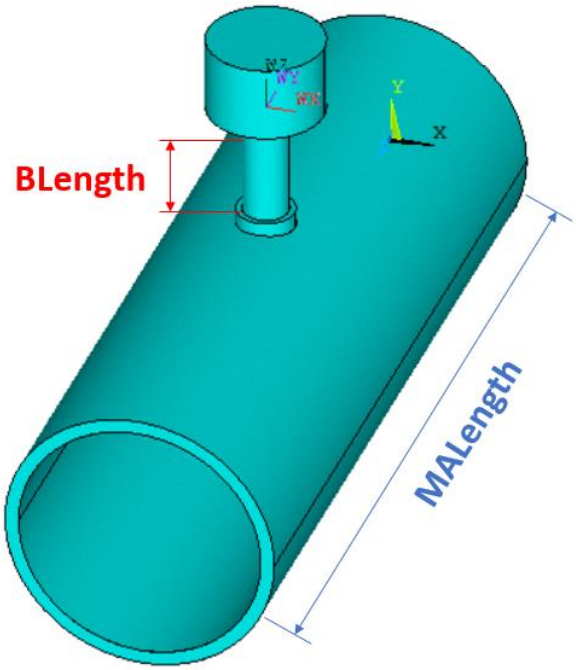

Figure 22**.** Main pipe & SBP lengths

The material used for the models was Carbon Steel (CS). CS is the most widely used material in pipework systems, due to the material's high strength and its wide availability [62]. Table 2 shows the properties of the material used.

Table 2. Carbon Steel (CS) Properties

Property	Value	Unit
Density	7850	kg / m^3
Thermal Expansion Coefficient	1.2×10^{-5}	C
Young's Modulus	2×10^{11}	Pa
Poison's Ratio	0.3	-
Bulk Modulus	1.666×10^{11}	Pa
Shear Modulus	7.692×10^{10}	Pa

A mesh sensitivity analysis was performed using the generated models. In this step, the number of nodes was taken as an independent variable, and outputs of maximum stress, tip velocity, and first natural mode of the system's frequency were recorded. The variation of these results was plotted against the number of nodes used and convergence of the results was observed. This study albeit straight forward, allowed the analysis to be performed for a wide variety of models with an optimum mesh sensitivity to optimize the processing time.

After determining the optimal mesh sensitivity, the trends of the maximum stress, tip velocity, and first natural mode of the system's frequency were examined against the system dimensions. The varied dimensions included:

1. The length of the SBP.
2. The length of the mainline.
3. The schedule of the SBP.
4. The schedule of the mainline.
5. The mass of the modeled valve.

The five (5) dimensions mentioned above were used to generate a total of 15 graphs for the variation in maximum stress, tip velocity, and first natural mode of the system's

frequency. These trends are explained in Chapter 4 - Results and Discussion.

The ANSYS-APDL code was used to run hundreds of mainline-SBP combinations as generated in Phase 1. The first natural frequency for each of the systems was recorded. The frequency results from this step were used to train the machine learning algorithm in Phase 4. Finally, a comparison was made between the four most commonly used guidelines (EI-AVIFF, VDI 3842, EFRC, and ASME OM-S/G) to assess their vibrations limits. The comparison was performed in order to examine their effectiveness and conservativeness.

Phase 3 Experimental Validations

The system that was used in the experimental analysis was of a different configuration to those that were modeled in Phase 2, as it included two SBPs connected to the mainline and had fixed support in the center of the mainline. However, a similar model was simulated in ANSYS and the APDL code that was written previously was used to output the first natural mode of the frequency of the system. The results outputted from the ANSYS code were then compared to those obtained experimentally, to verify and determine the accuracy of the code. When the results obtained from the program were out of the allowable tolerances, iterations were performed by going back to the ANSYS code which was tuned until the results were comparable.

Phase 4 Machine Learning

The purpose of using a machine learning model is to reduce the dependency on experimental data collection, which can be sometimes very impractical as in the case of this thesis. For example, the running fluid inside the pipe in addition to the outer coating around it makes the modes frequency measurement unrealistic. To install the sensors for data collection, the process needs to be shut down and that can cost money and increase unnecessary downtime. Furthermore, technicians have to be present at the

site for collecting this data. The collected data will then be sent to the engineer for further analysis. On the other hand, the machine learning model described in this research will be trained to determine the natural frequency based on pipe length, NPS, SBP length, and other parameters that can potentially be performed by any member of the maintenance team. This ML model (ANN) along with the suitable assessment guideline can then be used to quickly assess the pipe thereby minimizing system downtime, reduce the time the technician spends on data collection, and allows the engineer to make quick assessments. Additionally, the experience of the ML user does not take part in the obtained result whereas traditionally, the skills of technicians to record measurements do.

Machine learning was used to predict the system's first mode by inputting the geometrical properties of a sample pipework system. The first step was to train the machine learning program by feeding it with a database consisting of hundreds of calculations. Of the inputted data, 80% was used for learning purposes whereas the remaining was used to predict the natural frequency by the program. The 20% of data that was interpreted by the ML code and the frequency results were then compared to the known values from the ANSYS code as part of the ML code verification process. The software that was used for the ML study is mentioned below:

1. Scikit-learn: a python module for machine learning.
2. Keras: a python-based deep learning application programming interface (API).
3. Tensorflow: a deep learning library and framework from Google.

In order to evaluate the regression model, a variety of metrics taken into account and calculated;

1. R^2: the coefficient of determination: The variance proportions in the dependent variable which is anticipated from the independent variable [63]. (Which is used during the evaluation stage of the ML model)
2. Mean absolute error [MAE]: The difference measurement between two continuous variables [64]. Which is, in this case, represents the MAE difference between the simulation-based prediction and the ML-based prediction.
3. Mean absolute error percentage [MAPE]: Error percentage prediction method for the forecasting results [65]. Which represents the MAE in terms of percentage. Where it's used to indicate the relative magnitude difference between the simulation-based prediction and the ML-based prediction.
4. Mean squared error [MSE]: A method of measurement of an estimator measures the average square error difference between the actual value (simulation-based prediction) and the estimated value (ML-based prediction) [66].
5. Root mean squared error [RMSE]: The standard deviation of the predicted error. RMSE measures the concentration of the data around the best fit line [66].

The machine learning features are the system's geometrical parameters (described in Phase 1 of the methodology) and are as follows:

1. MaOD
2. MaID
3. MaLength
4. BLength
5. BOD
6. BID

Three different methods were used in order to find a relationship between the system features (geometrical parameters) and the first mode frequency of the system:

1. Neural Network
2. Random Forest
3. Multiple Linear Regression

The data was shuffled and randomly split into an 80% training set and a 20% testing set. Three (3) types of models were trained: multiple linear regression, random forest, neural network. The tuning of the algorithm (e.g. ANN) was carried out by utilizing readily available Big ML servers that conduct calculations using supercomputers and assisted in determining the weighted factors and to build mapped connections between the neurons.

Chapter 4: Results & Discussion

Mesh Sensitivity

Before starting to generate data from the finite element model, a mesh sensitivity study takes place in order to ensure the quality of the results as well as managing the time to optimize the functionality of the code. In this section, different parameters have been measured and the used mesh sensitivity is recorded.

The mesh sensitivity study was conducted for three different obtained measurements (modes, stress, and velocity) where the processing time of each calculation is noted and plotted versus the used number of nodes.

Both mesh size and mesh concentration are taken into consideration during this analysis where the mesh size sensitivity was conducted first and a variation of mesh size for different system components been tested. Secondly, after deciding the optimal mesh size, a refinement near the Hotspot (the weldment edges) was evaluated and a second mesh sensitivity analysis took place. Finally, the best-obtained results are considered for the remaining work (see Figure 23).

The sensitive mesh analysis conducted for the structure geometry shown in Table 3:

Table 3. Meshed pipe's geometry (m)

MaOD	MaID	MaLength	BOD	BIN	BLength
0.168	0.158	1.00	0.060	0.057	0.30

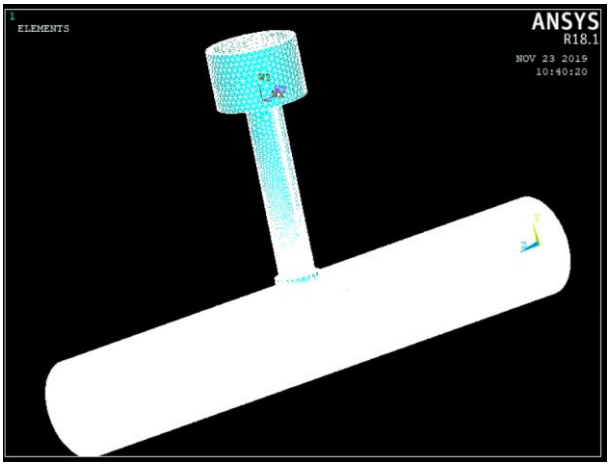

Figure 23. Meshed Pipe

Figure 24 elaborates on the change of the first mode natural frequency as the number of nodes is increased. Where the results started to converge at 200,000 nodes. Similarly, Figure 25 also shows a convergence of results when the number of nodes is above 200,000.

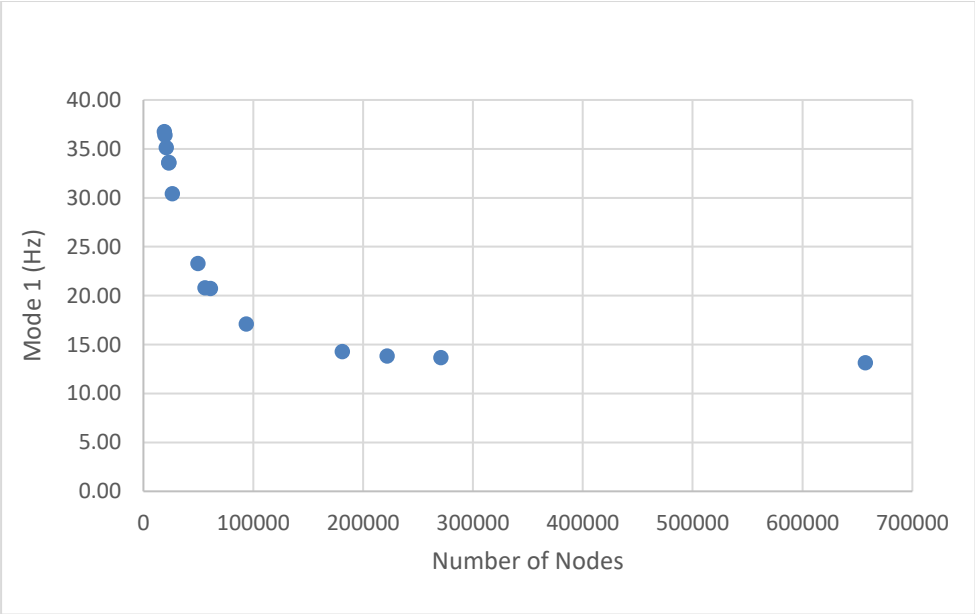

Figure 24. Modes (Hz) mesh sensitivity

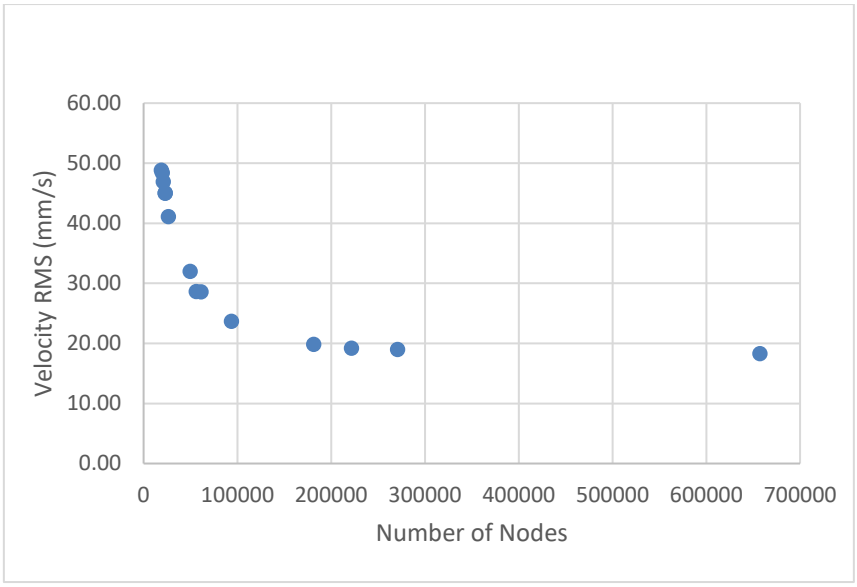

Figure 25. Velocity mesh sensitivity

The stress measurement also was evaluated for the number of nodes above 200,000 and as Figure 26 shows it is safe to consider the current mesh size assumptions to obtain accurate results for the mode frequency, velocity, and stress.

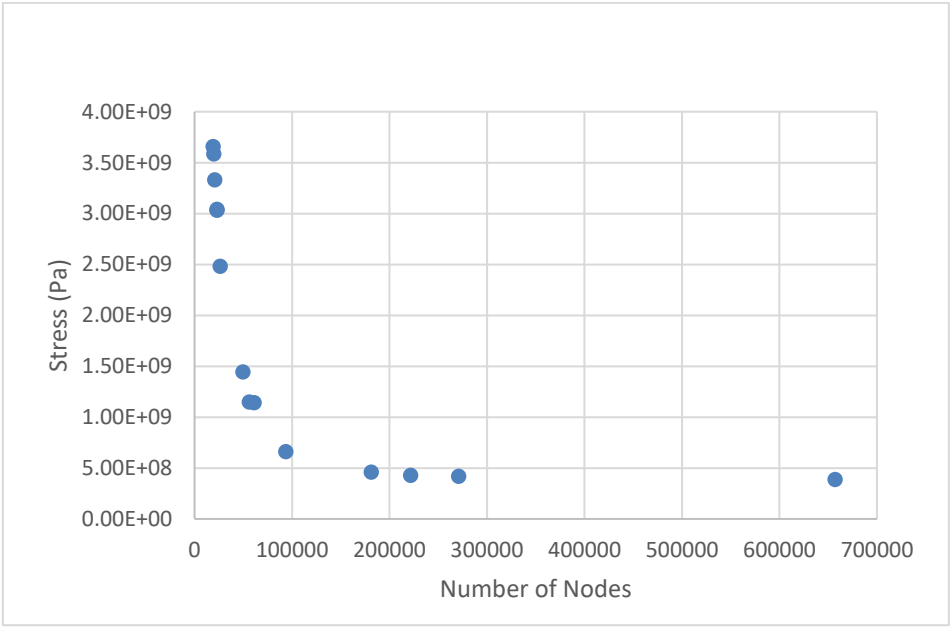

Figure 26. Stress (Pa) Mesh Sensitivity

Figure 27 presents a meshed model of the main pipe, SBC, and SBP. It is clearly showing a difference of element condensation since the element size is different is each different section.

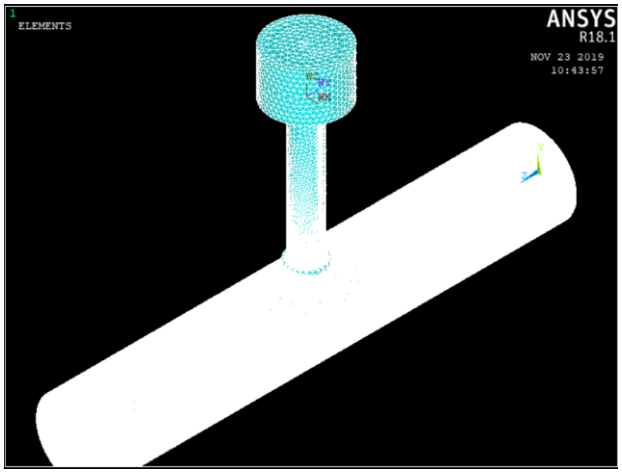

Figure 27. Meshed model

In order to maintain and improve the speed efficiency of the model, the required simulation time was calculated where Figure 28 proves that using 270777 nodes will cut down the time by 6 times (compared to using 700,000 nodes). On the other hand, the quality of the results is barely affected.

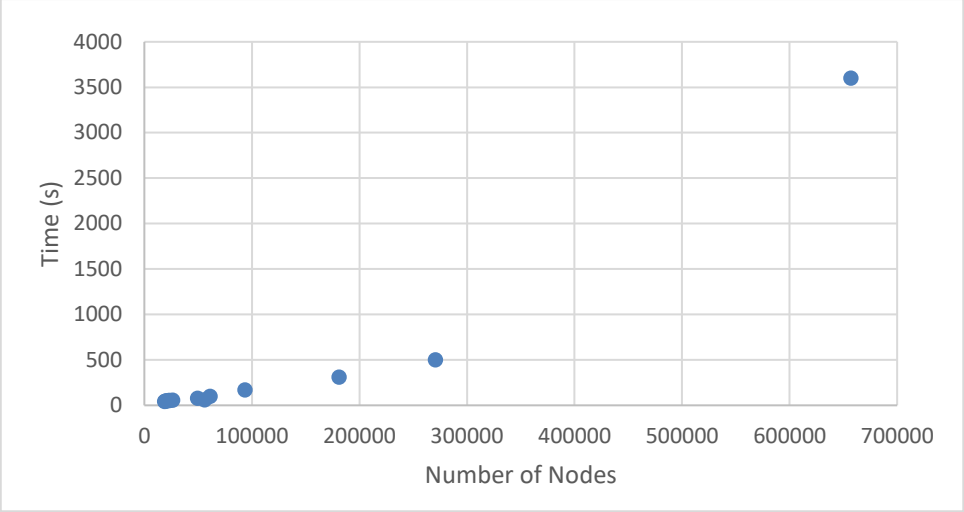

Figure 28. Time Vs. number of nodes

Refinement:

Since the stress is mainly located at the SBC edges, Thus, these two locations are considered as hotspots. Therefore, a mesh refinement has been generated with different refinement factors, and a new mesh sensitivity analysis been conducted. (See the zoomed mesh model in Figure 29).

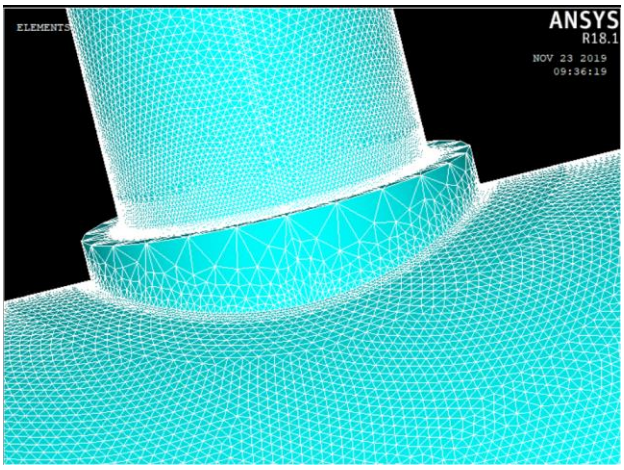

Figure 29. Zoomed meshed model

Following the first mesh sensitivity analysis, a refinement at the SBC edges helped to improve the obtained results and thus the main three factors of study (Modes, Stress, and velocity) are evaluated again and Figure 30 to Figure 32 below illustrate how the data is converging whenever the number of elements is approaching 1,000,000 nodes. Alternative meshing views are presented in Figure 33.

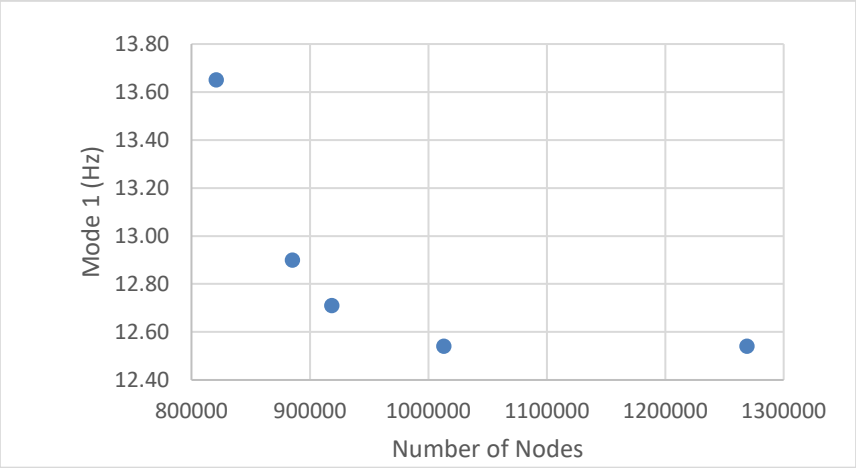

Figure 30. Modes (Hz) Mesh sensitivity after refinement

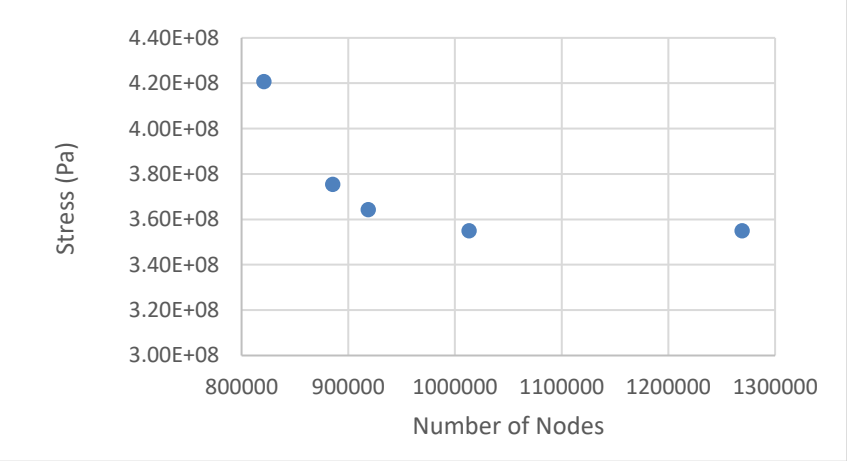

Figure 31. Stress (Pa) Mesh sensitivity after refinement

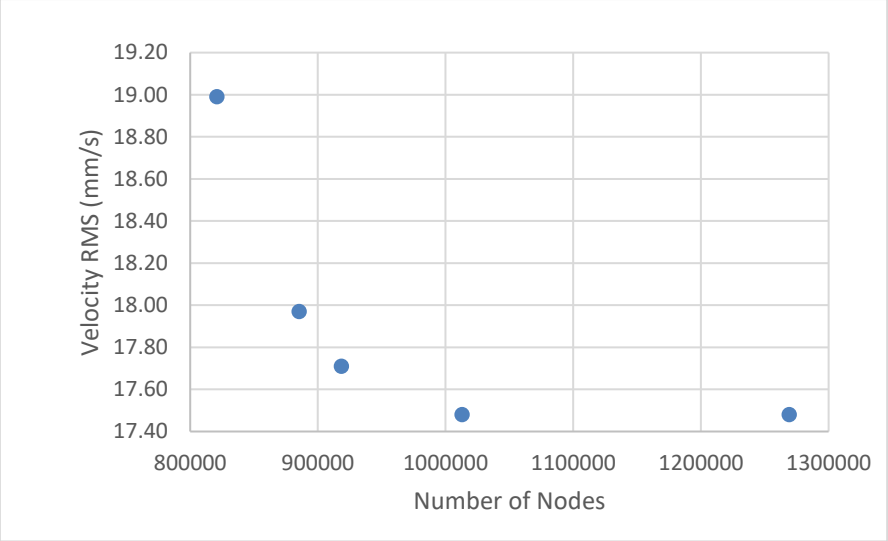

Figure 32. Velocity (mm/s) Mesh sensitivity after refinement

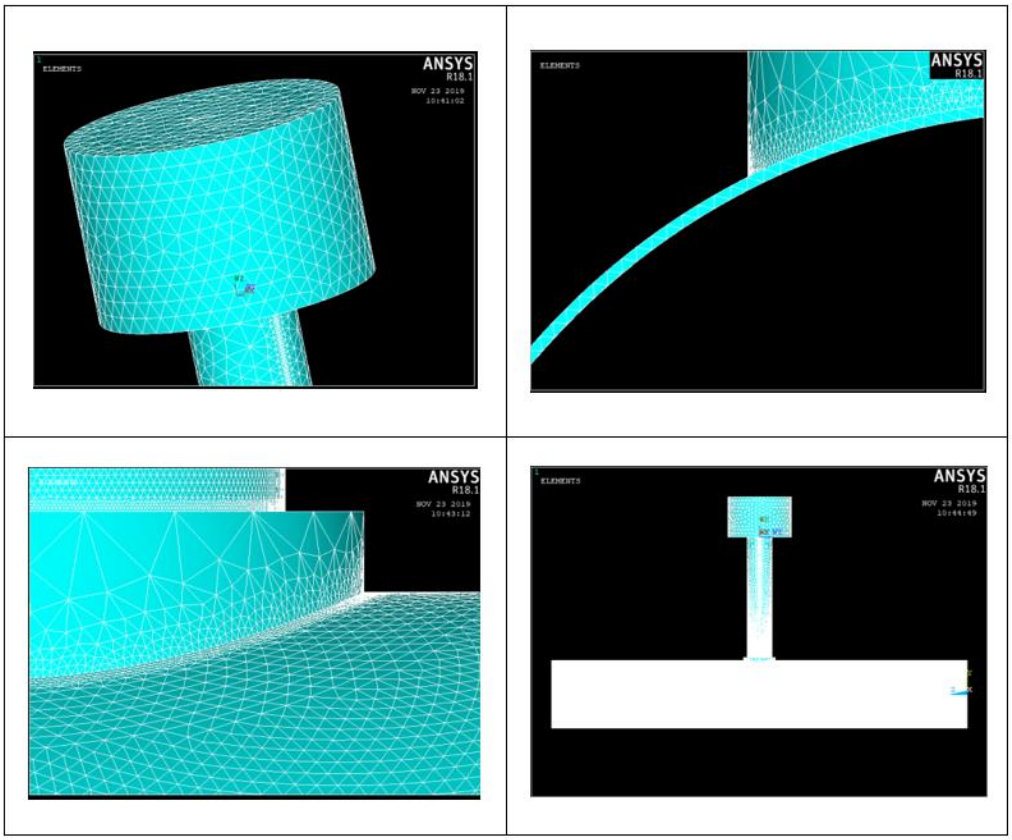

Figure 33. Alternative meshing views

Since the model has different parameters, a study concerning the impact of each individual parameter has been conducted. This study will help in the future to build a relationship between the parameters and the simulation outcomes. Thus, establishing a correlation between results and each parameter.

Mode Shapes

Mode shapes are found by ANSYS/APDL and represent the natural frequencies of the entire system and components demonstrated by the following figures.

Figure 34 represents the first mode of natural frequency where the SBP is oscillating in the X-Y plane. The maximum stress is concentrated in the SBC.

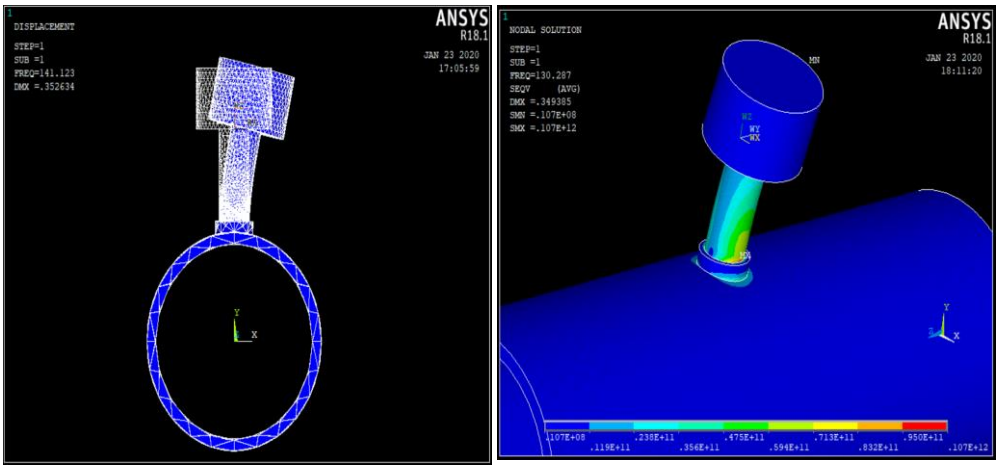

Figure 34. System mode 1

Figure 35 represents the second mode of natural frequency where the SBP is oscillating in the Y-Z plane. The maximum stress is concentrated in the SBC.

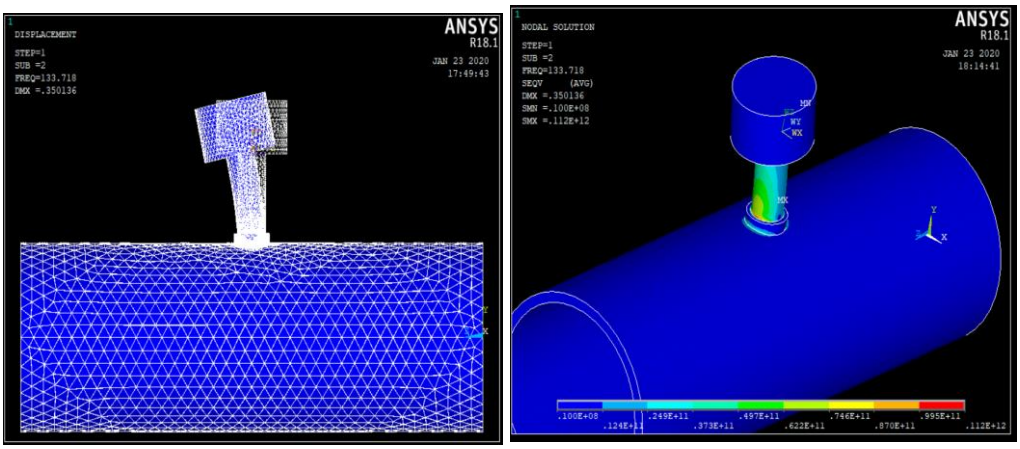

Figure 35. System mode 2

Figure 36 represents the third mode of natural frequency where the SBP is expanding and retracting radially. This mode is not critical for the SBC since the stress is not concentrated at the connection.

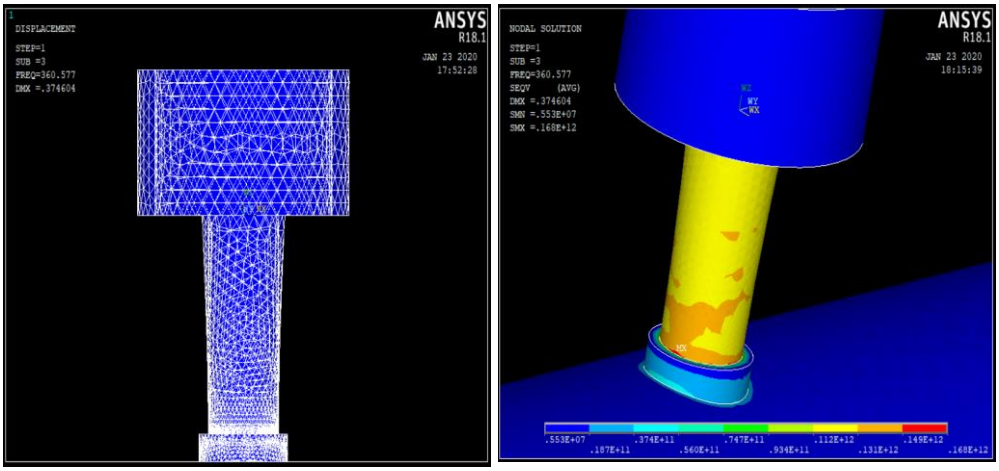

Figure 36. System mode 3

Figure 37 represents the fourth mode of natural frequency where the SBP is being displaced along the y-axis. The maximum stress is concentrated in the SBC.

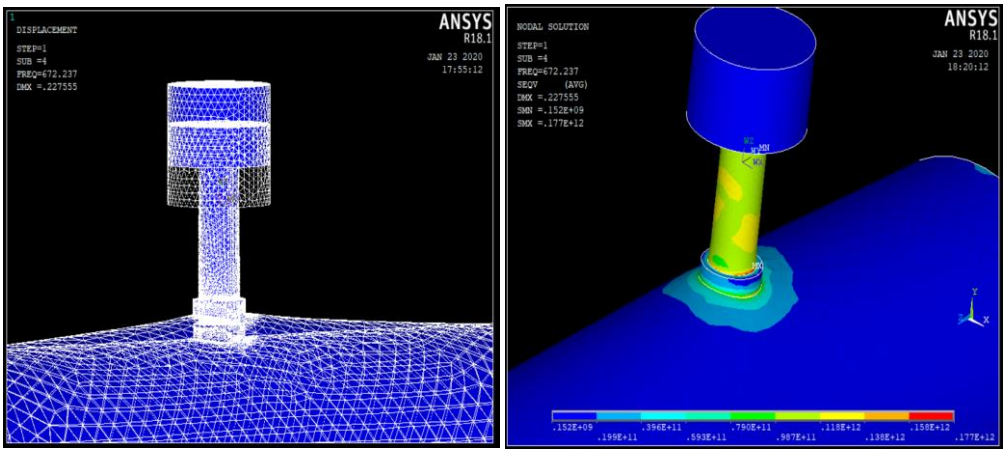

Figure 37. System mode 4

The fifth mode of natural frequency demonstrates that the SBP is bending as shown in Figure 38. Unlike previous modes, the maximum stress does not occur in the SBC but rather in the area between the SBP end and the attached valve.

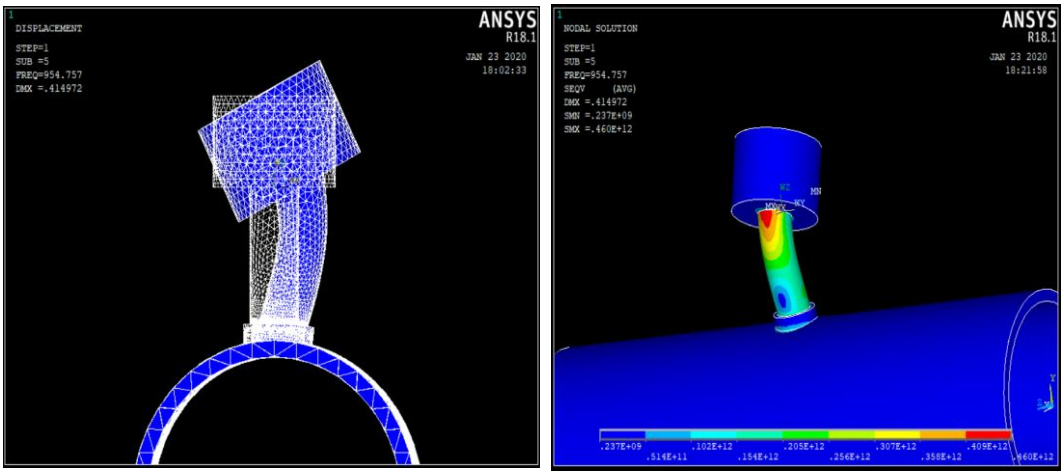

Figure 38. System mode 5

The Effect of the Main Pipeline Dimensions

This section studies the effect of the Main pipe's length and schedule on the first natural frequency, SBP's tip velocity, and the stress at the SBC.

The Effect of the Main Pipe Length

Table 4 shows a study of six (6) identical structures with only length variation of the main pipe been conducted in order to understand the relationship between the length of the main pipe and the simulation outcomes.

Table 4. Pipes dimensions (m) 1

MaOD	MaID	MALength	BOD	BIN	BLength
0.1143	0.1008	**0.40**	0.0603	0.0493	0.30
0.1143	0.1008	**0.50**	0.0603	0.0493	0.30
0.1143	0.1008	**0.80**	0.0603	0.0493	0.30
0.1143	0.1008	**0.90**	0.0603	0.0493	0.30
0.1143	0.1008	**1.00**	0.0603	0.0493	0.30
0.1143	0.1008	**1.10**	0.0603	0.0493	0.30

Figure 39 shows that the First mode of natural frequency is decreased as the main pipe length is increased. However, the increment of the main pipe length does not have a serious impact on the natural frequency in contrary to an increment within the SBP (see Figure 45). This could be explained by the fact that the SBP's 1st Mode is always lower than the main pipe's 1st Mode and thus the entire system's first natural frequency is mainly affected by the SBP parameters.

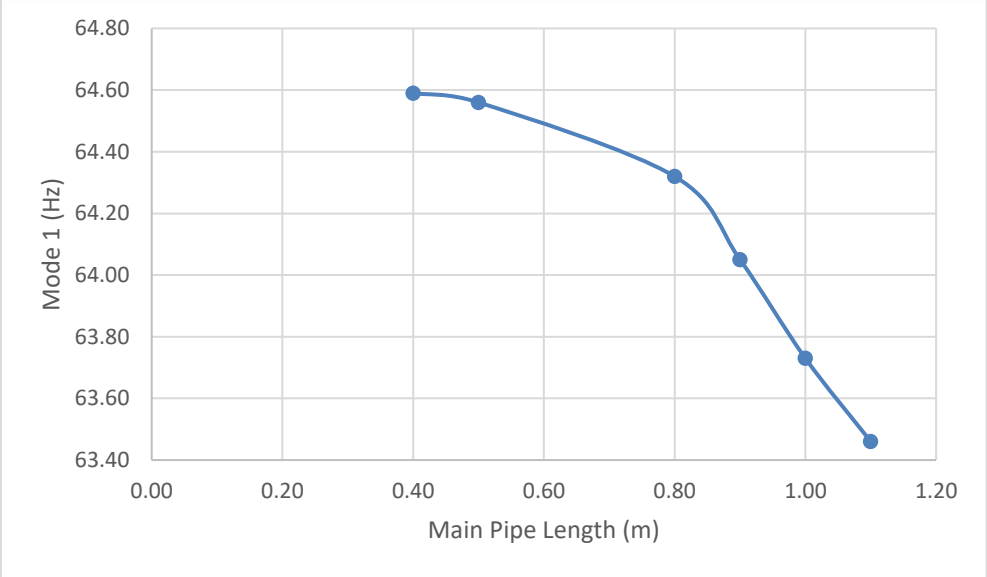

Figure 39. Modes 1 for different Main Pipe Lengths

The trend in Figure 40 shows that the SBP's tip velocity is increased as the length of the main pipe is incremented. Thus, a high-velocity RMS is expected in the field when measurements are taken for the main pipeline with long interval supports.

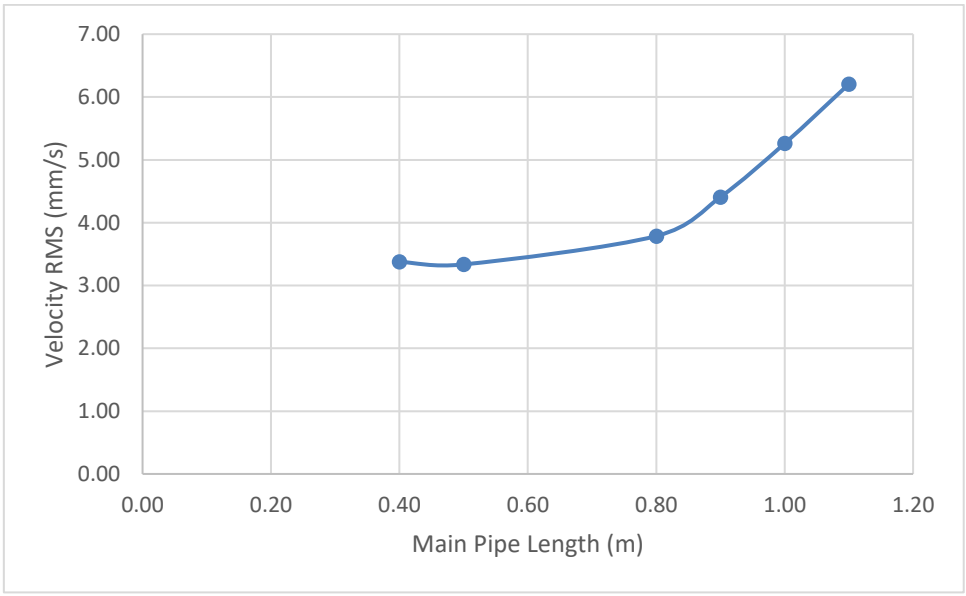

Figure 40. Velocity values for different Main Pipe Lengths

Figure 41 shows that the stress value on the SBC (these values are mass normalized mode) is decreasing as the main pipe length is increasing. In reality, the stiffness of the main pipe (which the SBC is welded on) is decreased as the main pipe length is increasing. Thus, the SBC will have relatively more flexibility which will lead to a decrease in the stress.

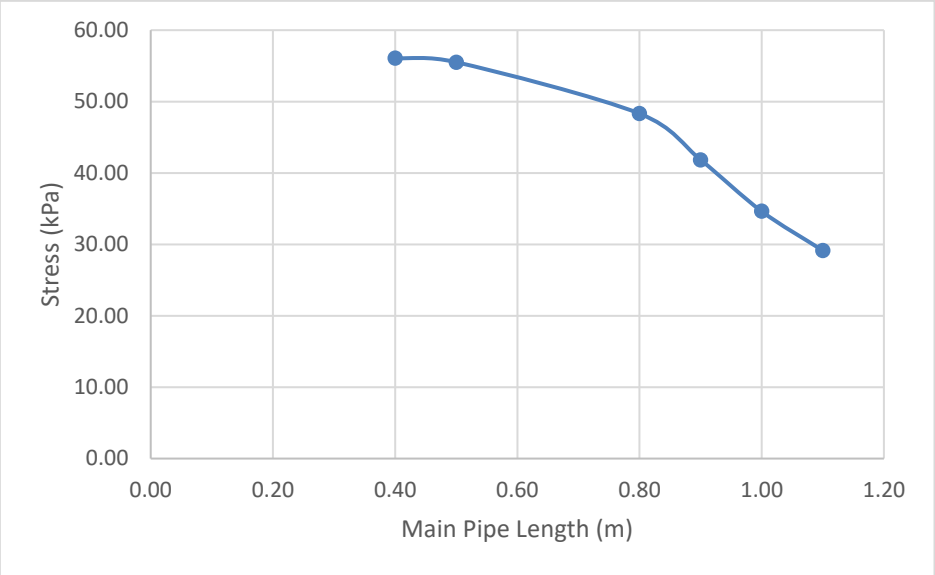

Figure 41. Stress values for different Main Pipe Lengths

The Effect of the Main Pipe Schedule

Another major parameter in this model is the main pipe schedule. The following graphs are obtained by varying the schedule for the main pipe and monitoring the change in the 1st natural frequency, maximum stress, and the SBP's tip velocity. For this purpose, Table 5 represents 8 identical models where the only variable is the main pipe schedule.

Table 5. Pipes dimensions (m) 2

MaOD	MaID	MALength	BOD	BIN	BLength
0.1143	**0.1008**	1.00	0.0603	0.0495	0.30
0.1143	**0.1020**	1.00	0.0603	0.0495	0.30
0.1143	**0.1030**	1.00	0.0603	0.0495	0.30
0.1143	**0.1040**	1.00	0.0603	0.0495	0.30
0.1143	**0.0860**	1.00	0.0603	0.0495	0.30
0.1143	**0.0880**	1.00	0.0603	0.0495	0.30
0.1143	**0.0850**	1.00	0.0603	0.0495	0.30
0.1143	**0.0750**	1.00	0.0603	0.0495	0.30

The obtained results in Figure 42 shows that the First Mode Natural Frequency is affected by the Main Pipe Schedule where the graph below affirms that the 1st Mode frequency will increase as the Main pipe schedule increases.

.

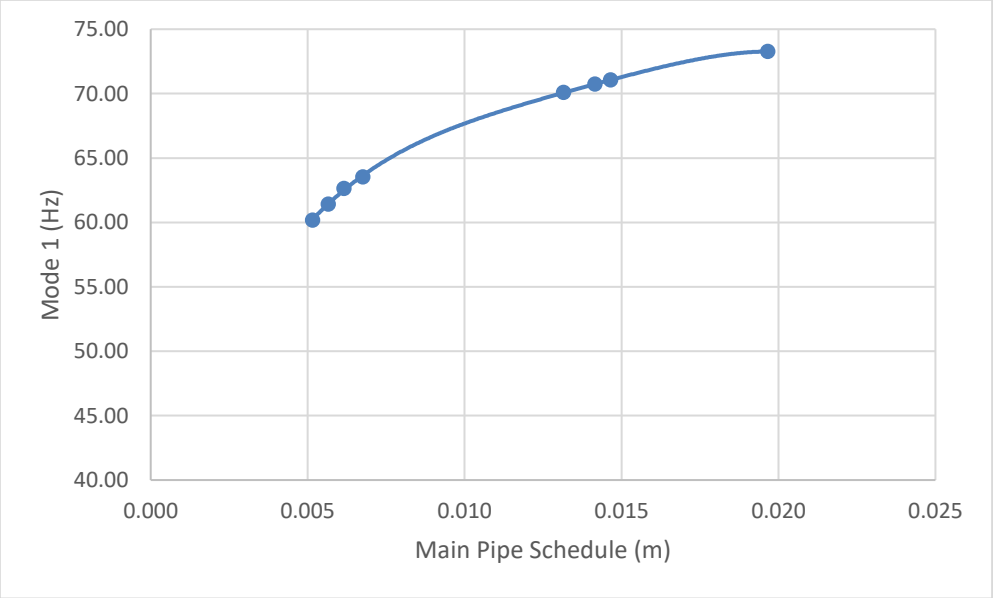

Figure 42. Mode 1 for different Mainline Schedules

The maximum stress variation to the main pipeline's schedule curve below validates the importance of the pipe schedule on the stress results. However, increasing the main pipeline's schedule will certainly lead to an increase in the pipe's stiffness which automatically causes a restriction of motion for the SBP and then generates high stress

on SBC (see Figure 43).

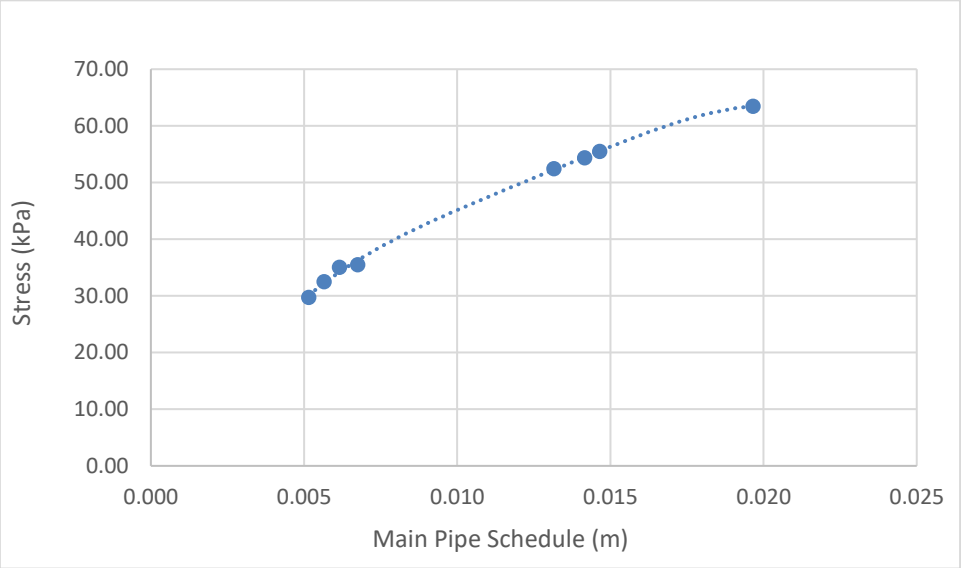

Figure 43. Stress values for different Mainline Schedules

Figure 44 shows that the velocity of the SBP's tip is a function of the mainline schedule. In fact, the graph below proves that the relationship is inversely proportional.

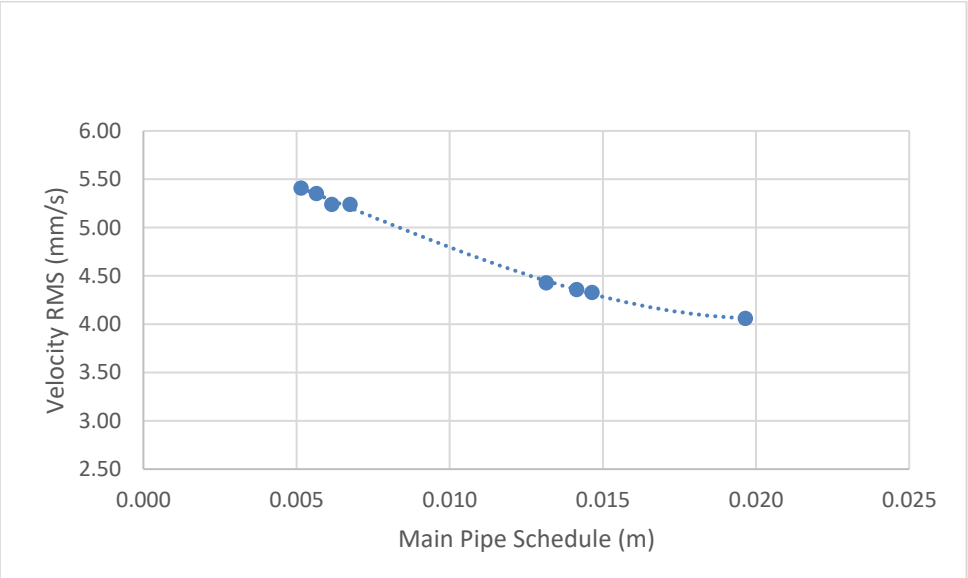

Figure 44. Velocity values for different Mainline Schedules

The Effect of SBP Dimensions

The Effect of the SBP Length

A study of 8 identical structures with the only variation of SBP's length value has been conducted in order to understand the relationship between the length of the SBP and the simulation outcomes (see Table 6).

Table 6. Pipes dimensions (m) 3

MaOD	MaID	MALength	BOD	BIN	BLength
0.1143	0.1008	1.0000	0.0603	0.0493	**0.05**
0.1143	0.1008	1.0000	0.0603	0.0493	**0.10**
0.1143	0.1008	1.0000	0.0603	0.0493	**0.15**
0.1143	0.1008	1.0000	0.0603	0.0493	**0.20**
0.1143	0.1008	1.0000	0.0603	0.0493	**0.25**
0.1143	0.1008	1.0000	0.0603	0.0493	**0.26**
0.1143	0.1008	1.0000	0.0603	0.0493	**0.28**
0.1143	0.1008	1.0000	0.0603	0.0493	**0.30**

According to the EI-guideline recommendations, the length of the SBP needs to be minimized. Accordingly, the obtained results from increasing the length of the SBP shows that the First Natural frequency (Mode 1) is decreasing. Thus, the system will have a higher chance of failure during the operation stage, where lower natural frequency leads to higher excitation probability due to the flow running in the system which has a low frequency. (see Figure 45) Additionally, as the length increased, the rate of change in the mode frequency reduced.

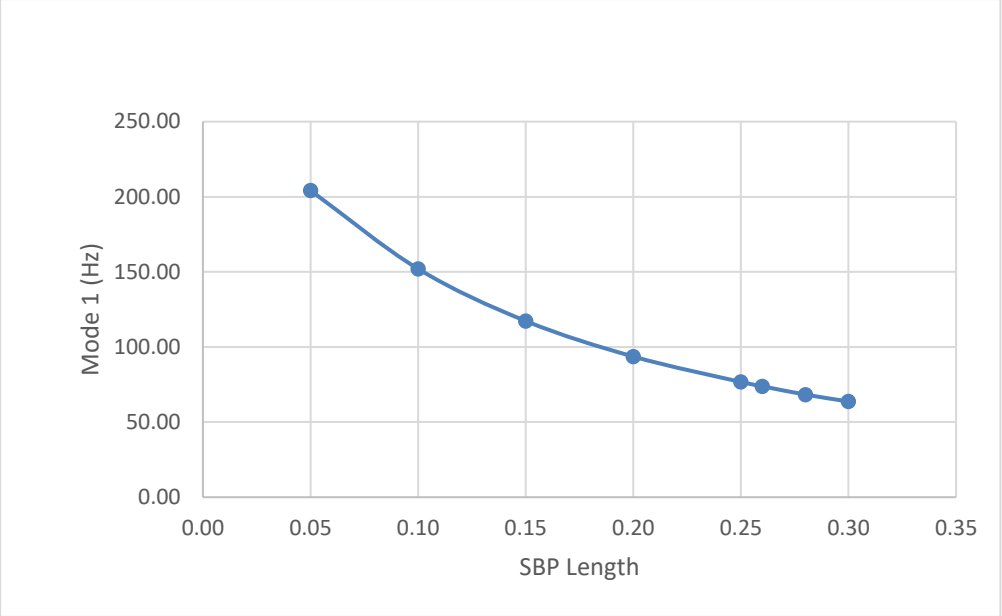

Figure 45. Modes 1 for different SBP Lengths

Figure 46 demonstrates the severity of using a long SBP within the structure and the graph below shows a significant increase of 10 kPa in the SBC edges if the SBP length is only increased by 10 cm.

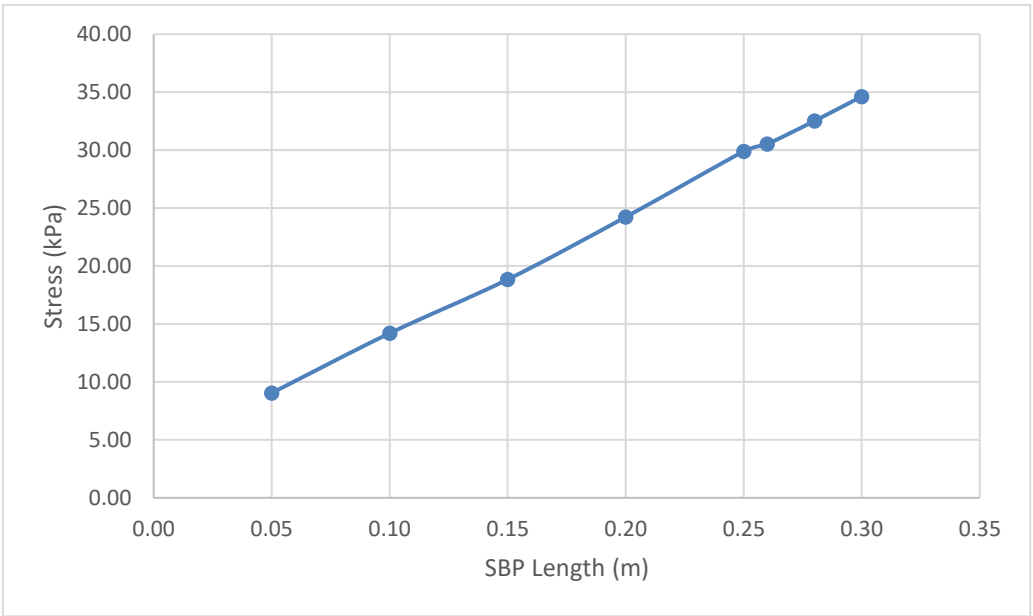

Figure 46. Stress Variation for different SBP Lengths

An expected relation is shown in Figure 47 where the velocity of the SBP upper tip is decreasing as the SBP Length is increasing.

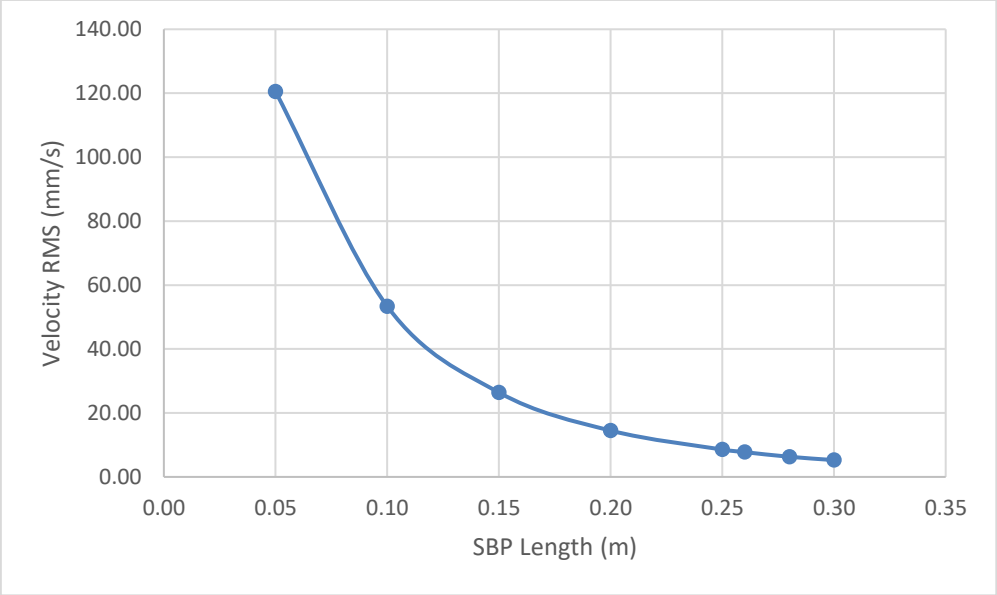

Figure 47. Velocity variation for different SBP Lengths

The Effect of the SBP Schedule

Similarly to the previous 2 studies (the impact of the SBP and main pipe lengths) a new simulation consisted of 8 identical structures with the only variation in the SBP schedule value been conducted to determine the relationship between the SBP schedule and the 1st Mode, SBP's tip velocity, and the SBC's maximum stress (see Table 7).

Table 7. Pipes dimensions (m) 4

MaOD	MaID	MALength	BOD	BIN	BLength
0.1143	0.1008	1.00	0.0603	**0.0495**	0.3
0.1143	0.1008	1.00	0.0603	**0.0500**	0.3
0.1143	0.1008	1.00	0.0603	**0.0505**	0.3
0.1143	0.1008	1.00	0.0603	**0.0510**	0.3
0.1143	0.1008	1.00	0.0603	**0.0520**	0.3
0.1143	0.1008	1.00	0.0603	**0.0525**	0.3
0.1143	0.1008	1.00	0.0603	**0.0530**	0.3
0.1143	0.1008	1.00	0.060	**0.0535**	0.3

Figure 48 shows that the First Mode Natural Frequency is affected by the SBP Schedule where the graph below affirms that the 1st Mode frequency will be 10% higher more if the SBP schedule is only increased by 36%.

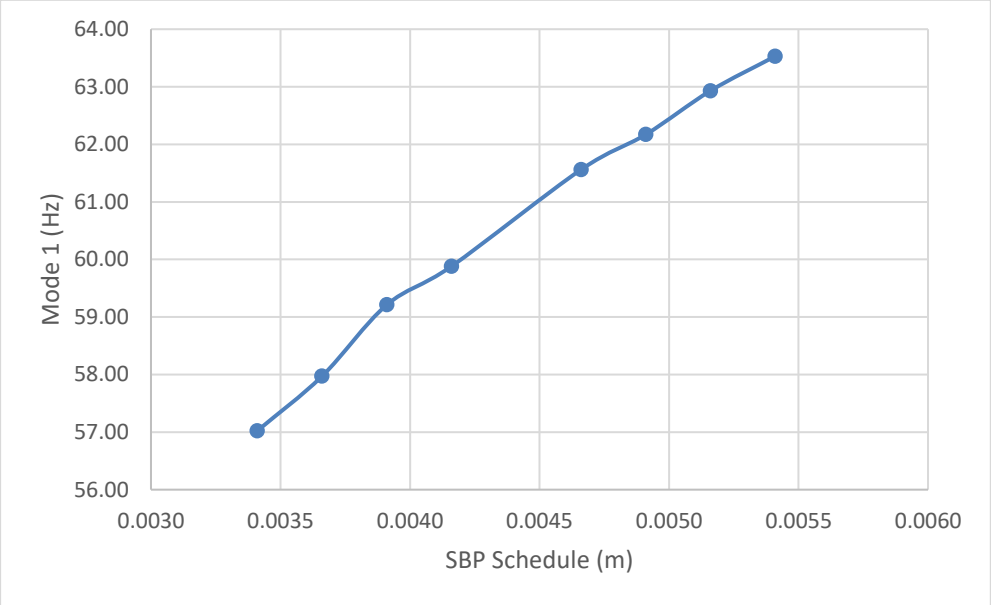

Figure 48. Modes 1 for different SBP Schedules

Figure 49 presents the relative relationship between the maximum stress generated at the SBC against the SBP schedule. This study proves that maximum stress decreases as the SBP schedule is increasing. However, increasing the SBP schedule around 35% will help to reduce the stress by 27%.

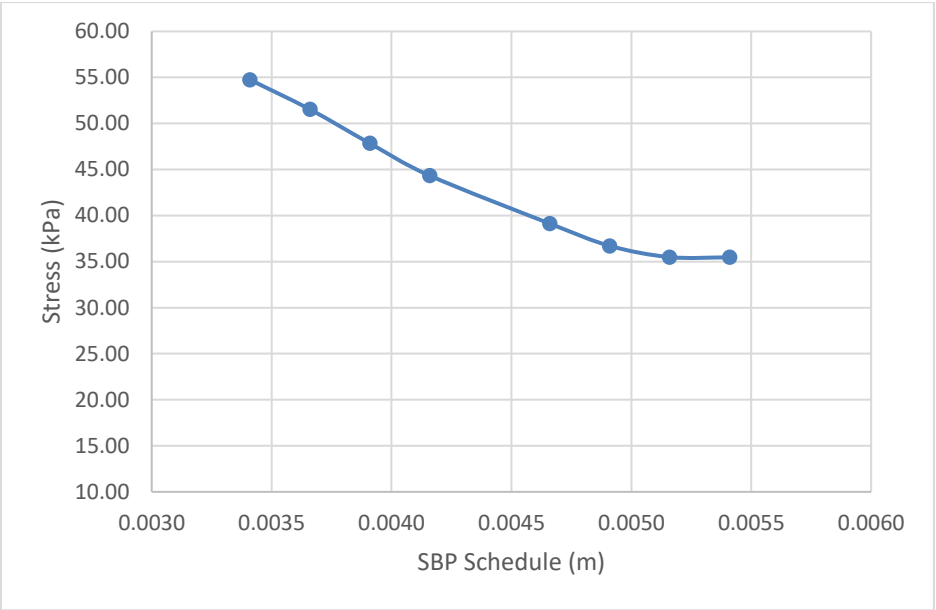

Figure 49. Stress values for different SBP Schedules

The relationship between the SBP's tip velocity and the SBP schedule is represented in Figure 50. The graph below shows a directly proportional relation. The study demonstrates that increasing the SBP schedule increases the SBP's tip velocity.

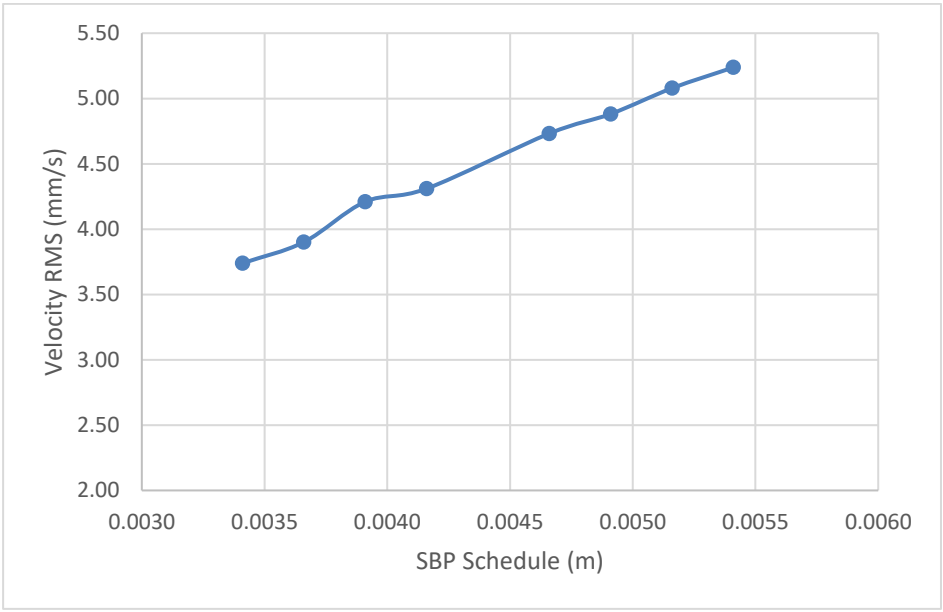

Figure 50. Velocity values for different SBP Schedules

The Effect of the Attached Valve Mass

The last parameter evaluated in this study is the impact of an attached mass to the SBP (e.g. valve) where all the other parameters are identical for the eight (8) simulated models (refer to Table 8). Performing this study will demonstrate the real contribution of any attached equipment to the natural frequency, stress, and velocity of the SBC's tip.

Table 8. Pipes dimensions (m) and mass (Kg)

MaOD	MaID	MALength	BOD	BIN	BLength	Mass
0.1143	0.1008	1.00	0.0603	0.0495	0.30	**1.00**
0.1143	0.1008	1.00	0.0603	0.0495	0.30	**2.00**
0.1143	0.1008	1.00	0.0603	0.0495	0.30	**3.00**
0.1143	0.1008	1.00	0.0603	0.0495	0.30	**4.00**
0.1143	0.1008	1.00	0.0603	0.0495	0.30	**5.00**
0.1143	0.1008	1.00	0.0603	0.0495	0.30	**6.00**
0.1143	0.1008	1.00	0.0603	0.0495	0.30	**7.00**
0.1143	0.1008	1.00	0.0603	0.0495	0.30	**8.00**

Figure 51 confirms that if the weight of any attached mass on the SBP (i.e. valve) increased it will certainly have a negative impact on the entire system as it will drastically decrease the modes of frequencies and thus a quick fatigue failure will be expected.

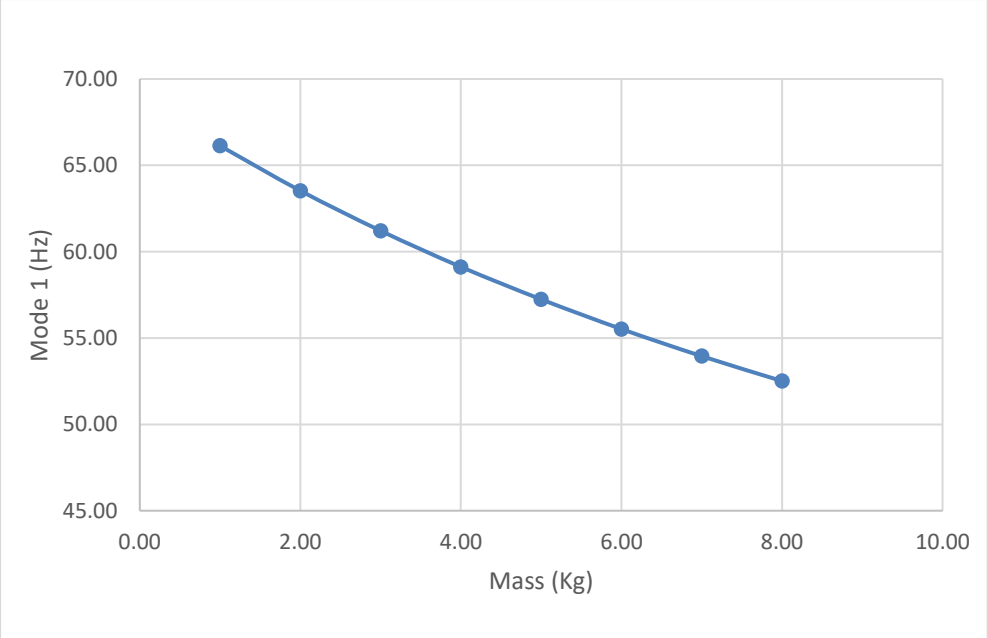

Figure 51. Mode 1 for different attached masses

Figure 52 ensures the danger of increasing the mass attached to the SBP. However, the measured stress on the SBC is plotted below and the graph clearly shows a positive slope which indicates that the stress will increase whenever the attached mass increased.

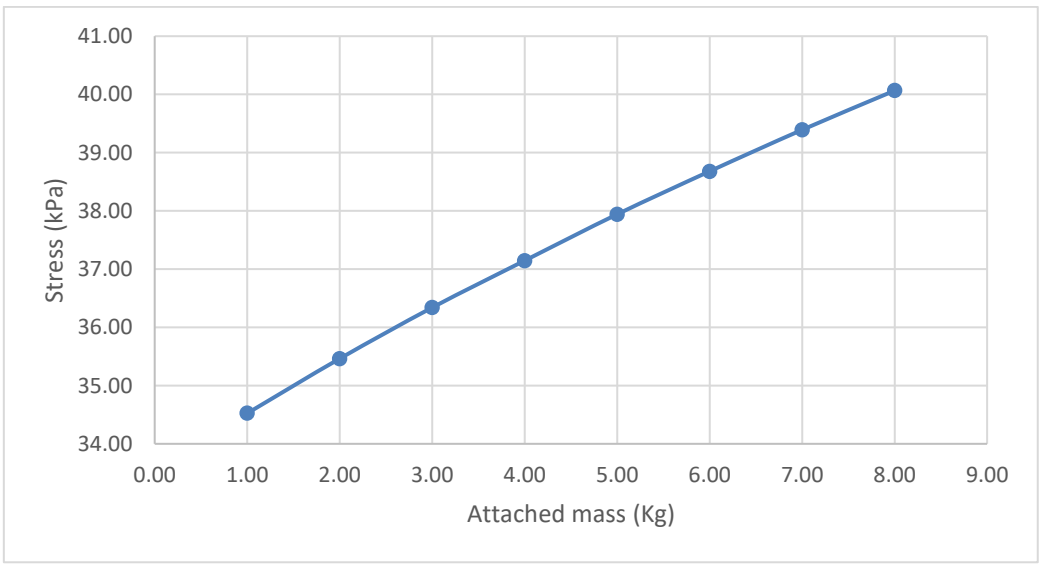

Figure 52. Stress values for different attached masses

The increment of a mass attached to the SBP will lead to a reduction in the velocity. The graph below explains the relationship between the velocity of SBP's tip and the mass attached to it (see Figure 53).

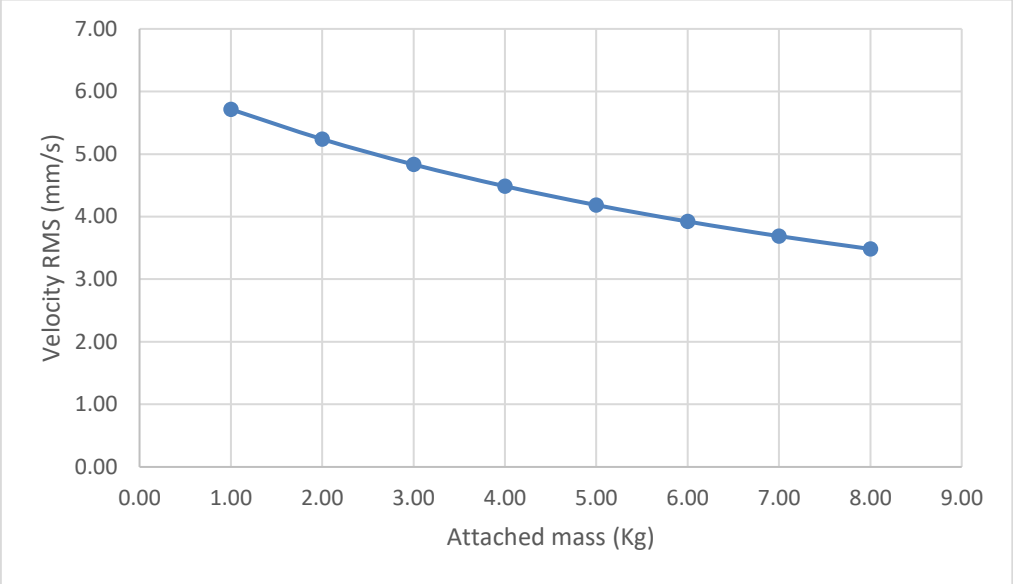

Figure 53. Velocity values for different attached masses

Piping Criterion Comparison

In this thesis, four (4) different techniques were reviewed, tested, and critiqued (VDI 3842, ASME OM-S/G, EI-AVIF, EFRC). The techniques all utilize the system's frequency plot along with custom vibrational Root Mean Square (RMS) limits to assess the SBC condition. Even though the techniques are empirical, the outcomes are fairly similar but with different limits of conservativeness.

The model below (Table 9) is used to compare the efficiency and accuracy of each of the 4 suggested methods.

Table 9. Model dimensions (m)

BIN	4.93E-02
BLENGTH	5.00E-02
BOD	6.03E-02
MAID	0.381
MALENGTH	2
MAOD	0.4064

The first step was to determine the model's frequency modes. This is for the reason that one of the suggested methods is based on the 1st natural frequency. In addition, these frequencies will help to understand the behavior of the structure in case of resonance excitation (see Table 10).

Table 10. Structure modes of vibration

Modes	Frequency (Hz)
1	146.67
2	158.49
3	354.5
4	541.25
5	559.67

Following the modal analysis, a harmonic study with a fluctuating 100 N downward force is applied on the main pipeline from the interval of 10 Hz up to 1000 Hz with an increment of 10 Hz (see Figure 54).

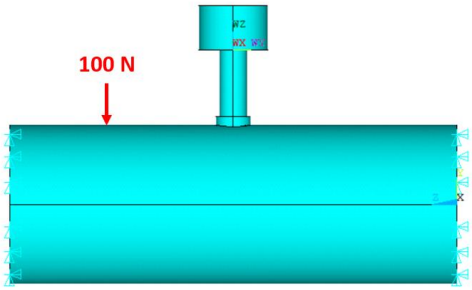

Figure 54. Harmonic Study (using 100N downward force)

Figure 55 shows the vibration (RMS vibration) results of the harmonic analysis. It is noted that the vibration reaches its peaks at 150 Hz, 540 Hz, and 700 Hz consecutively. These peaks represent the modes of the structure (see Table 10).

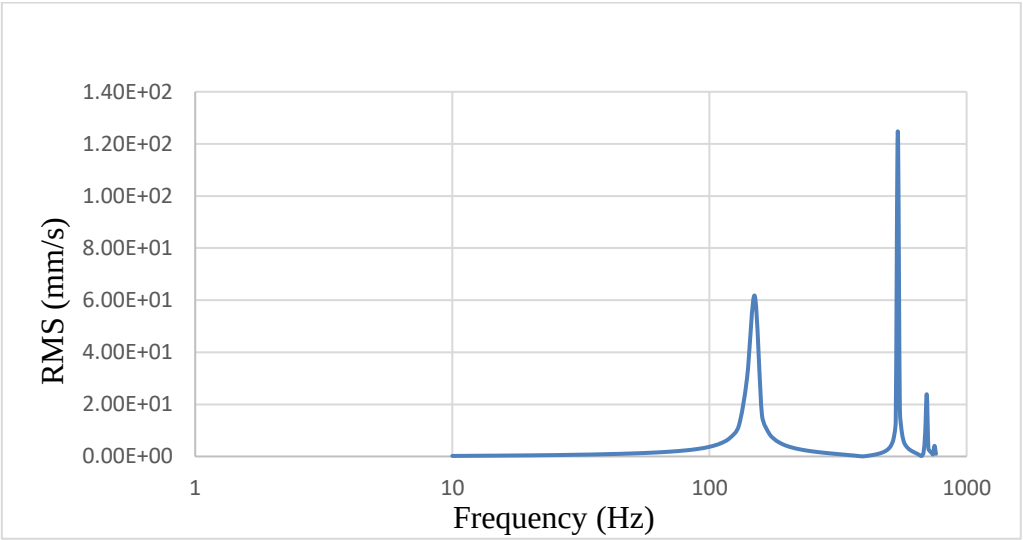

Figure 55. Harmonic response

By concluding the modal and the harmonic analyses, all the required data to assess the system through a range of frequencies [10Hz-1000Hz] is available.

From **Figure 56** to **Figure 58** the critical regions have been defined using a vertical line. Where the orange line is used for concern state and the red line is used to problem state (Please refer to Table 11).

Table 11. Concern and Problem lines

Concern	
Problem	

Critical Region 1

The graphs below (see Figure 56) study the first critical region using the four techniques (EI, ASME OM-S/G, VDI 3842, EFRC). The first critical region is where the first and second frequency modes reside. It is apparent from the graphs that the ASME approach is the most conservative technique whereas the VDI method can only indicate concern when the critical region is entered. EI-AVIFF covers the beginning of the critical region and shows concern early however it doesn't indicate concern over the entire critical region. Finally, the EFRC technique covers a reasonable amount of the critical region and is less conservative when compared to the ASME approach

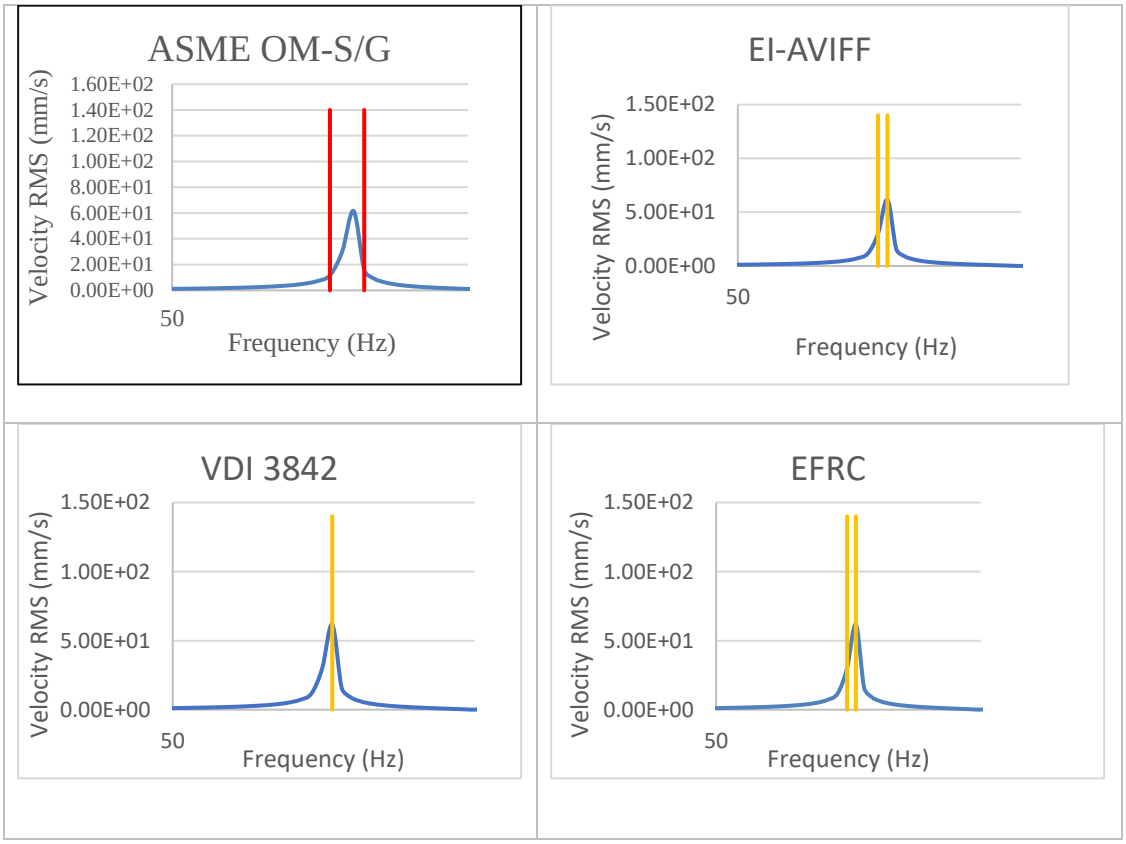

Figure 56. The frequency response of the first critical region

Critical Region 2

For the second critical region (Graph shows the frequency interval from 400 Hz to 1000 Hz), ASME continues to provide a conservative approach and indicates concern early. EFRC approach similarly covers the entire bounds of the critical region as a concern. Additionally, it also gives the danger zone warning very close to the critical region peak. However, VDI was only able to identify the critical region peak as a concern, it failed to indicate concern early. Finally, the EI-AVIFF technique is not usable for this critical region as the frequency is above 300 Hz which is the limit of the approach's capabilities (see Figure 57).

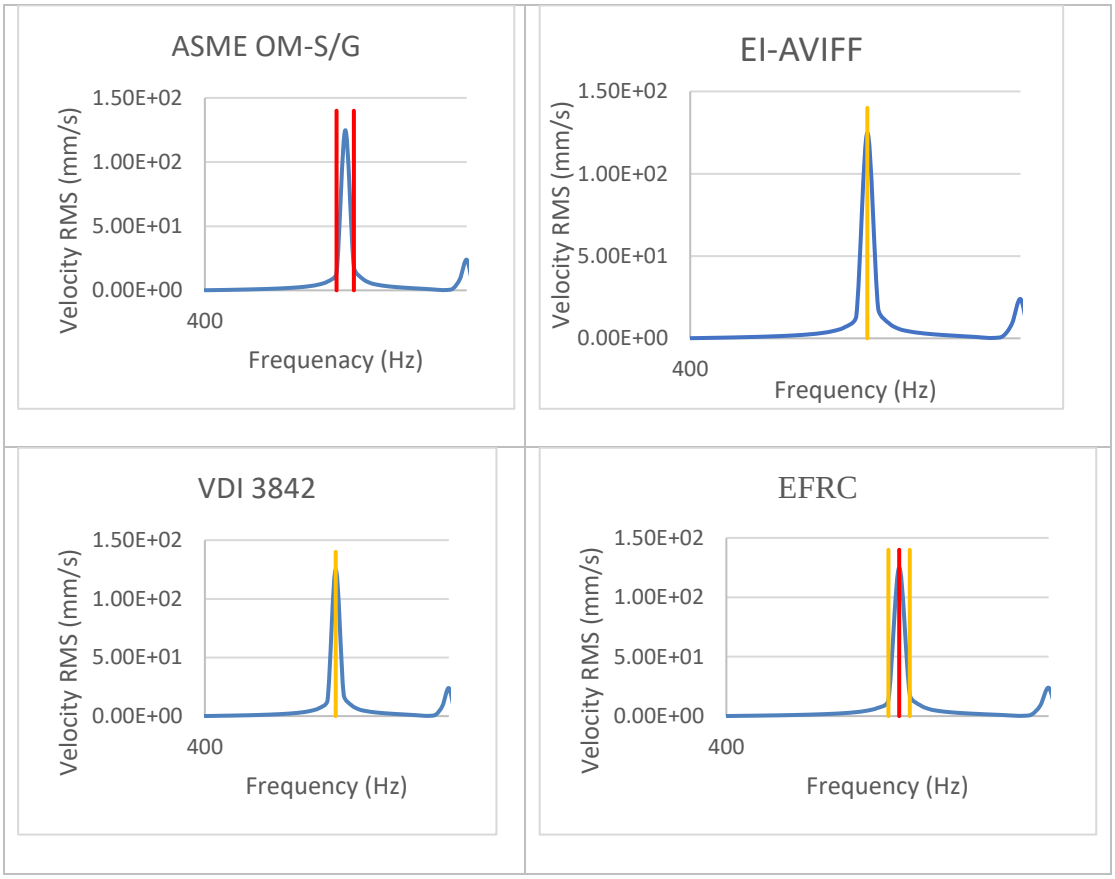

Figure 57. The frequency response of the second critical region

Critical Region 3

For the third critical region (Graph shows frequency interval from 400 Hz to 1000 Hz), only ASME and the EFRC approaches were able to identify the concern. None of the techniques were able to provide bounded concern regions. Consequently, technicians will not be warned early if any failure potentially occurs.

Much like for the previous critical region, the EI-AVIFF technique is not usable for this critical region as the frequency is above 300 Hz which is the limit of the approach's capabilities. whereas, VDI 3842 failed to predict any concern (see Figure 58).

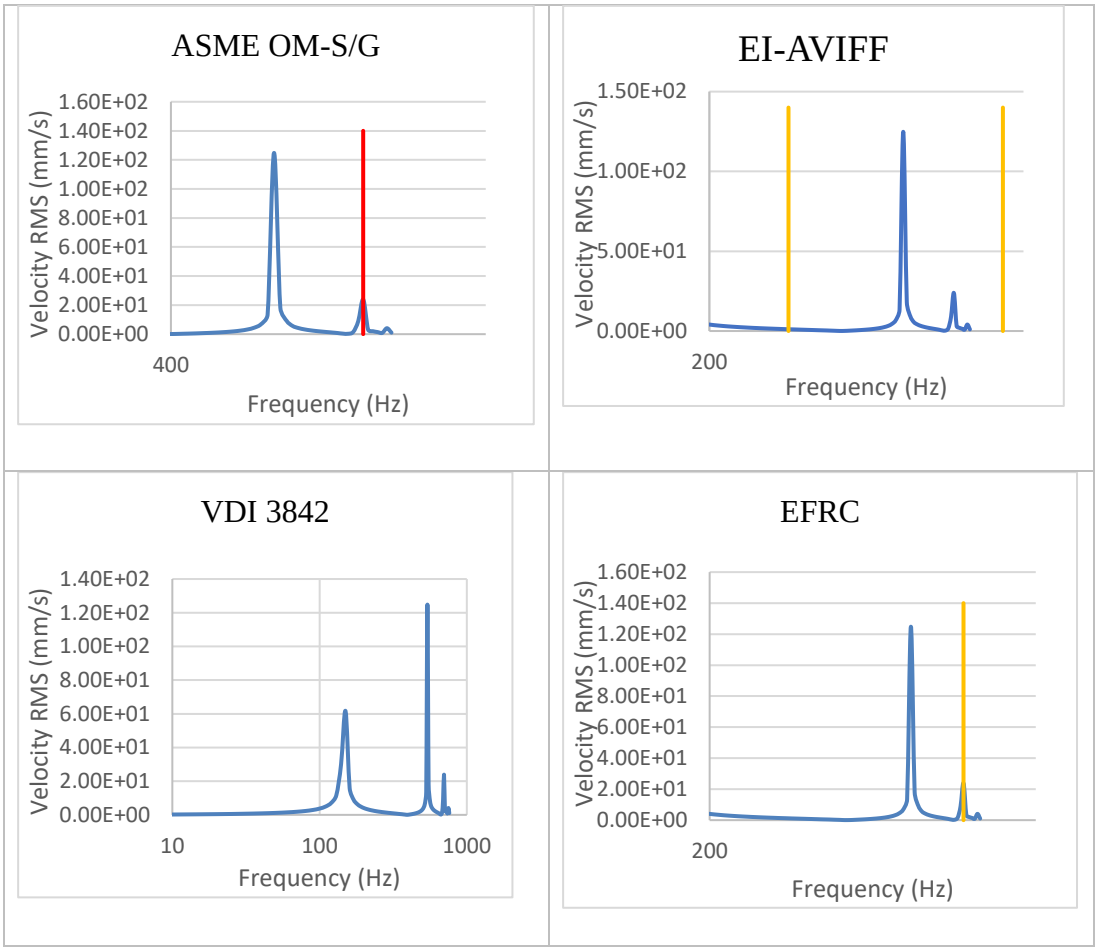

Figure 58. The frequency response of the third critical region

Machine Learning

All the models are regression models. Random forest and neural networks are nonlinear models although they can learn the linear effects if present within the data. Multiple linear regression cannot perform well for non-linear relationships.

As shown in Table 12, the random forest model is overfitting, while the multiple linear regression model is underfitting. The neural network gives a reasonable tradeoff between the two other models. A model that overfits (learns the data very well) cannot perform well when presented with new data that are outside the bounds of the dataset it was trained on. An underperforming model is likewise not useful for making predictions. The performance of the neural network, however, can be improved with more data. The linear regression model may not improve as much if the actual relationships within the independent features and the objective variable are nonlinear. Increasing the data will also help reduce the overfitting of the random forest (RF) model since the RF is not effective with big data.

Table 12. ML correlation factors

	R^2	MAE (HZ)	MAPE	RMSE
Multiple Linear Regression	0.77	17.4	27.47	23.25
Neural Network	0.97	6.1	8.41	8.3
Random Forest	0.98	4.12	5.79	6.19

Chapter 5: Validation

FE validation

In this section, an experimental test was performed to validate the FE model used to predict the mode frequency of the structure. A six-inch pipe with a total length of 240 cm and an “SHC 40” schedule with two SBPs (Small SBP and Long SBP) attached to it was analyzed (see Figure 59).

Specifications include:

- Small SBP: Two-inch pipe, with Schedule of “SCH 40” and a total length of 25 cm.
- Long SBP: Two-inch pipe, with Schedule of “SCH 40” and a total length of 35 cm.

Figure 59. Experimental setup

The setup shown in Figure 59 was modeled on the FE software using the same APDL code used for the structure with a single SBC (The APDL code used for this thesis). The material used was Carbon Steel and the dimensions are shown below in Figure 60.

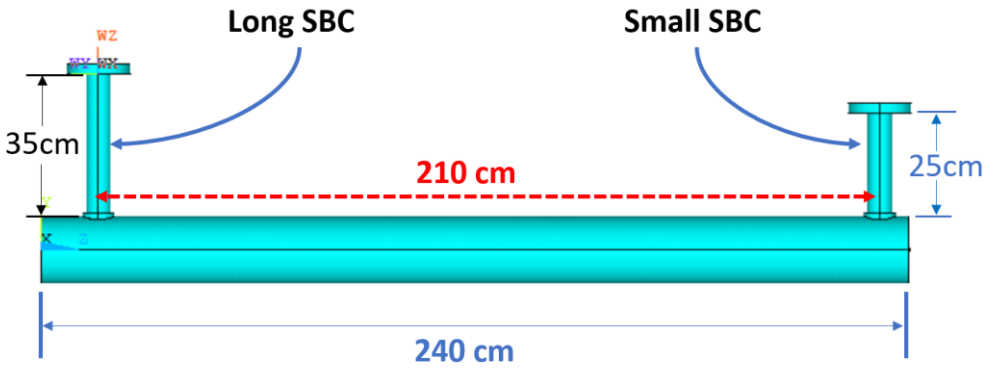

Figure 60. FE model for a pipe with two SBPs

The harmonic analysis was conducted in the workshop in order to obtain the modes of the structure's frequency (Please refer to Figure 67 in Appendix G). Similarly, modal analysis was performed using the FE (APDL algorithm) to determine the natural frequency (refer to Figure 61, Figure 62, and Figure 63).

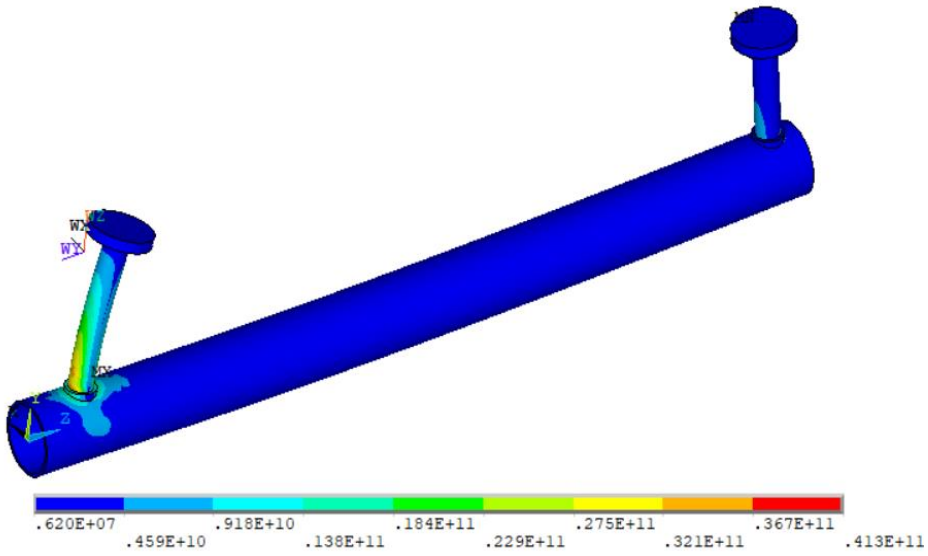

Figure 61. Stress associated with the first mode shape

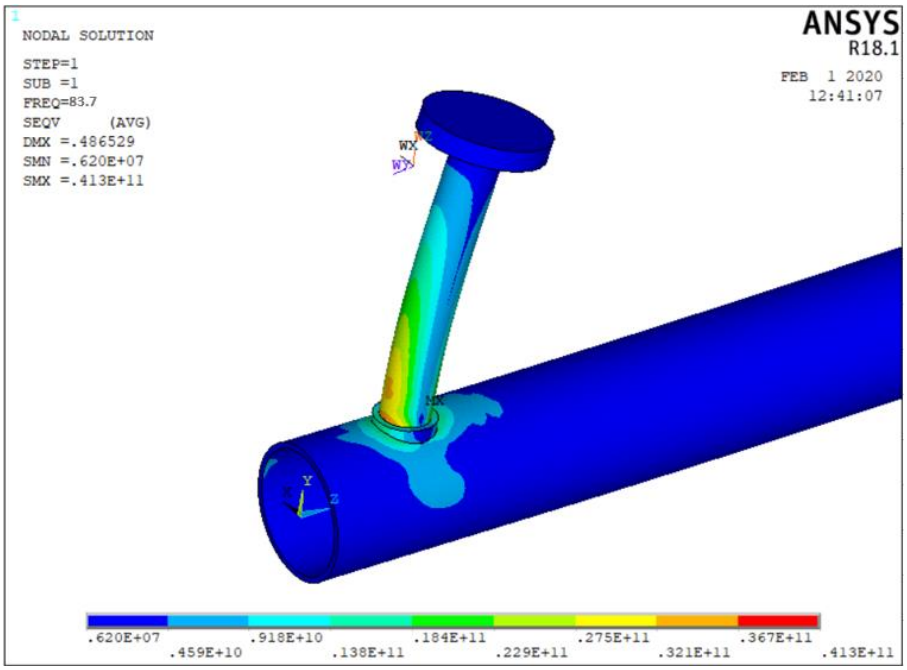

Figure 62. 1st mode shape of the long SBP and the stress associated

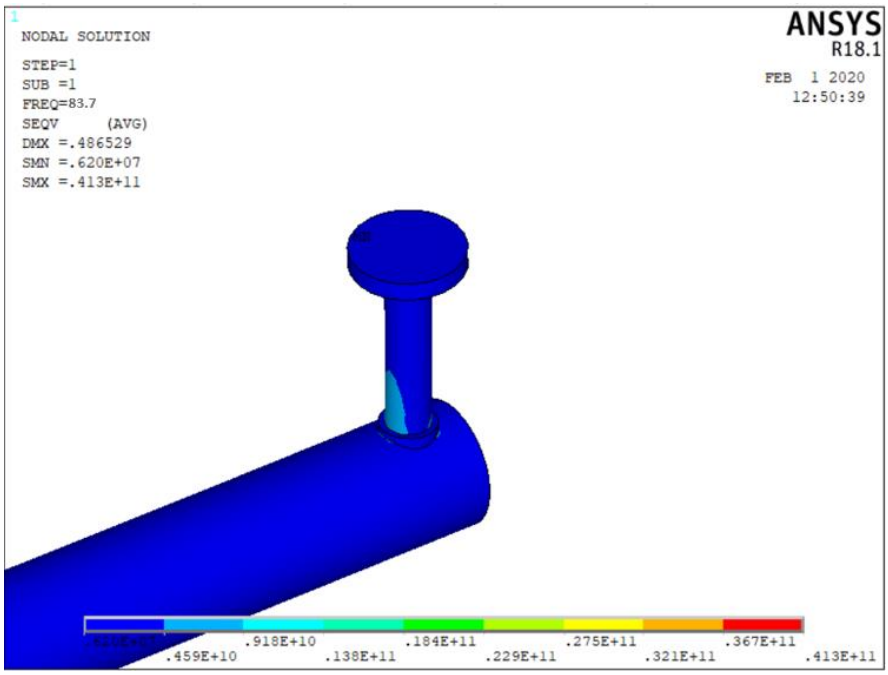

Figure 63. 1st mode shape of the short SBP and stress associated

The obtained results are summarized in Table 13. Where the FE modes obtained are reported along with the experimental modes of frequencies. In conclusion, the APDL code (model) is roughly accurate up to 95% to predict the exact value of the 1st natural

frequency. Thus, the output of the FE analysis that was used to train the ML algorithm is justified with the results obtained below in Table 13.

Table 13. FE and Experimental modes of frequencies

	FE (Hz)	Experimental (Hz)	Error %
Mode 1	**83.7**	**80.03**	**4.6%**
Mode 2	**116.5**	**112.8**	**3.3%**
Mode 3	**165**	**160**	**3.1%**

ML Projection Validation

In this section, the ML algorithm's ability was tested by predicting the first natural frequency for a system whose parameters were outside the bounds of those fed into the algorithm (i.e. length of the main pipe). The data that was fed to train the ML algorithm was obtained by testing systems whose main pipe length varied from 0.5m to 2.0m. Figure 64 shows how the 1st natural frequency is decreasing when the main pipe length is increasing (all other system parameters remain constant). Similarly to Figure 39 (1st natural frequency obtained from FE), the ML projection presents in Figure 64 shows the same patterns. As a conclusion, the ML algorithm could be used for prediction and projection analysis.

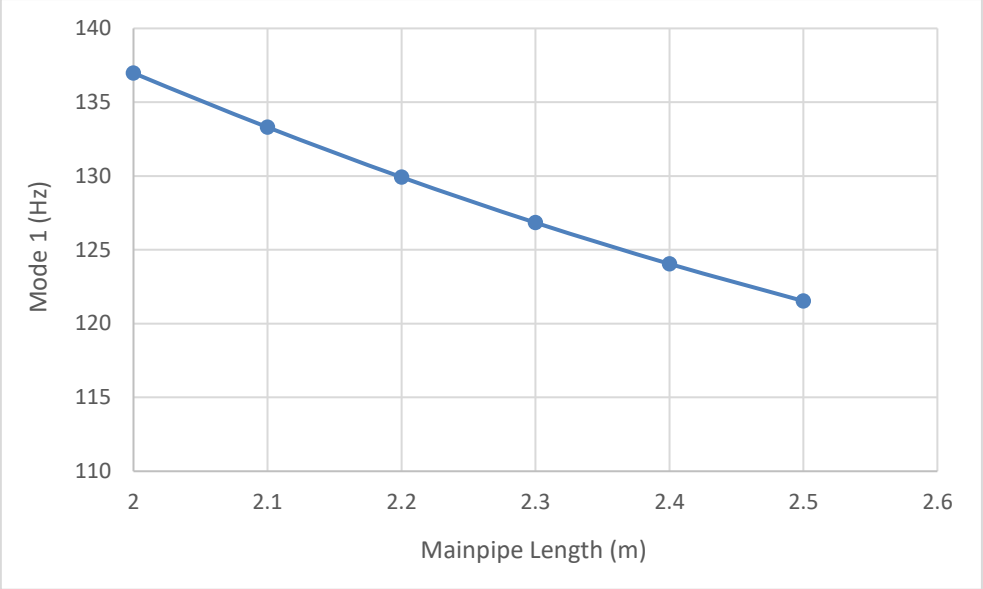

Figure 64. Mode 1 Vs Main pipe length (ML data)

Chapter 6: Conclusion & Recommendation

Conclusion

By studying the effects of the main pipeline dimensions on analysis results, the following recommendations are crucial for piping design & operation:

Point 1: The shorter the main pipe, the higher the first mode of the frequency of the entire system. These conditions could be satisfied by using short intervals supports.

Point 2: The longer the main pipe, the higher the RMS velocity of the SBP's tip and the lower the stress at the SBC.

Point 1&2 confirm that the position of the supports needs to be studied and simulated in order to ensure that the first natural frequency is higher than the operational frequency. An optimized solution is needed by creating a balance between the resulted stress at SBC and the first natural frequency. In this case, the outcome ML of this thesis could significantly contribute to optimizing the length of the main pipe.

Point 3: The first natural frequency is increasing as the main pipe schedule is increasing. On the other hand, the stress at the SBC is increasing as well.

Points 1, 2, and 3 affirm that higher stiffness of the main pipe (short interval support, thicker schedule) results in higher stress at the SBC.

Similarly, by studying the effect of the SBP dimensions on the analysis results, the following recommendations are crucial for piping design & operation:

Point 4: Increasing the length of the SBP results in a decrease in the first natural frequency and an increase of stress at the SBC. Thus, long SBP needs to be avoided.

Point 5: Increasing the schedule of the SBP results in an increase in the first natural frequency and a decrease in the stress at the SBC. In conclusion, increasing SBP is recommended.

Point 6: The effect of increasing the mass of the valve in this research is proved to have

a negative impact on both the 1st mode of the system and the stress at the SBC.

Point 7: Attaching an extra SBP to the main pipe will lead to a lower value of 1st natural frequency. It is recommended that the number of SBPs are minimized within the work pipe.

Point 8: For frequencies less than 300Hz, ASME OM-S/G guidelines are recommended to be used. However, the usage of this guideline recommends a prior knowledge of the 1st natural frequency. The ML algorithm created in this thesis provides the 1st mode of the system quickly by only knowing the system dimensions.

Point 9: Both EI-AVIFF and VDI 3842 guidelines are recommended to be avoided for frequencies above 300Hz. Where EI-AVIFF is too conservative in this frequency range while VDI 3842 is not capable to detect any concern.

Recommendation for Future Work

This thesis is a step closer to creating a new vibration criterion guideline. For this purpose, the following steps are needed:

Step 1: More data needs to be generated by varying the shape, location, and the material of the SBP. The provided APDL code is capable to accomplish this task.

Step 2: Various SBC shapes and dimensions need to be evaluated.

Step 3: Flow-induced vibration needs to be included in the analysis model to generalize the results.

Step 4: Different materials need to be tested withing the previous steps.

Step 5: Finally, Big Data needs to be utilized on supercomputers with the given APDL code and the ML algorithm.

REFERENCES

[1] L. Pook, Metal Fatigue What It Is, Why It Matters, London,UK: Springer, 2007.

[2] P. Maruschak, L. P. and T. Pyrig, "Fatigue an Brittle Fracture of Carbon Steel of Gas and Oil Pipelines," *TRANSPORT*, vol. 28, no. 3, pp. 270-275, 2013.

[3] A. Keprate, R. C. Ratnayake and H. DNV GL, "Vibration induced fatigue integrity evaluation of small bore piping using belief network," in *International Ocean and Polar Engineering Conference*, Hawaii, USA, 2019.

[4] S.Pewkliang, P.Janbanjong, P.Rahong, N.Muangsuankwan and S.Nokjib, "The Study of Effects from Small Bore Connection Geometry for High Vibrational Excitation," in *International Petroleum Exhibition & Confrence*, Abu Dhabi,UAE, 2017.

[5] P. v. Beek, R. Pijpers, K. Macdonald, J. Maljaars, K. Lunde, H. Korst and F. Hansen, "A Novel High Cycle Fatigue Assessment of Small-Bore Side Branches: Tailor-Made Acceptable Vibration Levels Based on the Remaining Life of Existing Structures," in *Proceedings of the ASME 2014 Pressure Vessels & Piping Conference*, California, 2014.

[6] A. McGillivray and J. Hare, "Offshore hydrocarbon releases 2001-2008," Health and Safety Laboratory, Buxton, 2008.

[7] American Petroleum Institute, Risk Based Inspection Technology, USA: API RP 581, 2016.

[8] American Petroleum Institute, Risk Based Inspection Technology, USA: API 580, 2016.

[9] H. Iqbala, S. Tesfamariama, H. Haiderb and R. Sadi, "Inspection and maintenance of oil & gas pipelines: a review of policies," *Structure and InfraStructure engIneer*, vol. 13, no. 6, pp. 794-815, 2016.

[10] P. K. Dey, S. O. Ogunlan and S. Naksuksaku, "Risk-based maintenancemodel for offshoreoil and gas pipelines:a case study," *Journal of Quality in Maintenance Engineering*, vol. 10, no. 3, pp. 169-183, 2004.

[11] Hydrocarbons Technology, "The world's longest oil and gas pipelines," Rockies Express, 17 OCTOBER 2012. [Online]. Available: https://www.hydrocarbons-technology.com/features/featureworlds-longest-oil-gas-pipelines-imports/. [Accessed 20 September 2019].

[12] I. Slav, "Pipeline Opponents Need A Shot Of Common Sense," Oil Price, 15 April 2018. [Online]. Available: https://oilprice.com/Energy/Crude-Oil/Pipeline-Opponents-Need-A-Shot-Of-Common-Sense.html. [Accessed 11 October 2019].

[13] code Steel, "Why inspections are so important with oil and gas piping," 20 April 2017. [Online]. Available: http://www.codesteel.com/oil-and-gas-piping-inspection/. [Accessed 08 October 2019].

[14] Petroleum Safety Authority Norway, "Investigation of Hydrocarbon Leak on Gudrun on 18 February 2015," ptil, Norway, 2015.

[15] G. Kacprzynski, A. Sarlashkar, M. Roemer, A. Hess and W. Hardman, "Predicting Remaining Life byFusing the Physics of FailureModeling with Diagnostics," *The Journal of The Minerals, Metals & Materials Society,* vol. 56, no. 3, pp. 29-35, 2004.

[16] M. Jasiulewicz, "The role of ergonomics in implementation of the social aspect of sustainability, illustrated with the example of maintenance," *Occupational Safety and Hygiene,* pp. 47-52, 2013.

[17] M. Jasiulewicz-Kaczmarek and P. Dro_zyne, "The Role of Maintenance in Reducingthe Negative Impact of a Businesson the Environment," in *Sustainability Appraisal: Quantitative Methodsand Mathematical Techniques for Environmental Performance Evaluation*, Germany, Springer, 2013, p. 141–166.

[18] R. Tovo, "On the fatigue reliability evaluation of structural components underservice loading," *International Journal of Fatigue,* vol. 27, no. 7, p. 587–598, 2001.

[19] Y.-L. LEE and D. TAYLOR, "Stress-Based Fatigue Analysis And Design.," in *Fatigue Testing and Analysis*, UK, Elsevier, 2005, pp. 103-180.

[20] D. E. Olson, "Companion Guide to the ASME Boiler & Pressure Vessel Code," in *Pipe Vibration Testing and Analysis*, USA, American Society of Mechanical Engineers, 2009, pp. 637-706.

[21] J. Wachel, "Displacement method for determining acceptable piping vibration amplitudes," in *Joint ASME/JSME Pressure Vessels and Piping Conference*, New York,USA, 1995.

[22] A. Ghaffar, K. K. Kong, Z. Ismail and W. T. Chong, "Determination of Vibration Borne Stress in a Pipeline Using Fluid Structure Interaction," in *International Conference on Mechanical Engineering Research*, Malaysia, 2013.

[23] A. Vepsä, "Operational displacement shape based estimation of vibration borne stress variation in a pipeline," in *A conference & Exposition on Structral Synamics*, Florida, USA, 2008.

[24] J. C. Wachel and C. L. Bates, "Escape piping vibrations while designing.," in *Hydrocarbon Processing*, 1976, pp. 152-156.

[25] C.-W. Lin, Design guide to reduce potential for vibration caused by fluid flow inside pipes-review and survey, New York: Welding Research Council, 1996.

[26] Southern Gas Association, Controlling the Effects of Pulsations and Fluid Transients in Piping Systems, USA: Southwest Research Institute, 1986.

[27] R. Motriuk, "Field measurement of piping vibration - the relationship of vibration velocity with dynamic strain and stress," in *Second international conference on motion and vibration control*, Yokohama, 1994.

[28] Wood, "Small-Bore Connections (SBC) Assessment," Wood, 2014. [Online]. Available: http://www.betamachinery.com/services/small-bore-connections-sbc-assessment. [Accessed 19 10 2019].

[29] C. B. Harper, "Integrity Evaluation of Small Bore Connections (Branch Connections)," in *European Forum for Reciprocating Compressors (EFRC)*, Vienna, 2014.

[30] European Forum Reciprocating Compressors, Guidelines for Vibrations in Reciprocating Compressor, vol. 4, Germany: EFRC, 2017.

[31] M. MERIKOSKI, "Analysis and mitigation with the DIAM matrix tool," Energiforsk, Stockholm,Sweden, 2017.

[32] Energy Institute, Guidelines for the Avoidance of Vibration Induced Fatigue Failure in Process Pipework, UK: Energy Institute, 2008.

[33] S. Simons, B. White and F. Fierro, "Applying The Energy Institute And GMRC/PRCI Guidelines For The Avoidance Or Reduction Of Vibration Problems In Small Diameter Piping Branch Connections," in *turbomachinery and pump symposia*, Texas,USA, 2016.

[34] J. S. G. McGhee, S. MacDonald, J. P. Hamilton and G. Wally, "Definition of a Cut-Off Natural Frequency for Small Bore Pipework Connections," in *Pressure Vessels and Piping Conference*, Paris, France, 2014.

[35] F. Cobb, in *Structural Engineer's Pocket Book,* UK, Elsevier Butterworth Heinemann, 2014, p. 67.

[36] Gas Machinery Research Council, Design Guideline for Small Diameter Branch Connections, USA: Southwest Research Institute, 2011.

[37] M. HAMBLIN, "Fatigue of cantilevered pipe fittings subjected to vibration," *fatigue & fracture of engineering materials and structures,* vol. 26, no. 8, pp. 695-707, 2003.

[38] J. C. Wachel, S. J. Morton and K. E. Atkins, "Piping Vibration Analysis," in *19th Turbomachinery Symposium September 18-20, Turbomachinery Laboratory*, Texas,USA, 1990.

[39] S. Kaneko, T. Nakamura, F. Inada, M. Kato, K. Ishihara, T. Nishihara and M. A. Langthjem, "Vibration Induced by Pressure Waves in Piping," in *Flow-induced Vibrations*, USA, Academic Press, 2014, pp. 197-275.

[40] P. Drożyner, "Gas pipeline structural fatigue life prediction based on vibration signals analysis," *Journal of Vibroengineering,* vol. 18, no. 8, p. 5239–5251, 2016.

[41] R. Gamble and S. J. Tagart, "A method to assign failure rates for piping reliability assessments," in *American Society of Mechanical Engineers (ASME) pressure vessels and piping conference,* USA, 1991.

[42] American Society of Mechanical Engineers (ASME), Standards and Guides for Operation and Maintenance of Nuclear Power Plants, USA: IHS Markit, 2007.

[43] Y. Da, A.-Y. Abdullah, N. Tung, P. Seungbae and C. Soonwan, "High-cycle fatigue life prediction for Pb-free BGA under random vibration loading," *Microelectronics Reliability,* vol. 51, no. 3, pp. 649-656, 2011.

[44] K. A, "Application of time-frequency distributions in diagnostic signal processing problems: a case study," *Diagnostyka,* vol. 17, no. 2, pp. 95-103, 2016.

[45] X. Fei, W. Zhao-Xin, L. Lei, T. Wen-Xin, G. Ming-Xiang, L. Peng and S. Guo-Gang, "Experimental and numerical evaluation of the vibration fatigue of small bore pipe in PWR," *Advanced Materials Research,* vol. 97, no. 101, pp. 848-851, 2010.

[46] S. Chakraverty and K. K. Pradhan, Computational Structural Mechanics: Static and Dynamic Behaviors, UK: Elsevier, 2018.

[47] R. L. T. J. Z. Olek C Zienkiewicz, The Finite Element Method: Its Basis and Fundamentals, USA: Butterworth-Heinemann, 2013.

[48] D. L. Logan, A First Course in the Finite Element Method, CA,USA: Cengage Learning, 2011.

[49] Manor, "Manortool," 8 June 2018. [Online]. Available: https://www.manortool.com/finite-element-analysis. [Accessed 04 January 2020].

[50] K.-J. Bathe, Finite Element Procedures, Watertown,Ma: K.J.Bathe, 2016.

[51] Y. Saito, S. Torisaki and S. Miwa, "Two-phase flow regime identification using fluctuating force signals under machine learning techniques.," in *26th International Conference on Nuclear Engineering*, London,UK, 2018.

[52] V. Selvam and R. Babu, "An Overview of Machine Learning and its Applications," *International Journal of Electrical Sciences & Engineering (IJESE)*, vol. 1, no. 1, pp. 22-24, 2015.

[53] S. Guido and A. Mueller, Introduction to Machine Learning with Python, California,USA: O'Reilly Media, 2016.

[54] S. U. J.P. Patel, "Comparison between Artificial Neural Network and Support Vector Method for a Fault Diagnostics in Rolling Element Bearings," *Procedia Engineering*, vol. 144, pp. 390-397, 2016.

[55] S. Arangioa and F. Bontempi, "Structural health monitoring of a cable-stayed bridge with Bayesian neural networks," *Structure and Infrastructure Engineering*, vol. 11, no. 4, pp. 575-587, 2014.

[56] O. Abdeljaber, O. Avci and D. Inman, "Active vibration control of flexible cantilever plates using piezoelectric materials and artificial neural networks," *Journal of Sound and Vibration*, vol. 363, pp. 33-53, 2015.

[57] K. Zakikhani, T. Zayed, B. Abdrabou and A. Senouci, "Modeling Failure of Oil Pipelines," *American Society of Civil Engineers ASCE,* vol. 34, no. 1, pp. 88-98, 2020.

[58] A. Sawhney and A. Mund, "Adaptive probabilistic neural networkbased crane type selection system," *Journal of Construction Engineering and Management,* vol. 128, no. 3, pp. 265-273, 2002.

[59] G. S. Rao, V. Kumari and P. Rao, "Image Compression Using Neural Network for Biomedical Applications," in *Soft Computing for Problem Solving*, Singapore, Springer, 2019, pp. 107-119.

[60] K. Liao, Q. Yao, X. Wu and W. Jia, "A numerical corrosion rate prediction method for direct assessment of wet gas gathering pipelines internal corrosion," *Energies,* vol. 5, no. 10, p. 3892–3907, 2012.

[61] M. Rezakazemi, S. Razavi, T. Mohammadi and A. Nazari, "Simulation and determination of optimum conditions of pervaporative dehydration of isopropanol process using synthesized PVA–APTEOS/TEOS nanocomposite membranes by means of expert systems," *Journal of Membrane Science,* vol. 379, no. 2, pp. 224-232, 2011.

[62] R. A.Parisher and R. A.Rhea, "Steel Pipe," in *Pipe Drafting and Design*, USA, Gulf Professional Publishing, 2012, pp. 4-12.

[63] B. S. Everitt and A. Skrondal, The Cambridge Dictionary of Statistics, UK: Cambridge University Press, 2010.

[64] C. J. Willmott and K. Matsuura, "Advantages of the mean absolute error (MAE) over the root mean square error (RMSE) in assessing average model performance," *CLIMATE RESEARCH,* vol. 30, no. 12, pp. 79-82, 2005.

[65] A. d. Myttenaere, B. Golden, B. L. Grand and F. Rossi, "Mean Absolute Percentage Error for Regression Models," *Neurocomputing,* vol. 192, pp. 38-48, 2016.

[66] G. James, D. Witten, T. Hastie and R. Tibshirani, An Introduction to Statistical Learning: with Applications in R, USA: Springer, 2017.

[67] American Society of Mechanical Engineers, ASME B31.3 Process Piping Guide, USA: AMSE, 2009.

APPENDICES

Appendix A: SBC Coordinate System

SBC coordinate system [29]

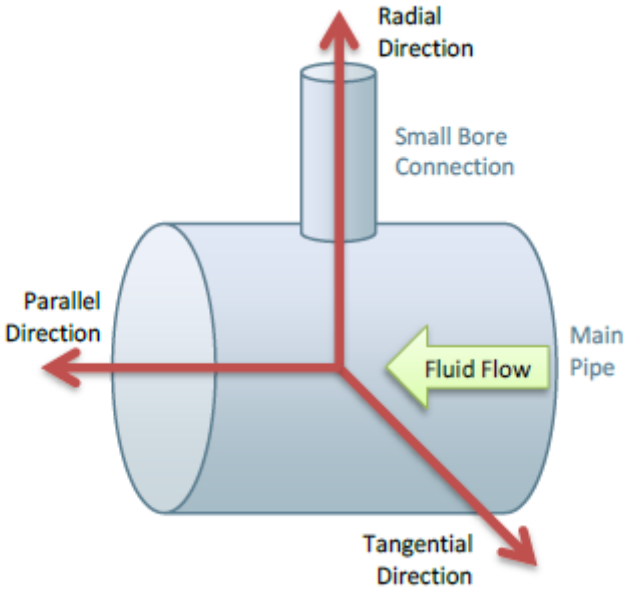

Figure 65. SBC coordinate system

Appendix B: Allowable Factors of Vibration

Table 14. Allowable factors of vibration [29]

Configuration	Diagram	K_a
Fixed-Free	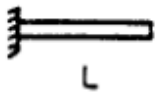	0.0569
Simply Supported	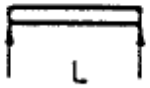	0.0203
Fixed-Supported	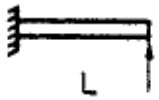	0.00979
Fixed-Fixed	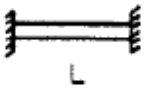	0.00710
L-Bend, Out-of-Plane, Equal Leg Length	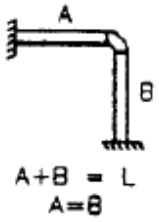	0.0110
L-Bend, In-Plane, Equal Leg Length	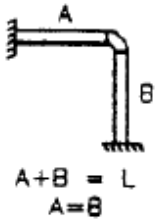	0.00267
U-Bend, Out-of-Plane, Equal Leg Length	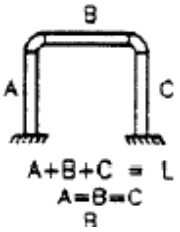	0.00746

Appendix C: APDL Code

APDL Code:

! These commands are used to start the software

FINISH

/CLEAR,START

! The for-Loop function is used to read multiple pipe dimensions rows

! Each Run is referred by the term "case"

*DO,case,1,100,1

/PREP7

!APDL call to open another script which is responsible to model the system

!Refer to "Model_loop" for details.

/CWD,'C:\Users\mehdi\Dimensions V5'

!/INPUT, Fname, Ext, Dir, LINE, LOG

/CWD,'C:\Users\mehdi\Model_loop'

/INPUT, Model_loop, txt ,,,,

! Boundary Conditions for the pipe are applied

!=====================================

DL,1,,ALL

DL,2,,ALL

DL,3,,ALL

DL,4,,ALL

DL,9,,ALL

DL,10,,ALL

DL,11,,ALL

DL,12,,ALL

!This section is responsible to generate the meshing for parts of the model

!=====================================

! Meshing of the attached mass

!=====================================

ESIZE,0.01,0

MSHKEY,0

MSHAPE,1,3d

VMESH,4

!=====================================

! Meshing of the SBP

!=====================================

BThickness = BOD - BIN

ESIZE,BThickness*0.7,0

MSHKEY,0

MSHAPE,1,3d

VMESH,1

!=====================================

! Meshing of the Main Pipe

!=====================================

MThickness = MaOD - MaID

ESIZE,MThickness*1.5,0

MSHKEY,0

MSHAPE,1,3d

```
VMESH,3


!=====================================
! Meshing of the weldolet (O-let)
!=====================================
ESIZE,0.01,0 ! Select the according to the schedule of the pipe
MSHKEY,0
MSHAPE,1,3d
VMESH,2
!LREFINE,53,56,1,3,1,1,1
!LREFINE,21,24,1,1,1,1,1


!=====================================
! This section is used to create models with different attached masses
!=====================================
ET,2,MASS21
R,1,2,2,2, , , ,
type,2
E, nmass
!=====================================
! This script is responsible for running the Modal analysis and
! finds the modes of frequencies needed.
!=====================================
/SOL
ANTYPE,2
```

MODOPT,LANB,1

EQSLV,SPAR

MXPAND,5, , ,1

LUMPM,0

PSTRES,0

MODOPT,LANB,5,1,1004, ,OFF

solve

finish

!=====================================

! After performing the analysis, the data will be written to an external file

! The following for-loop will study the 3 modes of frequencies and get the following:

! 1- The natural frequencies

! 2- The maximum stress at the SBC

! 3- The displacement of the SBP tip

!=====================================

/post1

PI=ACOS(-1)

*DO,J,1,2,1

*DEL,sigma1

*DEL,smax1

*DEL,sigma2

*DEL,smax2

*DEL,disp

*DEL,dispmax

SET,,, ,,, ,J

LSEL,S, , ,53,56,1

NSLL,S,1

*GET,nodenumber1,node,,count

*DIM,sigma1,array,nodenumber1,6

*VGET,sigma1(1,1),node,,S,1

*VGET,sigma1(1,2),node,,S,2

*VGET,sigma1(1,3),node,,S,3

*DIM,smax1,array,3,1

!=====================================

! Find the maximum value in each principal stress direction

!=====================================

*VSCFUN,smax1(1,1),max,sigma1(1,1)

*VSCFUN,smax1(2,1),max,sigma1(1,2)

*VSCFUN,smax1(3,1),max,sigma1(1,3)

!=====================================

! Find the maximum (principal) stress in the three directions

!=====================================

*VSCFUN,smaxt1,max,smax1(1,1)

!=====================================

! Get the value of the first natural frequency

!=====================================

*GET, f, Mode, J, FREQ, , ,

!=====================================

! Finding the stress at the connection of the branch and the o-let

!=====================================

ALLSEL,ALL,ALL

LSEL,S, , ,21,24,1

NSLL,S,1

*GET,nodenumber2,node,,count

*DIM,sigma2,array,nodenumber2,6

*VGET,sigma2(1,1),node,,S,1

*VGET,sigma2(1,2),node,,S,2

*VGET,sigma2(1,3),node,,S,3

*DIM,smax2,array,3,1

*VSCFUN,smax2(1,1),max,sigma2(1,1)

*VSCFUN,smax2(2,1),max,sigma2(1,2)

*VSCFUN,smax2(3,1),max,sigma2(1,3)

! Find the maximum (principal) stress in the three directions

*VSCFUN,smaxt2,max,smax2(1,1)

!=====================================

! Find velocity at tip of SBC

!=====================================

ALLSEL,ALL,ALL

LSEL,S, , ,69,72,1

NSLL,S,1

*GET,nodenumber3,node,,count

*DIM,disp,array,nodenumber3,3

*VGET,disp(1,1),node,,U,X

*VGET,disp(1,2),node,,U,Y

*VGET,disp(1,3),node,,U,Z

*DIM,dispmax,array,3,1

*VSCFUN,dispmax(1,1),max,disp(1,1)

*VSCFUN,dispmax(2,1),max,disp(1,2)

*VSCFUN,dispmax(3,1),max,disp(1,3)

*VSCFUN,dispmaxt,max,dispmax(1,1)

!=====================================

! Writing the outputs into an external file

!=====================================

*CFOPEN,STRCAT('Result',CHRVAL(MAOD)),TXT,,APPEND

*vwrite,MaOD,MaID,MALength,BOD,BIN,BLength,f,smaxt1,smaxt2,f*2*PI*dispm

axt

(E14.4,7x,E14.4,7x,E14.4,7x,E14.4,7x,E14.4,7x,E14.4,7x,E14.4,7x,E14.4,7

x,E14.4)

*CFCLOS

```
*ENDDO
```

Model Loop:

```
!=====================================
! The model Loop file is called at the begging of the APDL code
! This Script is used to build the model based on the geometry dimensions
! These geometry dimensions are inserted through a sperate txt file.
!=====================================
to_skip=1
/INQUIRE,numlines,LINES,ApdlExcel,txt
to_read=numlines-to_skip
*DEL,mytable,,NOPR
*DIM,mytable,TABLE,to_read-1,9
*TREAD,mytable,ApdlExcel,txt,,to_skip
*DEL,xyz,,NOPR
*DIM,xyz,ARRAY,to_read,10
*DO,I,1,10,1
        *vfun,xyz(1,I),copy,mytable(0,I-1)
*ENDDO
!=====================================
! For every model there is ID assigned to it (case)
! The following script will read the matrix and define the parameters.
! Each element in the matrix will be assigned to a parameter.
!=====================================
I = case
```

ID = xyz(I,10)

BOD = xyz(I,1)

BIN = xyz(I,2)

BLength = xyz(I,3)

MaOD = xyz(I,4)

MaID = xyz(I,5)

MALength = xyz(I,6)

!=====================================

! Create the mainline

!=====================================

CYL4,0,0,MaID/2,0,MaOD/2,0,MALength

!=====================================

Create keypoint for the SBC

!=====================================

K,,1.25*MaOD,0,

K,,1.25*MaOD,1.1*MaOD/2,

K,,-1.25*MaOD,1.1*MaOD/2,

K,,-1.25*MaOD,0,0,

!=====================================

Create the lines form the keypoint then generate the SBC volume

!=====================================

LSTR, 2, 17

LSTR, 17, 18

LSTR, 18, 19

LSTR, 19, 20

LSTR, 20, 3

AL,3,4,21,22,23,24,25

VOFFST,7,-MAlength

OID = xyz(I,7)

OTHICKNESS = xyz(I,9)

OOD = xyz(I,8)

K = MaOD + 2*OTHICKNESS

WPOFFS,0,0,MALength/2

WPROTA,0,270,0

CYL4,0,0,0,0,OOD/2,0,2*MaOD

VINP,2,3

CYL4,0,0,0,0,BIN/2,0,2*MaOD

VSBV,ALL,2,

WPOFFS,0,0,1.1*MaOD /2

!=====================================

Create the SBP with a mass attached to it

!=====================================

CYL4,0,0,BIN/2,0,BOD/2,0,BLength

WPOFFS,0,0,BLength

CYL4,0,0,0,0,OOD,0,0.1

VGLUE, 1,2

VGLUE, 1,3

VGLUE, 2,5

!=====================================

Assign to Material Model Carbon Steel

!=====================================

```
MP,EX,1,210E9              ! Young's modulus
MP,PRXY,1,0.3              ! Poisson's ratio
MP,DENS,1,7850             ! Density
!MP,ALPX,1,1.2E-5          ! Coefficient of Thermal Expansion
!MP,THSX,1,22              ! Zero-Thermal strain reference temperature
!MP,GXY,1,7.6923E10        ! Shear Modulus
ET,1,SOLID185
```

Appendix D: ML Code

Machine learning code:

In [1]: **import pandas as pd**

import numpy as np

import seaborn as sns

from sklearn.model_selection import train_test_split

from sklearn.preprocessing import RobustScaler

from sklearn.neural_network import MLPRegressor

from sklearn.ensemble import RandomForestRegressor

from sklearn.linear_model import LinearRegression

from sklearn.metrics import r2_score, mean_squared_error, mean_absolute_error

In [2]: df=pd.read_csv('mehdi.csv', sep=',')

In[3]:df.boxplot(figsize=(10,6),

column=['MaOD','MaID','MALength','BLength','BOD','BIN'], grid

In [4]: df.boxplot(figsize=(10,6), column=['f'], grid=**False**)

Out[4]: <matplotlib.axes._subplots.AxesSubplot at 0x7f8a7c2f3e80>

In [47]: sns.pairplot(df,kind='scatter')

Out[47]: <seaborn.axisgrid.PairGrid at 0x7f8a78a61a90>

In [5]: sns.pairplot(df,kind='reg')

Out[5]: <seaborn.axisgrid.PairGrid at 0x7f8a7a24d208>

In [6]: df.head(5)

Out[6]: MaOD MaID MALength BLength BOD BIN f

0 0.356 0.328 0.6 0.15 0.0603 0.0576 104.0

1 0.356 0.328 0.6 0.15 0.0603 0.0564 119.0

2 0.356 0.328 0.6 0.15 0.0603 0.0548 135.0

3 0.356 0.328 0.6 0.15 0.0603 0.0516 163.0

4 0.356 0.328 0.6 0.15 0.0603 0.0493 172.0

In [7]: X=df.iloc[:,:6]

In [8]: X.head(3)

Out[8]: MaOD MaID MALength BLength BOD BIN

0 0.356 0.328 0.6 0.15 0.0603 0.0576

1 0.356 0.328 0.6 0.15 0.0603 0.0564

2 0.356 0.328 0.6 0.15 0.0603 0.0548

In [9]: y=df.iloc[:,6:]

In [10]: y.head(3)

Out[10]: f

0 104.0

1 119.0

2 135.0

In [11]: df.corr()

Out[11]: MaOD MaID MALength BLength BOD BIN f

MaOD 1.000000 0.997763 -0.089438 0.421079 -0.129601 -0.024895 -0.133577

MaID 0.997763 1.000000 -0.085966 0.424026 -0.130266 -0.023982 -0.170451

MALength -0.089438 -0.085966 1.000000 0.168737 0.674421 0.003741 -0.083977

BLength 0.421079 0.424026 0.168737 1.000000 -0.156491 -0.009618 -0.534244

BOD -0.129601 -0.130266 0.674421 -0.156491 1.000000 0.004324 0.141666

BIN -0.024895 -0.023982 0.003741 -0.009618 0.004324 1.000000 -0.240531

f -0.133577 -0.170451 -0.083977 -0.534244 0.141666 -0.240531 1.000000

In [12]: X_train_unscaled, X_test_untransformed, y_train, y_test =

train_test_split(X,y,

test_size=0.2,train_size=0.8,shuffle='True',random_state=7)

In [13]: len(X_train_unscaled)

Out[13]: 828

In [14]: len(X_test_untransformed)

Out[14]: 208

In [15]: robust=RobustScaler()

In [16]: X_train=robust.fit_transform(X_train_unscaled)

In [17]: X_test=robust.transform(X_test_untransformed)

In [18]: y_train=np.ravel(y_train)

In [19]: y_test=np.ravel(y_test)

1 Neural Network

In [20]: NN=

MLPRegressor(hidden_layer_sizes=(156,230),alpha=0.01,learning_rate_init=0.08,

max_iter=1000, verbose=**False**, early_stopping=**True**, random_state=7)

In [21]: neural_network=NN.fit(X_train,y_train)

In [22]: neural_network.score(X_test,y_test)

Out[22]: 0.8844888591755858

In [23]: nn_predicted=neural_network.predict(X_test)

In [24]: mean_absolute_error(y_test,nn_predicted)

Out[24]: 8.427311486282091

In [25]: mean_squared_error(y_test,nn_predicted)

Out[25]: 276.9490883473978

In [26]:

nn_pred=pd.DataFrame(zip(y_test,nn_predicted),columns=['actual','nn_predicted'])

In [27]: nn_pred.head(5)

Out[27]: actual nn_predicted

0 71.30 76.732667

1 45.24 51.374761

2 175.20 176.712352

3 40.05 28.190364

4 72.40 59.501277

2 Random Forest

In [28]: RF=RandomForestRegressor(random_state=7)

In [29]: random_forest=RF.fit(X_train,y_train)

In [30]: random_forest.score(X_test,y_test)

Out[30]: 0.9840288344388856

In [31]: rf_predicted=random_forest.predict(X_test)

In [32]: mean_absolute_error(y_test,rf_predicted)

Out[32]: 4.124507211538456

In [33]: mean_squared_error(y_test,rf_predicted)

Out[33]: 38.29240807793256

In [34]:

rf_pred=pd.DataFrame(zip(y_test,rf_predicted),columns=['actual','rf_predicted'])

In [35]: rf_pred.head(5)

Out[35]: actual rf_predicted

0 71.30 77.8450

1 45.24 47.4220

2 175.20 173.6500

3 40.05 39.5784

4 72.40 72.9740

3 Linear Regression

In [36]: linear= LinearRegression()

In [37]: LR=linear.fit(X_train,y_train)

In [38]: LR.score(X_test,y_test)

Out[38]: 0.7745765551677833

In [39]: lr_predicted=LR.predict(X_test)

In [40]: mean_absolute_error(y_test,lr_predicted)

Out[40]: 17.40888395084471

In [41]: mean_squared_error(y_test,lr_predicted)

Out[41]: 540.474426040965

In [42]:

lr_pred=pd.DataFrame(zip(y_test,lr_predicted),columns=['actual','lr_predicted'])

In [43]: lr_pred.head(5)

Out[43]: actual lr_predicted

0 71.30 74.930935

1 45.24 58.830277

2 175.20 140.155708

3 40.05 43.943037

4 72.40 69.330246

In [44]: predictions=pd.DataFrame(zip(y_test,lr_predicted,rf_predicted,nn_predicted),

columns=['actual_f','lr_pred','rf_pred','nn_pred'])

In [45]: X_test_untransformed.reset_index(drop=**True**,inplace=**True**)

In [46]: pd.concat([X_test_untransformed,predictions],

axis=1,sort=**False**).to_csv('predictions.csv',sep=',')

Appendix E：Pipe Schedule Parameter

Pipe Schedule Parameter [67]

Nom. Pipe Sizes		OD	OD	Schedule	Wall	Wall	Lbs/Ft	Kg/m
Inches	mm DN	inches	mm	Designations ANSI/ASME	Thickn. inches	Thickn. mm		
1/8"	6	0.405	10.29	10/10S	0.049	1.24	0.1863	0.28
1/8″	6	0.405	10.29	STD/40/40S	0.068	1.73	0.2447	0.36
1/8"	6	0.405	10.29	XS/80/80S	0.095	2.41	0.3145	0.47
1/4"	6	0.540	13.72	10/10S	0.065	1.65	0.3297	0.49
1/4″	8	0.540	13.72	STD/40/40S	0.088	2.24	0.4248	0.63
1/4″	8	0.540	13.72	XS/80/80S	0.119	3.02	0.5351	0.80
3/8″	10	0.675	17.15	10/10S	0.065	1.65	0.4235	0.63
3/8"	8	0.675	17.15	STD/40/40S	0.091	2.31	0.5676	0.84
3/8"	10	0.675	17.15	XS/80/80S	0.126	3.20	0.7388	1.10
1/2"	10	0.840	21.34	5/5S	0.065	1.65	0.5383	0.80
1/2"	15	0.840	21.34	10/10S	0.083	2.11	0.671	1.00
1/2"	15	0.840	21.34	STD/40/40S	0.109	2.77	0.851	1.27
1/2″	15	0.840	21.34	XS/80/80S	0.147	3.73	1.088	1.62
1/2″	15	0.840	21.34	160	0.188	4.78	1.309	1.95
1/2″	15	0.840	21.34	XX	0.294	7.47	1.714	2.55
3/4"	20	1.050	26.67	5/5S	0.065	1.65	0.684	1.02
3/4"	20	1.050	26.67	10/10S	0.083	2.11	0.857	1.28
3/4"	20	1.050	26.67	STD/40/40S	0.113	2.87	1.131	1.68
3/4″	20	1.050	26.67	XS/80/80S	0.154	3.91	1.474	2.19
3/4″	20	1.050	26.67	160	0.219	5.56	1.944	2.89
3/4″	20	1.050	26.67	XX	0.308	7.82	2.441	3.63
1″	25	1.315	33.40	5/5S	0.065	1.65	0.868	1.29
1″	25	1.315	33.40	10/10S	0.011	2.77	1.404	2.09
1″	25	1.315	33.40	STD/40/40S	0.133	3.38	1.679	2.50
1″	25	1.315	33.40	XS/80/80S	0.179	4.55	2.172	3.23
1″	25	1.315	33.40	160	0.250	6.35	2.844	4.23
1″	25	1.315	33.40	XX	0.358	9.09	3.659	5.45
1 1/4″	32	1.660	42.16	5/5S	0.065	1.65	1.107	1.65
1 1/4″	32	1.660	42.16	10/10S	0.109	2.77	1.806	2.69
1 1/4″	32	1.660	42.16	STD/40/40S	0.140	3.56	2.273	3.38
1 1/4″	32	1.660	42.16	XS/80/80S	0.191	4.85	2.997	4.46
1 1/4″	32	1.660	42.16	160	0.250	6.35	3.765	5.60
1 1/4″	32	1.660	42.16	XX	0.382	9.70	5.214	7.76
1 1/2″	40	1.900	48.26	5/5S	0.065	1.65	1.274	1.90
1 1/2″	40	1.900	48.26	10/10S	0.109	2.77	2.085	3.10
1 1/2″	40	1.900	48.26	STD/40/40S	0.145	3.68	2.718	4.05
1 1/2″	40	1.900	48.26	XS/80/80S	0.200	5.08	3.631	5.40

Nom. Pipe Sizes		OD	OD	Schedule Designations ANSI/ASME	Wall Thickn. inches	Wall Thickn. mm	Lbs/Ft	Kg/m
Inches	mm DN	inches	mm					
1 1/2″	40	1.900	48.26	160	0.281	7.14	4.859	7.23
1 1/2″	40	1.900	48.26	XX	0.400	10.16	6.408	9.54
2″	50	2.375	60.33	5/5S	0.065	1.65	1.604	2.39
2″	50	2.375	60.33	10/10S	0.109	2.77	2.638	3.93
2″	50	2.375	60.33	STD/40/40S	0.154	3.91	3.653	5.44
2″	50	2.375	60.33	XS/80/80S	0.218	5.54	5.022	7.47
2″	50	2.375	60.33	160	0.344	8.74	7.462	11.11
2″	50	2.375	60.33	XX	0.436	11.07	9.029	13.44
2 1/2″	65	2.875	73.03	5/5S	0.083	2.11	2.475	3.68
2 1/2″	65	2.875	73.03	10/10S	0.120	3.05	3.531	5.26
2 1/2″	65	2.875	73.03	STD/40/40S	0.203	5.16	5.793	8.62
2 1/2″	65	2.875	73.03	XS/80/80S	0.276	7.01	7.661	11.40
2 1/2″	65	2.875	73.03	160	0.375	9.53	10.01	14.80
2 1/2″	65	2.875	73.03	XX	0.552	14.02	13.69	20.37
3″	80	3.500	88.90	5/5S	0.083	2.11	3.029	4.51
3″	80	3.500	88.90	10/10S	0.120	3.05	4.332	6.45
3″	80	3.500	88.90	STD/40/40S	0.216	5.49	7.576	11.27
3″	80	3.500	88.90	XS/80/80S	0.300	7.62	10.250	15.25
3″	80	3.500	88.90	160	0.438	11.13	14.320	21.31
3″	80	3.500	88.90	XX	0.600	15.24	18.580	27.65
3 1/2″	90	4.000	101.60	5/5S	0.083	2.11	3.472	5.17
3 1/2″	90	4.000	101.60	10/10S	0.120	3.05	4.973	7.40
3 1/2″	90	4.000	101.60	STD/40/40S	0.226	5.74	9.109	13.56
3 1/2″	90	4.000	101.60	XS/80/80S	0.318	8.08	12.500	18.60
3 1/2″	90	4.000	101.60	XX	0.636	16.15	22.850	34.01
4″	100	4.500	114.30	5/5S	0.083	2.11	3.915	5.83
4″	100	4.500	114.30	10/10S	0.120	3.05	5.613	8.35
4″	100	4.500	114.30	STD/40/40S	0.237	6.02	10.790	16.06
4″	100	4.500	114.30	XS/80/80S	0.337	8.56	14.980	22.29
4″	100	4.500	114.30	120	0.438	11.13	19.000	28.28
4″	100	4.500	114.30	160	0.531	13.49	22.510	33.50
4″	100	4.500	114.30	XX	0.374	17.12	27.540	40.99
5″	125	5.563	141.30	5/5S	0.109	2.77	6.349	9.45
5″	125	5.630	143.00	10/10S	0.134	3.4	7.770	11.56
5″	125	5.630	143.00	STD/40/40S	0.258	6.55	14.620	21.76
5″	125	5.630	143.00	XS/80/80S	0.375	9.53	20.780	30.93
5″	125	5.630	143.00	160	0.500	12.70	27.040	40.24

Nom. Pipe Sizes		OD	OD	Schedule	Wall	Wall	Lbs/Ft	Kg/m
Inches	mm DN	inches	mm	Designations ANSI/ASME	Thickn. inches	Thickn. mm		
5″	125	5.630	143.00	XX	0.625	15.88	32.960	49.05
5″	125	5.630	143.00	5/5S	0.750	19.05	38.550	57.37
6″	150	6.625	168.28	5/5S	0.109	2.77	7.585	11.29
6″	150	6.625	168.28	10/10S	0.134	3.40	9.289	13.82
6″	150	6.625	168.28	STD/40/40S	0.280	7.11	18.970	28.23
6″	150	6.625	168.28	XS/80/80S	0.432	10.97	28.570	42.52
6″	150	6.625	168.28	120	0.562	14.27	36.390	54.16
6″	150	6.625	168.28	160	0.719	18.26	45.350	67.49
6″	150	6.625	168.28	XX	0.864	21.95	53.160	79.12
8″	200	8.625	219.08	5/5S	0.109	2.77	9.914	14.75
8″	200	8.625	219.08	10/10S	0.148	3.76	13.600	19.94
8″	200	8.625	219.08	20	0.250	6.35	22.360	33.28
8″	200	8.625	219.08	30	0.277	7.04	24.700	36.76
8″	200	8.625	219.08	STD/40/40S	0.322	8.18	28.550	42.49
8″	200	8.625	219.08	60	0.406	10.31	34.640	53.04
8″	200	8.625	219.08	XS/80/80S	0.500	12.70	43.390	64.58
8″	200	8.625	219.08	100	0.594	15.09	50.950	75.83
8″	200	8.625	219.08	120	0.719	18.26	60.710	90.35
8″	200	8.625	219.08	140	0.812	20.62	67.760	100.84
8″	200	8.625	219.08	XX	0.875	22.23	72.420	107.78
8″	200	8.625	219.08	160	0.906	23.01	74.690	111.16
10″	250	10.750	273.05	5S	0.134	3.40	15.190	22.61
10″	250	10.750	273.05	10S	0.165	4.19	18.700	27.83
10″	250	10.750	273.05	20	0.250	6.35	28.040	41.73
10″	250	10.750	273.05	30	0.307	7.80	34.240	50.96
10″	250	10.750	273.05	STD/40/40S	0.365	9.27	40.480	60.24
10″	250	10.750	273.05	XS/60/80S	0.500	12.70	54.740	81.47
10″	250	10.750	273.05	80	0.594	15.09	64.430	95.89
10″	250	10.750	273.05	100	0.719	18.26	77.030	114.64
10″	250	10.750	273.05	120	0.844	21.44	89.290	132.89
10″	250	10.750	273.05	140/XX	1.000	25.40	104.130	154.97
10″	250	10.750	273.05	160	1.250	28.58	115.640	175.10
12″	300	12.750	323.85	5S	0.156	3.96	20.980	31.22
12″	300	12.750	323.85	10S	0.180	4.57	24.200	36.02
12″	300	12.750	323.85	20	0.250	6.35	33.380	49.68
12″	300	12.750	323.85	30	0.330	8.38	43.770	65.14
12″	300	12.750	323.85	STD/40S	0.375	9.53	49.560	73.76

Nom. Pipe Sizes		OD	OD	Schedule	Wall	Wall	Lbs/Ft	Kg/m
Inches	mm DN	inches	mm	Designations ANSI/ASME	Thickn. inches	Thickn. mm		
12″	300	12.750	323.85	40	0.406	10.31	53.520	79.65
12″	300	12.750	323.85	XS/80S	0.500	12.70	65.420	97.36
12″	300	12.750	323.85	60	0.562	14.27	73.150	108.87
12″	300	12.750	323.85	80.00	0.688	17.48	88.630	11.90
12″	300	12.750	323.85	100	0.844	21.44	107.320	159.72
12″	300	12.750	323.85	120/XX	1.000	25.40	125.490	186.76
12″	300	12.750	323.85	140	1.125	28.58	139.670	207.86
12″	300	12.750	323.85	160	1.312	33.32	160.270	238.52
14″	350	14.000	355.60	10S	0.188	4.78	27.730	41.27
14″	350	14.000	355.60	10	0.250	6.35	36.710	54.63
14″	350	14.000	355.60	20	0.312	7.92	45.610	67.88
14″	350	14.000	355.60	STD/30/40S	0.375	9.53	54.570	81.21
14″	350	14.000	355.60	40	0.438	11.13	63.440	94.41
14″	350	14.000	355.60	XS/80S	0.500	12.70	72.090	107.29
14″	350	14.000	355.60	60	0.594	15.09	85.050	126.58
14″	350	14.000	355.60	80	0.750	19.05	106.130	157.95
14″	350	14.000	355.60	100	0.938	23.83	130.850	194.74
14″	350	14.000	355.60	120	1.094	27.79	150.900	224.58
14″	350	14.000	355.60	140	1.250	31.75	170.210	253.32
14″	350	14.000	355.60	160	1.406	35.71	189.100	281.43
16″	400	16.000	406.40	10S	0.188	4.78	31.750	47.25
16″	400	16.000	406.40	10	0.250	6.35	42.050	62.58
16″	400	16.000	406.40	20	0.312	7.92	62.270	77.79
16″	400	16.000	406.40	STD/30/40S	0.375	9.53	62.580	93.13
16″	400	16.000	406.40	XS/40/80S	0.500	12.70	82.770	123.18
16″	400	16.000	406.40	60	0.656	16.66	107.500	159.99
16″	400	16.000	406.40	80	0.844	21.44	136.610	203.31
16″	400	16.000	406.40	100	1.031	26.20	164.820	245.29
16″	400	16.000	406.40	120	1.219	30.96	192.430	286.37
16″	400	16.000	406.40	140	1.438	36.53	223.640	332.83
16″	400	16.000	406.40	160	1.594	40.49	245.250	364.99
18″	450	18.000	457.20	10S	0.188	4.78	35.760	53.22
18″	450	18.000	457.20	10	0.250	6.35	47.390	70.53
18″	450	18.000	457.20	20	0.312	7.92	58.940	87.72
18″	450	18.000	457.20	STD/40S	0.375	9.53	70.590	105.06
18″	450	18.000	457.20	30	0.438	11.13	82.150	122.26
18″	450	18.000	457.20	XS/80S	0.500	12.70	93.450	138.08

Nom. Pipe Sizes		OD	OD	Schedule	Wall	Wall	Lbs/Ft	Kg/m
Inches	mm DN	inches	mm	Designations ANSI/ASME	Thickn. inches	Thickn. mm		
18″	450	18.000	457.20	40	0.562	14.27	104.670	155.78
18″	450	18.000	457.20	60	0.750	19.05	138.170	205.63
18″	450	18.000	457.20	80	0.938	23.83	170.920	254.37
18″	450	18.000	457.20	100	1.156	29.36	207.960	309.50
18″	450	18.000	457.20	120	1.375	34.93	244.140	363.34
18″	450	18.000	457.20	140	1.562	39.67	274.220	408.11
18″	450	18.000	457.20	160	1.781	45.24	308.500	459.13
20″	500	20.000	508.00	10S	0.218	5.54	46.060	68.55
20″	500	20.000	508.00	10	0.250	6.35	52.730	78.48
20″	500	20.000	508.00	STD/20/40S	0.375	9.53	78.60	116.98
20″	500	20.000	508.00	XS/30/80S	0.500	12.70	104.130	154.97
20″	500	20.000	508.00	40	0.594	15.09	123.110	183.22
20″	500	20.000	508.00	60	0.812	20.62	166.400	247.65
20″	500	20.000	508.00	80	1.031	26.19	208.870	310.85
20″	500	20.000	508.00	100	1.281	32.54	256.100	381.14
20″	500	20.000	508.00	120	1.500	38.10	296.370	441.07
20″	500	20.000	508.00	140	1.750	44.45	341.090	507.63
20″	500	20.000	508.00	160	1.969	50.01	379.170	564.30
24″	600	24.000	609.60	10/10S	0.250	6.35	63.410	94.37
24″	600	24.000	609.60	STD/20/40S	0.375	9.53	94.620	140.82
24″	600	24.000	609.60	XS/80S	0.500	12.70	125.490	186.76
24″	600	24.000	609.60	30	0.562	14.27	140.680	209.37
24″	600	24.000	609.60	40	0.688	17.48	171.290	254.92
24″	600	24.000	609.60	60	0.969	24.61	238.350	354.72
24″	600	24.000	609.60	80	1.219	30.96	296.580	441.39
24″	600	24.000	609.60	100	1.531	38.89	367.390	546.77
24″	600	24.000	609.60	120	1.812	46.02	429.390	639.04
24″	600	24.000	609.60	140	2.062	52.37	483.100	718.97
24″	600	24.000	609.60	160	2.344	59.54	542.130	806.3
30″	750	30.000	762.00	10	0.361	7.92	98.930	147.23
30″	750	30.000	762.00	STD/40S	0.375	9.53	118.650	176.58
30″	750	30.000	762.00	XS/20/80S	0.500	12.70	157.530	234.44
30″	750	30.000	762.00	30	0.625	15.88	196.080	291.82
36″	900	36.000	914.40	10	0.312	7.92	118.920	176.98
36″	900	36.000	914.40	STD/40S	0.375	9.53	142.680	212.34
36″	900	36.000	914.40	XS/80S	0.500	12.70	189.570	282.13

Appendix F: Model Supports

Figure 66 shows how the system is supported; both ends of the main pipe have fix supports.

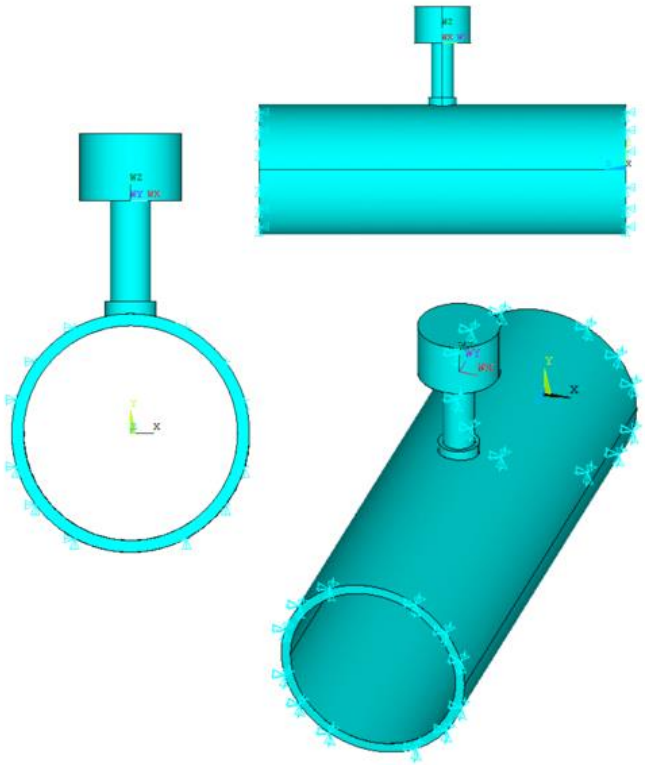

Figure 66. Model fixed support

Appendix G: Modes Frequencies

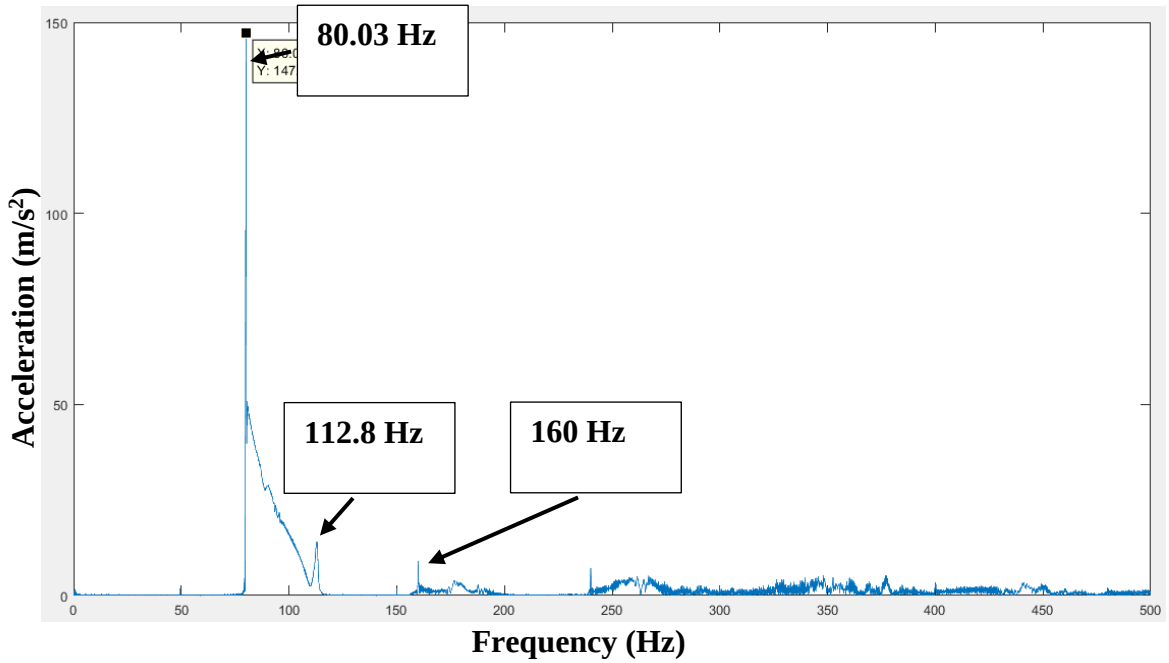

Figure 67. Harmonic response with the modes peaks (experimental)